Tephra fallout probabilistic hazard maps for Cotopaxi and Guagua Pichincha volcanoes (Ecuador) with uncertainty quantification

Alessandro Tadini[1], Nourddine Azzaoui[2], Olivier Roche[1], Pablo Samaniego[3], Benjamin Bernard[4], Andrea Bevilacqua[5], Silvana Hidalgo[4], Arnaud Guillin[2], and Mathieu Gouhier[1]

[1]Laboratoire Magmas et Volcans (Université Clermont Auvergne-CNRS-IRD)
[2]Laboratoire de Mathématiques Blaise Pascal (Université Clermont Auvergne)
[3]Insitut de Recherche et Développment
[4]Instituto Geofísico-Escuela Politécnica Nacional
[5]National Institute of Geophysics and Volcanology

November 24, 2022

Abstract

Tephra fallout hazard assessment is commonly undertaken with the development of probabilistic maps that rely on numerical models. Among the steps for map production, the definition of input parameters of the model (including atmospheric conditions), the physical approximations of the numerical simulations, and the probabilities of occurrence of different eruption types in specific time frames are among the most critical sources of uncertainty. In this paper, we present a tephra fallout hazard assessment study for two volcanoes (Cotopaxi and Guagua Pichincha) in Ecuador. We utilize the coupled PLUME-MoM/HYSPLIT models, and we develop a procedure for uncertainty quantification where: i) we quantify the uncertainty on eruptive source parameters and eruption type occurrence through expert elicitation; ii) we implement a new procedure for correlations between the different parameters, and iii) we quantify the uncertainty of the numerical model by testing it with past eruptions and by deriving coefficients of mean model overestimation/underestimation. Probability maps of exceedance, given a deposit thickness threshold, and thickness maps, given a probability of exceedence, are produced for eruption of sub-Plinian and Plinian types, which are then merged into single maps concerning the next eruption. These are described according to the uncertainty distribution of eruption type occurrence probabilities, in terms of their 5^{th} percentile, mean and 95^{th} percentile values. We finally present hazard curves describing exceeding probabilities in 10 sensitive sites within the city of Quito. Additional information includes the areal extent and the people potentially affected by different isolines of tephra accumulation.

Hosted file

`essoar.10507518.1.docx` available at https://authorea.com/users/552017/articles/604592-tephra-fallout-probabilistic-hazard-maps-for-cotopaxi-and-guagua-pichincha-volcanoes-ecuador-with-uncertainty-quantification

A. Tadini[1], N. Azzaoui[2], O. Roche[1], P. Samaniego[1,3], B. Bernard[3], A. Bevilacqua[4], S. Hidalgo[3], A. Guillin[2], M. Gouhier[1]

[1]Université Clermont Auvergne, Laboratoire Magmas et Volcans, UCA-CNRS-IRD, 6 Avenue Blaise Pascal, 63178 Aubière, France.

[2]Université Clermont Auvergne, Laboratoire de Mathématiques Blaise Pascal, 3 place Vasarely, 63178 Aubière, France.

[3]Escuela Politécnica Nacional, Instituto Geofísico, Ladrón de Guevara E11-253 y Andalucía, Quito, Ecuador.

[4]Istituto Nazionale di Geofisica e Vulcanologia, Sezione di Pisa, via Cesare Battisti 53, 56125 Pisa, Italy.

Corresponding author: Alessandro Tadini (Alessandro.TADINI@uca.fr)

Key Points:

- We use the PLUME-MoM/HYSPLIT model and a probabilistic approach
- We quantify uncertainty of the input parameters, the model, and eruption occurrences
- Probability/isopach maps and hazard curves in 10 sensitive sites in Quito for sub-Plinian/Plinian eruption types for the next eruption

Index Terms and Keywords

4314 Mathematical and computer modeling, 3275 Uncertainty quantification, 8428 Explosive volcanism, 8488 Volcanic hazards and risks

Tephra fallout, volcanic hazard assessment, Cotopaxi, Guagua Pichincha, uncertainty quantification

Abstract

Tephra fallout hazard assessment is commonly undertaken with the development of probabilistic maps that rely on numerical models. Among the steps for map production, the definition of input parameters of the model (including atmospheric conditions), the physical approximations of the numerical simulations, and the probabilities of occurrence of different eruption types in specific time frames are among the most critical sources of uncertainty. In this paper, we present a tephra fallout hazard assessment study for two volcanoes (Cotopaxi and Guagua Pichincha) in Ecuador. We utilize the coupled PLUME-MoM/HYSPLIT models, and we develop a procedure for uncertainty quantification where: i) we quantify the uncertainty on eruptive source parameters and eruption type occurrence through expert elicitation; ii) we implement a new procedure for correlations between the different parameters, and iii) we quantify the uncertainty of the numerical model by testing it with past eruptions and by deriving coefficients of mean model overestimation/underestimation. Probability maps of exceedance, given a deposit thickness threshold, and thickness maps, given a probability of exceedence, are produced for eruption of sub-Plinian and

Plinian types, which are then merged into single maps concerning the next eruption. These are described according to the uncertainty distribution of eruption type occurrence probabilities, in terms of their 5^{th} percentile, mean and 95^{th} percentile values. We finally present hazard curves describing exceeding probabilities in 10 sensitive sites within the city of Quito. Additional information includes the areal extent and the people potentially affected by different isolines of tephra accumulation.

Plain language summary

We present a tephra fallout (i.e. volcanic ash accumulation on the ground due to sedimentation from volcanic clouds) hazard assessment for two ecuadorian volcanoes, Cotopaxi and Guagua Pichincha. The novelties of this study are that i) we use the coupled PLUME-MoM/HYSPLIT models (never used in similar studies with uncertainty quantification) and ii) we quantify the main sources of uncertainties that normally affect probabilistic hazard maps produced using numerical models. In particular, resulting maps are presented as probability maps of exceedance, given a deposit thickness threshold, and thickness maps, given a probability of exceedence. For the two volcanoes, maps are related to the case that next eruption will be sub-Plinian or Plinian: to obtain this, we merged the maps for these two eruption types into a single map according to the different probability of occurrence of such eruption types (along with their uncertainties). Moreover, we also present hazard curves describing exceeding probabilities of tephra accumulation in 10 sensitive sites within the city of Quito, and the areal extent and the people potentially affected by different isolines of tephra accumulation.

1 Introduction

Among the numerous hazards related to volcanic eruptions, tephra fallout is certainly one of the most severe because it may affect large areas (> 100 km^2; Blong, 1996) and has a dramatic impact on both human settlements and activities Brown *et al.*, 2017(). While tephra residence in the atmosphere can lead to near-total disruption of air traffic over a vast region Budd *et al.*, 2011Bursik *et al.*, 2009Folch *et al.*, 2012Folch and Sulpizio, 2010(e.g., Eyjafjallajokull 2010 eruption; ; ; ;), tephra accumulation on the ground affects human health Baxter, 1990Baxter and Horwell, 2015(;), buildings stability Macedonio and Costa, 2012Spence *et al.*, 2005(;), roads/transportation systems Blake *et al.*, 2017Guffanti *et al.*, 2009(;), electrical infrastructure Bebbington *et al.*, 2008Wilson *et al.*, 2014(;), farmland/livestock Annen and Wagner, 2003() or water reservoirs and vegetation Wilson *et al.*, 2012(). In response to this threat, many researches have been conducted with the aim of providing authorities, stakeholders and population with tools either for both real-time volcanic crises management or long-term planning. Particularly, in this latter case, tephra fallout hazard maps have been produced using different strategies that rely on field data of past eruptions e.g., Orsi *et al.*, 2004() or which combine field data and numerical modelling Barberi *et al.*, 1990Bursik, 2001Cioni *et al.*, 2003Macedonio *et al.*, 1988(; ; ;).This latter approach is normally coupled with semi-probabilistic to

fully probabilistic Monte Carlo techniques Hurst and Smith, 2004() to sample model input parameters, and takes advantage of the great availability of tephra transport and deposition numerical models. As examples, tephra fallout hazard maps have been produced using HAZMAP Bonasia *et al.*, 2011Capra *et al.*, 2008Costa *et al.*, 2009Macedonio *et al.*, 2005(; ; ;), TEPHRA2 Biass and Bonadonna, 2013Biass *et al.*, 2014Bonadonna *et al.*, 2005Tsuji *et al.*, 2017Yang *et al.*, 2021(; ; ; ;), FALL3D Costa *et al.*, 2006Folch *et al.*, 2009Folch *et al.*, 2020Prata *et al.*, 2021Scaini *et al.*, 2012Vázquez *et al.*, 2019(; ; ; ; ;), VOLCALPUFF Barsotti *et al.*, 2018Barsotti and Neri, 2008Barsotti *et al.*, 2008(; ;) and ASH3D Alpízar Segura *et al.*, 2019IG-EPN *et al.*, 2019Schwaiger *et al.*, 2012Yang *et al.*, 2020(; ; ;) models. The key elements for the modelling of tephra dispersal and for the development of probabilistic maps are: i) the identification of the eruptive scenarios that describe the eruptive history of the volcano; ii) the quantification of the uncertainty range of the eruptive source parameters (ESPs) related to each scenario; and iii) the estimation of the temporal recurrence rate and/or the probability of occurrence of the identified scenarios within defined temporal frames Sandri *et al.*, 2016(). Especially for the second two elements, uncertainty was quantified in recent hazard-related studies mostly through comparison between available field data and existing global databases see for example Biass and Bonadonna, 2013(). How the input uncertainty propagates through the model, and interacts with wind field variability has been the topic of several studies Bursik *et al.*, 2012Macedonio *et al.*, 2016Madankan *et al.*, 2014Pouget *et al.*, 2016Scollo *et al.*, 2008Stefanescu *et al.*, 2014(; ; ; ; ;). An important source of uncertainty that has a direct impact on final map production has been however poorly considered so far, that is the uncertainty related to the inadequacy of the numerical model itself, which is linked to the necessary physical approximations that allow acceptable computational times. Constraining the model-related uncertainty is an open challenge in common with other geophysical mass flow modeling efforts, and requires a statistically-based and multi-model approach Bevilacqua *et al.*, 2019Costa *et al.*, 2016bPatra *et al.*, 2020Patra *et al.*, 2018(; ; ;).

This paper presents a tephra fallout hazard assessment study, which focuses on the area of Quito, Ecuador's capital city. In order to perform this study, we focus on Cotopaxi and Guagua Pichincha, which are located nearby the city and are currently active volcanoes with recent eruptions. Two main novelties are included in this study: i) a modelling strategy that employs a coupling between the plume model PLUME-MoM de'Michieli Vitturi *et al.*, 2015() and the tephra dispersal model HYSPLIT Stein *et al.*, 2015(); ii) a procedure that takes into account the three above-mentioned major sources of uncertainty during the production of tephra fallout hazard maps (on the ESPs, on the model, and on the eruption type occurrence probability). Particularly, the preliminary definition of these uncertainties has been the topic of two precedent studies Tadini *et al.*, 2020, 2021(), which are propedeutical to this work, and have been developed in the ambience of the same research project.
In summary, in this study we firstly introduce Cotopaxi and Guagua Pichincha

volcanoes (section 2). Then we describe the modelling strategy (section 3.1), the uncertainty quantification for ESPs and eruption type occurrence (section 3.2), and the procedure for hazard maps and hazard curves production. Finally, section 4 focuses on the presentation of the maps/curves and the discussion of their main implications, including the areas and the people potentially involved by each hazard isoline.

2 Background

Quito, Ecuador's capital city, is located in the inter-andean valley, within the province of Pichincha (Fig. 1a). With almost three millions of inhabitants it is also the largest city in the country, it hosts the largest country's airport and it is in the middle of the most important road systems (e.g. the "Pan-American highway"; Fig. 1a).

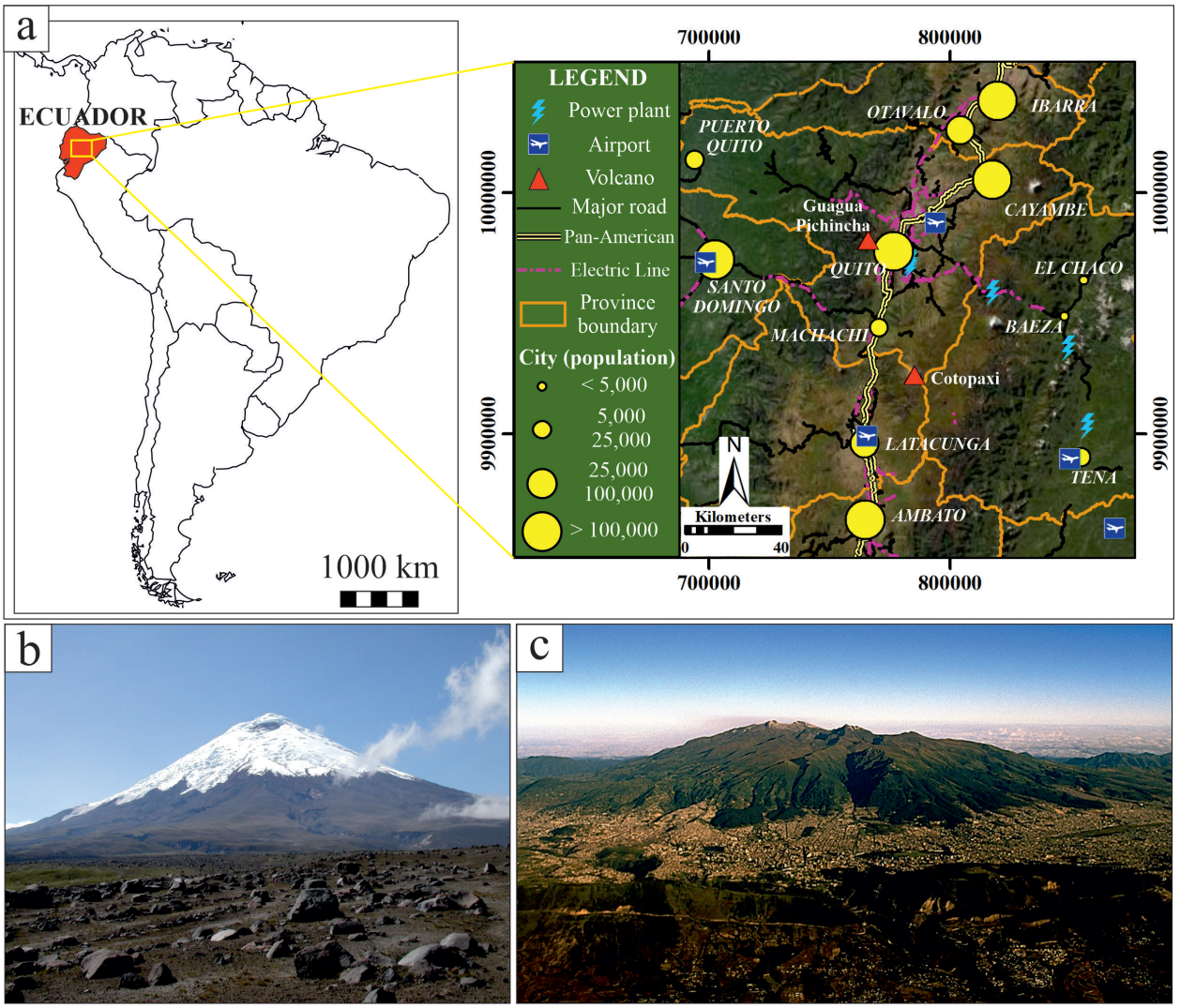

Figure 1. a) Location of Cotopaxi and Guagua Pichincha volcanoes with respect to the capital city Quito and the main towns and infrastructures in the region. Service Layer Credits, source: Esri, DigitalGlobe, GeoEye, Earthstar Geographics, CNES/Airbus DS, USDA, USGS, AeroGRID, IGN and the GIS User Community; b) Cotopaxi volcano seen from North; c) Guagua Pichincha volcanic complex and the city of Quito seen from East.

2.1 Cotopaxi

Cotopaxi volcano (Fig. 1a and b) is characterized by a bimodal volcanism involving rhyolitic (70–75 wt.% SiO_2) and andesitic (56–62 wt.% SiO_2) magmas. According to Hall and Mothes (2008), rhyolitic magmas were erupted mostly in

the early stages of Cotopaxi activity (Plinian eruptions with VEI 4-5 or greater), while from ~4 ka until present day, magmas erupted were almost all andesitic in composition. The latter period of activity with andesitic magmas include violent Strombolian VEI 2-3 in the XIX century, Pistolesi *et al.*, 2011(), sub-Plinian VEI 3-4 AD 1877 or XVIII century, Pistolesi *et al.*, 2011() and Plinian VEI 4-5 Layer 3 - 820±80 years BP; Layer 5 - 1180± 80 years BP, Biass and Bonadonna, 2011Tsunematsu and Bonadonna, 2015(;) eruptions. The last eruption of Cotopaxi is the AD 2015 VEI 1-2 eruption, characterized by an opening hydrovolcanic phase Bernard *et al.*, 2016() followed by a ~3 months long ash emission Gaunt *et al.*, 2016Hidalgo *et al.*, 2018(;).

Cotopaxi volcano has been the topic of tephra fallout hazard Biass and Bonadonna, 2013Hall *et al.*, 2004aHall *et al.*, 2004bHall and von Hillebrandt, 1988aMiller *et al.*, 1978(; ; ; ;) and risk Biass *et al.*, 2013() assessment studies. Particularly, Biass and Bonadonna (2013) performed a probabilistic tephra fallout hazard assessment for five eruption scenarios (two with fixed ESPs and three with ESPs defined as a variation range), with magnitudes ranging from VEI 3 to 5. For each eruption scenario, 1,000 runs were done by using the TEPHRA2 model. As input parameters for this model, Biass and Bonadonna (2013) considered, for each run, i) a wind profile sampled from the NOAA NCEP/NCAR Reanalysis 1 database Kalnay *et al.*, 1996() and ii) erupted volume, plume height and median grainsize sampled from a specific distribution. The probability of tephra accumulation in a given time window was presented by the authors through three different outputs, i) probability maps for a given tephra accumulation, ii) isomass maps for a given probability value and iii) hazard curves for several locations, including Quito city center and the town of Latacunga. Moreover, using data from the global volcanism program database, the authors calculated the probability of occurrence of an eruption of VEI 3 for the next 10 (~36%) and 100 (~99%) years. Additionally, Biass *et al.* (2013) performed a risk assessment for eruptions with VEI 4, highlighting the possible roof collapse due to tephra loading of several thousands of houses in the proximity of the volcano, the destruction of agriculture and the possible disruption of major roads. Then, Volentik and Houghton (2015) performed a more extended hazard assessment focused on the potential impact of tephra fallout on Quito International airport from explosive eruptions of different Ecuadorian volcanoes. They used the TEPHRA2 model and NCEP/NCAR Reanalysis 1 wind data, while plume height, eruption duration, total mass and median/sorting of grain size were sampled from uniform, log-uniform or log-normal distributions. Specifically for Cotopaxi, the study indicated, at Quito airport, a probability of mass accumulation of 1 mm and 10 mm of, respectively, ~14% and 2.5%. Recently, a multi-hazard map for Cotopaxi was released divided in three sectors, North Mothes *et al.*, 2016a(), South Mothes *et al.*, 2016b() and East Vasconez *et al.*, 2017(). In the first two maps, tephra fallout hazard assessment was treated as the expected tephra accumulation (with thresholds of 5 and 25 cm) in case of an eruption with VEI 3-5, based on field data of past eruptions with similar magnitudes. In the map of Vasconez

et al. (2017), instead, the authors present the most likely (80%) distribution for a VEI 3 eruption (similar to the AD 1877) based on 120 simulations (1 per month for 10 years, windfield reanalysis 2007-2017) using the ASH3D model Schwaiger *et al.*, 2012(). In this map Quito is potentially (<20% probability) affected by ashfalls between 10 and 100 mm. Finally, additional tephra fallout maps have been presented in the work of Cruz Roja Ecuatoriana (2020), which include maps for 5 eruptive scenarios (120 simulations each using the ASH3D model) for different probability thresholds (1, 25, 50, 75 and 99%)

2.2 Guagua Pichincha

The Pichincha volcanic complex (Fig. 1a and c) is composed of three distinct edifices, the youngest of which is Guagua Pichincha (4,784 m a.s.l.). During the eruptive history of this latter (starting from 60 ka), all the erupted products were of andesitic to dacitic composition (59-66 wt.% SiO_2; Robin *et al.*, 2010). Guagua Pichincha volcano has been affected by two major lateral collapses (at ~11 ka and ~4 ka): after the latter one "Toaza" lateral collapse; Robin *et al.*, 2008() the eruptive history has been characterized mainly by phases of growth and destruction of a summit dome ("Cristal Dome"), divided into three major eruptive cycles (I century, X century, Historic) and separated by repose periods of the order of 300–500 years. Each cycle was initiated with phases of dome emplacement and explosive episodes, and involved a final Plinian-like eruption Robin *et al.*, 2008(). The closing eruption of the Historic cycle occurred in AD 1660 Robin *et al.*, 2008() and caused severe ash fallout in Quito and pyroclastic density currents on the western side of the volcano testified by historical accounts, Wolf, 1904(). After more than 300 years of quiescence, a new eruptive cycle started in AD 1999, lasting for almost 2 years until AD 2001, including several Vulcanian events and a series of dome-forming eruptions Garcia-Aristizabal *et al.*, 2007Wright *et al.*, 2007(;).

The first tephra fallout hazard assessments at Guagua Pichincha have been done by Hall and von Hillebrandt (1988b) and Barberi *et al.* (1992). Particularly, the latter authors considered the Plinian-like eruptions of the X century and Historic cycles as the maximum expected events, and they calculated the expected tephra accumulation using the model of Armienti *et al.* (1988). For this model they considered two single meteorological profiles (i.e. wind) and specific eruptive source parameters for each of the two eruptions. Resulting maps described tephra accumulation in term of thickness (from 5 to 50 cm) and a zonation of the area surrounding Guagua Pichincha in different classes according to the impact of tephra fall and other volcanic-related hazards. Volentik and Houghton (2015), in the case of an eruption from Guagua Pichincha volcano indicated at Quito airport a probability of accumulation of 1 mm and 10 mm of ash of 17.5 and 7 %, respectively. Finally, a multi-hazard map for Guagua Pichincha was published IG-EPN *et al.*, 2019() within the already cited work of Cruz Roja Ecuatoriana (2020). For such map it has been used the ASH3D model Schwaiger *et al.*, 2012(), and tephra fallout hazard assessment has been treated in a semi-probabilistic way. Three scenarios linked to three past eruptions (AD 1999-2001, X century,

AD 1660-Historic) have been considered with fixed eruptive source parameters, while wind profiles were statistically sampled at each iteration. Resulting maps described the expected tephra thickness (in mm) for given probabilities (1, 25, 50, 75 and 99%).

3 Methods

3.1 Numerical modelling

3.1.1 PLUME-MoM/HYSPLIT model

In this work, we used a coupling between the integral plume model PLUME-MoM and the tephra transport and dispersion model HYSPLIT, as already performed by Tadini *et al.* (2020) and Pardini *et al.* (2020). With PLUME-MoM, through a post-processing procedure, we computed the mass released from the plume at intervals of fixed height, which were the source locations for HYSPLIT.

In this paper we use a newly released version of PLUME-MoM PLUME-MoM-TSM, with "TSM" standing for "two-sized moments"; de' Michieli Vitturi and Pardini, 2021(). As in the first version of de'Michieli Vitturi *et al.* (2015), PLUME-MoM solves the equations for the conservation of mass, momentum, energy, and the variation of heat capacity and mixture gas constant. The model accounts for particle loss during the plume rise and for radial and crosswind air entrainment parameterized using two entrainment coefficients, and it adopts the method of moments to describe a continuous size distribution of one or more group of particles (e.g., with different densities, shapefactors,etc.). In particular, among the new features of PLUME-MoM-TSM, we used: i) the initial spreading of the umbrella cloud injecting from the volcanic column into the atmosphere, simulated through a transient shallow-water system of equations that models the intrusive gravity current and ii) the modelling of terminal fall velocity according to Ganser (1993).

The HYSPLIT model Stein *et al.*, 2015() belongs to the family of Lagrangian Volcanic ash transport and dispersion models, and solves the Lagrangian motion equations for the horizontal transport of pollutants (i.e. particles), while vertical motion depends on the pollutant terminal fall velocity. The dispersion of a pollutant is described using three main types of configuration, "3D particle","puff" or hybrid "particle/puff". Particularly, in the "puff" configuration, pollutants are described by packets of ash particles ("puffs") having a horizontal gaussian distribution of mass described by a standard deviation . The puffs expand with atmospheric turbulence until they exceed the size of the meteorological grid cell (either horizontally or vertically) and then split into several new puffs, each with their respective pollutant mass. We have used the hybrid "particle/puff" configuration, in which the horizontal packets of particles have a "puff" distribution, while in the vertical direction they move like 3D particles. As discussed in Tadini *et al.* (2020) this configuration allows to use a limited number of puffs (thus reducing computationl times) to properly capture both the horizontal dispersion and the vertical wind shears. In this work we have used

the April 2018 release version of HYSPLIT, with the modifications detailed in Tadini *et al.* (2020).

3.1.2 Uncertainty quantification for the numerical model

In this paper we apply the procedure for the quantification of the uncertainty of tephra fallout model described in Tadini *et al.* (2020). In the latter, the coupled PLUME-MoM/HYSPLIT model has been tested through simulations of four past eruptions of different magnitudes and styles from three Andean volcanoes (Tungurahua and Cotopaxi in Ecuador and Puyehue-Cordòn Caulle in Chile). Such uncertainty was quantified by evaluating the differences between modeled and observed data of plume height above the vent, and mass loading and grain size at given stratigraphic sections. Regarding mass loading (kg/m^2) in particular, for each eruption type and meteorological dataset tested, Tadini *et al.* (2020) calculated the mean overestimation (MO) and the mean underestimation (MU),

$$\begin{cases} MO = \frac{\sum_{i=1}^{N_o} {}_i}{N_o} & \text{for } {}_i > 0 \\ MU = \frac{\sum_{i=1}^{N_u} {}_i}{N_u} & \text{for } {}_i < 0 \end{cases} \quad (1)$$

where N_o and N_u are the number of sections with overestimation and underestimation, respectively. These two values were divided by the mean value of mass loading measured in the field (MML), thus giving two coefficients (MO/MML and MU/MML), which we will use in section 3.3.1 to account for, respectively, model overestimation and underestimation. Given the new features introduced in PLUME-MoM (see Section 3.1.1), we ran the simulations again for all the eruptions used by Tadini *et al.* (2020). In order to take into account the full uncertainty of the model, we chose the two MO/MML and MU/MML worst values related to the GDAS meteorological database (used in this work, see section 3.2.2), both deriving from the Puyehue-Cordon Caulle 2011 sub-Plinian eruption, which were

MO/MML = 2.2

MU/MML = -0.12

3.2 Eruption type probabilities and input parameters for the numerical model

3.2.1 Eruption type probabilities

To provide a quantification of the uncertainty in future eruption occurrences at both Cotopaxi and Guagua Pichincha volcanoes, Tadini *et al.* (2021) performed an expert elicitation session aimed at quantifying such values, which we will use in the merging of maps/curves (see section 3.3.3). In general, during an elicitation session Aspinall, 2006Aspinall *et al.*, 2019Bevilacqua *et al.*, 2015Neri *et al.*, 2008Tadini *et al.*, 2017a(; ; ; ;) selected experts are asked to provide their judgements (in the form of three percentiles, normally the 5^{th}, 50^{th} and 95^{th}) on two different questionnaires. Firstly they are asked factual questions with known answers to the organizers, in which they are asked to provide credible

intervals that capture the 'true' values (seed questions). The score that each expert got assigned after filling this first questionnaire is then used to pool all experts' judgements on a second questionnaire. This questionnaire enlists a number of "target" questions with unknown answer, which specifically address the problem(s) under investigation, in order to obtain group synthesized answers called 'decision-maker'.

In Tadini *et al.* (2021), a total of 20 experts (with different background, experience and knowledge on the studied volcanoes) were calibrated through 14 seed questions on south American (particularly Ecuadorian) volcanism and numerical modelling of tephra transport and dispersal. Thus the experts were weighted using two performance-based schemes: the CM Classical Model, Cooke, 1991() and ERF Expected Relative Frequency, Flandoli *et al.*, 2011() methods, and compared to an equal weight combination. The experts were then asked to provide their answers on 55 target questions on both future eruption occurrences and eruptive source parameter uncertainty ranges (see section 3.2.2). Regarding future eruption occurrences, two time frames were distinguished, the next eruption case and the next 100 years case: the former was aimed at assessing what would be the probability for the next eruption of a specific type (the mean elicited values summed up to 100%), while the 100 years focused on the probability of having at least one eruption of a specific type within the next 100 years (no constraints on the elicited values sum). This was made in order to consider the case of new large scale eruptions in the next 100 years, albeit preceded by smaller size events. The comparison to previous estimates based on temporal models of the eruptive record is thoroughly discussed in Tadini et al. (2021). A major advance was related to having obtained a probability distribution of eruption occurrence over an uncertainty range, thus enabling a doubly stochastic approach Bevilacqua *et al.*, 2020Bevilacqua *et al.*, 2018Bevilacqua *et al.*, 2016Marzocchi *et al.*, 20082010Neri *et al.*, 2008Tadini *et al.*, 2017b(; ; ; ; ; ;).

In this paper we use the results related to the CM model, and the corresponding probability distributions for the eruption types considered in this study (i.e. sub-Plinian and Plinian) are reported in Fig. 2. Mean values of the probability distributions are reported in Table 1, while the three percentiles for each eruption type are reported in Table S1 from the supporting information.

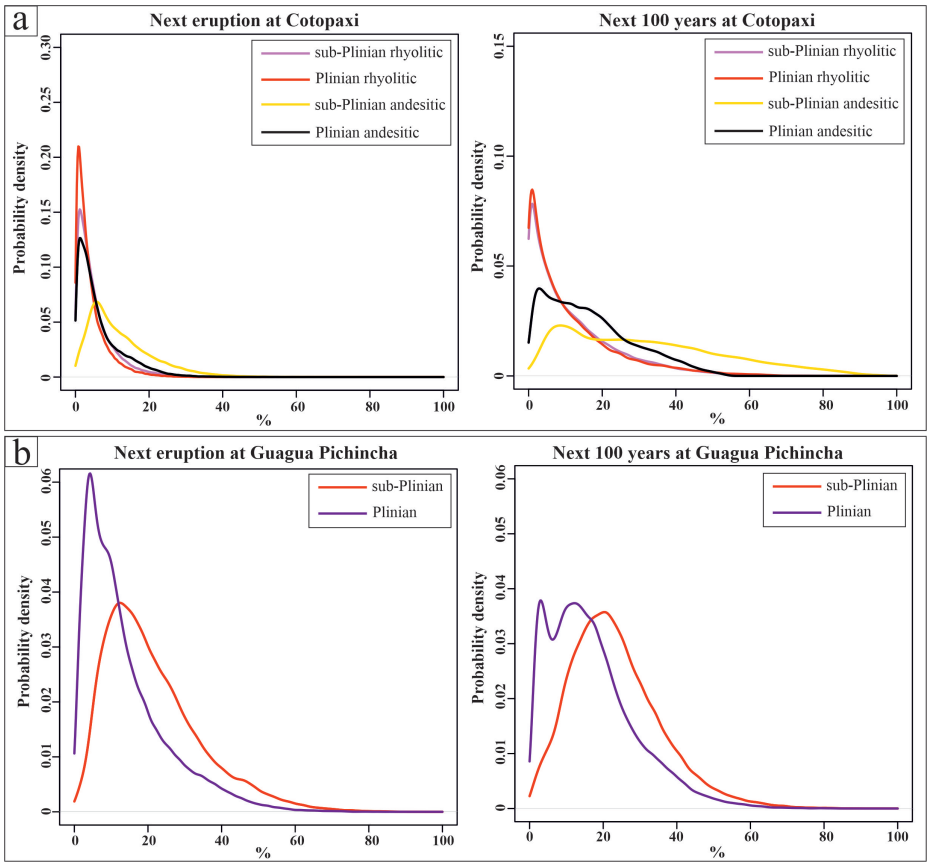

Figure 2. Uncertainty distributions according to the Classical Model method for the probability of occurrences of the sub-Plinian and Plinian eruption types for a) Cotopaxi and b) Guagua Pichincha volcanoes. y-axis describes the density of the probability density function. Data from Tadini *et al.* (2021).

Eruption Cotopaxi	**Next eruption (%)**	**Next 100 years (%)**
sub-Plinian Rhyolitic	5.9	12
Plinian Rhyolitic	4.6	12
sub-Plinian Andesitic	12	31
Plinian Andesitic	6.9	17
Eruption Guagua Pichincha	**Next eruption (%)**	**Next 100 years (%)**
sub-Plinian	22	28
Plinian	14	21

Table 1. Mean values obtained from the distributions of Figure 2. Data from Tadini *et al.* (2021).

3.2.2 Input parameters for the numerical model

We used detailed uncertainty distributions to sample three important parameters for tephra fallout hazard assessment and numerical modeling, which are eruption duration, total mass of the fallout deposit, and average plume height. Such distributions were defined by the expert elicitation session thoroughly described in Tadini *et al.* (2021) and summarized in section 3.2.1. We report these uncertainty distributions in Fig. 3 and the mean values of such distributions in Table 2, while the three elicited percentiles (5^{th}, 50^{th}, and 95^{th}) are reported in Tables S1 and S2 from the supporting information.

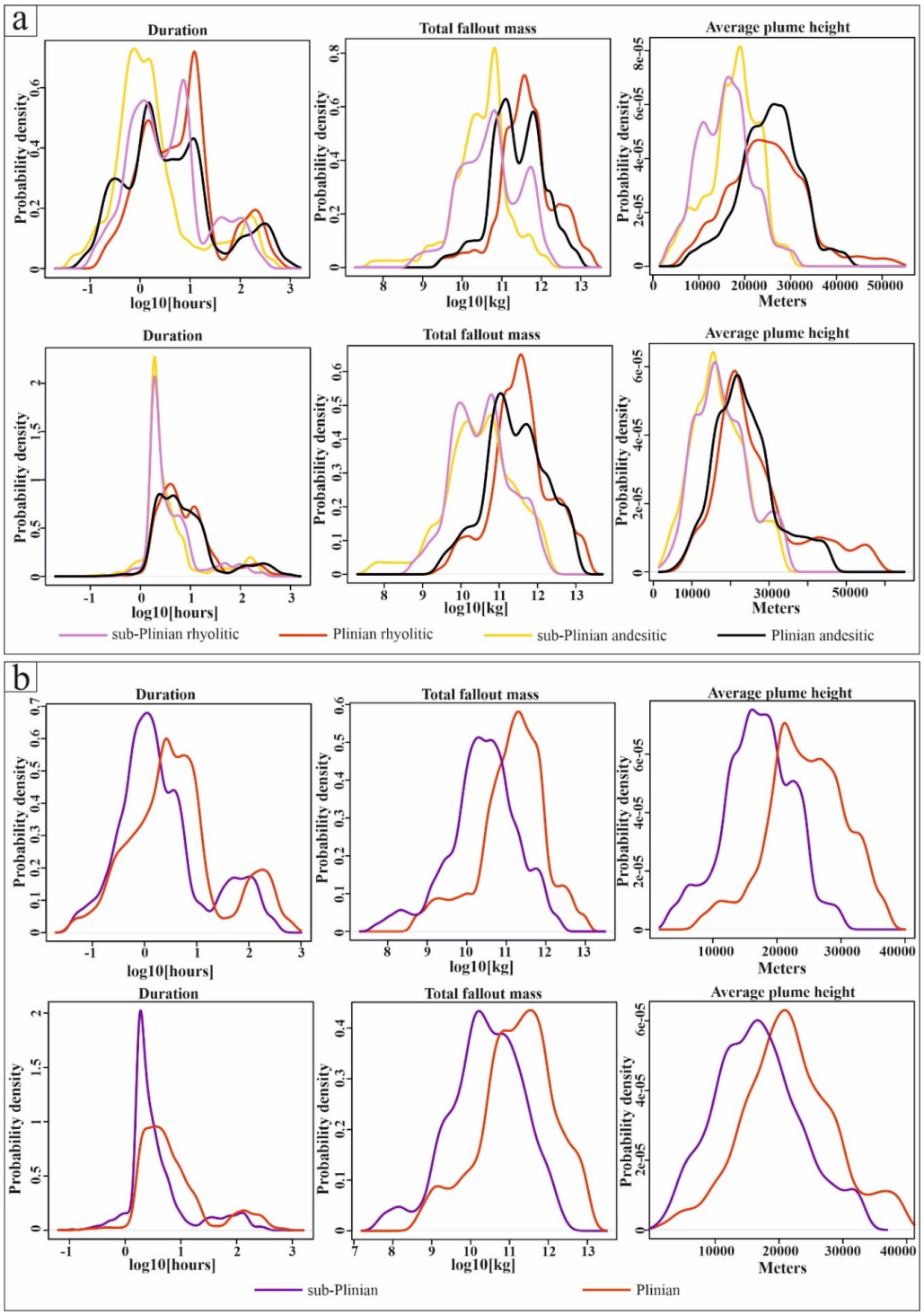
a
Duration
Total fallout mass
Average plume height
Probability density
log10[hours]
log10[kg]
Meters
sub-Plinian rhyolitic
Plinian rhyolitic
sub-Plinian andesitic
Plinian andesitic
b
sub-Plinian
Plinian

Figure 3. Eruptive source parameters (total eruption duration, total fallout mass and average plume height), uncertainty distributions according to the Classical Model method from Tadini *et al.*, 2021; upper panels() and uncertainty distributions recalculated after the application of the relation of Mastin *et al.* (2009) (lower panels) for a) Cotopaxi and b) Guagua Pichincha volcanoes. y-axis describes the density of the probability density function.

Eruption Cotopaxi	**Duration [hours]**	**Total mass fallout [10^9 kg]**	**Average plume he**
sub-Plinian Rhyolitic	3.3 (4.1)	49 (36)	14 (18)
Plinian Rhyolitic	6.2 (7.6)	270 (365)	22 (27)
sub-Plinian Andesitic	1.8 (3.8)	27 (31)	16 (17)
Plinian Andesitic	2.2 (7.7)	240 (262)	24 (24)
Eruption Guagua Pichincha	**Duration [hours]**	**Total mass fallout [10^9 kg]**	**Average plume he**
sub-Plinian	2.2 (3.8)	24 (25)	16 (16)
Plinian	4 (7)	130 (150)	24 (21)

Table 2. Mean values for duration, total fallout mass and average plume height Figure 3 and Tadini *et al.*, 2021() and maximum-minimum values for median (MdΦ) and sorting (Φ) of the total grain-size distributions Costa *et al.*, 2016a(). Values in square brackets are mean values after the application of the relation of Mastin *et al.* (2009) described in section 3.3.1.

For other parameters, such as total grain-size distribution (TGSD), particle densities, particle shape factors, and initial volatile content of magma, we considered an uncertainty range variable between two end members. In detail, for particle density we considered that this parameter varies linearly between those typical of two grain size end-members. Uncertainty bounds for this latter parameter have been derived from Bonadonna and Phillips (2003) and Pistolesi *et al.* (2011). For TGSD, instead, we considered the relationship discussed in Costa *et al.* (2016a), who proposed that TGSD distributions (for each eruption and magma types) can be described by the sum of two log-normal distributions as a function of plume height and magma viscosity. Details of these relations are provided in the Appendix. In our study we have considered TGSD in the range Φ = -6 to Φ = 10 (see Table 2 for the range of median and sorting of the total grain size distributions used in the simulations). Regarding the uncertainty ranges of the other parameters, we relied on the constraints in literature for initial water mass fractions Andújar *et al.*, 2017Martel *et al.*, 2018Samaniego *et al.*, 2010Wright *et al.*, 2007(; ; ;), and particle shape factors Riley *et al.*, 2003() of other volcanoes. The complete list of the parameters (other than those reported in Table 2) is available in Table S3 from the supporting information.

For meteorological data, we have used those deriving from the GDAS forecast data NOAA, 2004(), covering the period December 2004 – December 2019. This meteorological dataset tested by Tadini *et al.*, 2020() collects atmospheric data on 23 pressure levels (plus ground data) with a spatial grid resolution of 1° x 1°

and a temporal resolution of 3 hours. An example of wind directions/velocities at a selected pressure level (200 hPa) above Cotopaxi volcano is provided in Figure S1 from the supporting information, which shows that main wind directions are toward NW/W/SW with the exceptions of December and January.

3.3 Hazard maps and curves

3.3.1 Parameters sampling and maps production

In this study, in order to explicitly quantify the different uncertainties, we have implemented a new and comprehensive procedure for parameter sampling and map production, as illustrated in Fig. 4. This figure shows the procedure for each eruption type and for each iteration.

The uncertainty affecting the eruptive source parameters (ESPs) was taken into account with a Monte Carlo sampling (Fig. 4a). Three major ESPs (eruption duration, total mass of tephra fallout deposit, and average plume height) have been sampled directly from the distributions provided by Tadini *et al.* (2021) and reported in Fig. 3.

However, in order to provide set of parameters consistent with real eruptions, we have used the relations described in Mastin *et al.* (2009) that link plume height (in km) with volumetric flow rate (VFR in m^3/s) and total volume (V in km^3) of the fallout deposit, which are

$$H = 2.00 * \mathrm{VFR}^{0.241} \quad (2)$$

$$H = 25.9 + 6.64 \log_{10}(V) \quad (3)$$

Therefore, we have defined three possible cases, imposing that one third of the Monte Carlo iterations follows each case:

- total mass is sampled and duration/plume height are calculated;
- plume height is sampled and total mass/duration are calculated;
- duration and total mass are sampled and plume height is calculated.

For the latter case, duration and total mass have been sampled independently due to the absence of a strong relationship between eruption duration and the other parameters as also pointed out by Mastin *et al.*, 2009(). In detail, the total mass of tephra fallout deposit (in kg) enabled the calculation of the mass flow rate (kg/s) using eruption duration. To convert our mass and mass flow rate to, respectively, volume and volumetric flow rate, we have used magma DRE densities, and we tabulated values from Spera (2000) of 2340, 2220 and 2110 kg/m^3 for, respectively, andesitic, dacitic and rhyolitic melts. Density values have been chosen corresponding to magma water contents compatible to the ranges used here (see Table S2 from the supporting information).This procedure has the advantage of creating set of parameters physically related for each simulation, although it introduces some alterations with respect to the original elicited values. We found these differences not significant, except for

eruption duration (see Fig. 3), which reduced the probability of samples below 60 minutes, and thus has mean values slightly higher than the elicited one for all the eruption types. Nevertheless, although this is significant to mention in terms of seeking future improvements of input parameters handling, the increment of duration is not significantly influencing our hazard assessment because it only affects the eruptions of shortest duration and, in absolute terms, prolongs them of a few tens of minutes.

We highlight that PLUME-MoM cannot take plume height as input parameter, and thus the plume height in our procedure (both sampled from the elicited distribution of Tadini *et al.,* 2021 or calculated after Mastin *et al.,* 2009) can be different with respect to the plume height calculated by PLUME-MoM for the inferred total mass and duration. In case the elicited plume height is sampled, we found that PLUME-MoM can provide plume height values ~30-40% lower, at the end of simulation, with respect to those used to calculate the total mass/duration. This is perhaps related to the fact that Mastin *et al.* (2009) mostly focus on the maximum plume height while we consider their average values, in our simulations. However, the uncertainty bounds provided by Mastin *et al.* (2009) and the uncertainty range of our elicitation are fully overlapping and greater than the above-mentioned differences.

As previously mentioned, plume height and magma viscosity enabled us to calculate total grain-size distribution according to the relation proposed by Costa *et al.* (2016a) (see previous section, Appendix, and Table 2). However, we found the differences in the TGSD because of the plume height discrepancy to be not significant.

We finally remark that the duration of the eruption was also used to select (from the GDAS meteorological file covering the period 2004-2019) a time period for meteorological data. To this time period, additional 6 hours of simulation (with no emission) have been added to allow the particles to settle. To account for monthly variations in atmospheric data (see Figure S1 from the supporting information), we have performed the same number of simulations for each month (250, chosen as the best compromise between output accuracy and computation time).

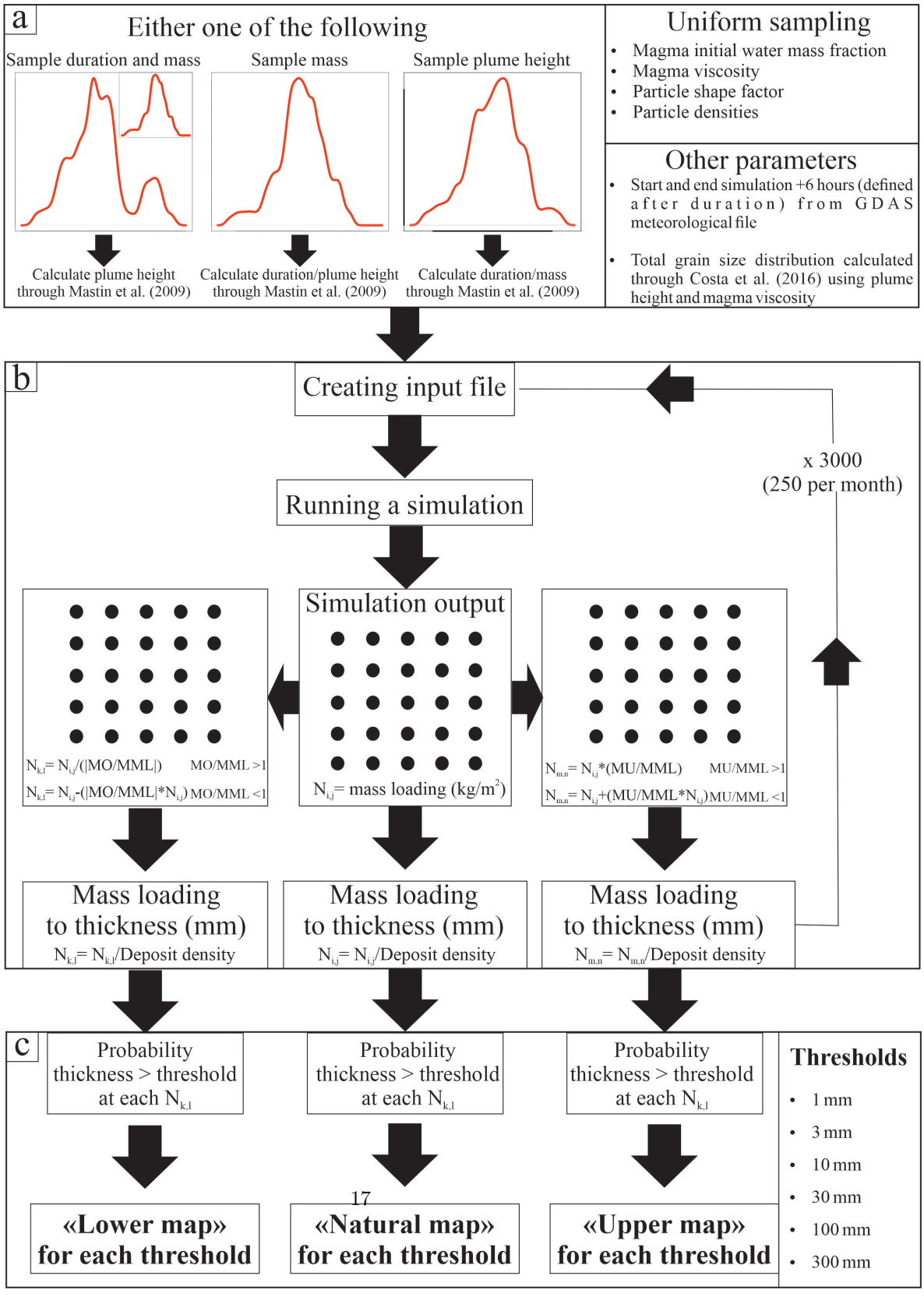
a
Either one of the following
Sample duration and mass
Sample mass
Sample plume height
Calculate plume height through Mastin et al. (2009)
Calculate duration/plume height through Mastin et al. (2009)
Calculate duration/mass through Mastin et al. (2009)
Uniform sampling
Magma initial water mass fraction
Magma viscosity
Particle shape factor
Particle densities
Other parameters
Start and end simulation +6 hours (defined after duration) from GDAS meteorological file
Total grain size distribution calculated through Costa et al. (2016) using plume height and magma viscosity
b
Creating input file
Running a simulation
Simulation output
x 3000
(250 per month)
$N_{k,l}= N_{i,j}/(|MO/MML|)$ MO/MML >1
$N_{k,l}= N_{i,j}-(|MO/MML|*N_{i,j})$ MO/MML <1
$N_{i,j}$= mass loading (kg/m^2)
$N_{m,n}= N_{i,j}*(MU/MML)$ MU/MML >1
$N_{m,n}= N_{i,j}+(MU/MML*N_{i,j})$ MU/MML <1
Mass loading to thickness (mm)
$N_{k,l}= N_{k,l}$/Deposit density
Mass loading to thickness (mm)
$N_{i,j}= N_{i,j}$/Deposit density
Mass loading to thickness (mm)
$N_{m,n}= N_{m,n}$/Deposit density
c
Probability thickness > threshold at each $N_{k,l}$
Probability thickness > threshold at each $N_{k,l}$
Probability thickness > threshold at each $N_{k,l}$
«Lower map» for each threshold
«Natural map» for each threshold
«Upper map» for each threshold
Thresholds
1 mm
3 mm
10 mm
30 mm
100 mm
300 mm

Figure 4. Sketch of a) parameter sampling for each iteration; b) processing of simulations; c) post processing and development of probability maps.

The uncertainty due to the numerical model has been quantified during the processing of simulations (Fig. 4b). During this stage, the sampled parameters have been assembled to create an input file for the model, and at the end of the simulation it has been provided an output in the form of a sampling grid, where each node $N_{i,j}$ (with latitude and longitude coordinates) has a mass loading value (in kg/m^2). By using the two coefficients MO/MML and MU/MML described in Tadini *et al.* (2020) and in section 3.1.2, two additional maps were created:

- a map with nodes $N_{k,l}$ that corrects model overestimation, such that $N_{k,l} = N_{i,j} - (N_{i,j}$*MO/MML), where MO/MML is the coefficient of overestimation;
- a map with nodes $N_{m,n}$ that corrects model underestimation, obtained by multiplying each mass loading value by the coefficient of underestimation (MU/MML).

The mass loading values of each map (in kg/m^2) were then converted into thickness values (in mm) by dividing them with deposit density average values. For Cotopaxi we have used 825 kg/m^3 for andesitic average among values used by Tsunematsu and Bonadonna, 2015() and 560 kg/m^3 for rhyolitic Bonadonna *et al.*, 2015() magmas. For Guagua Pichincha, given the general paucity of published data, we have collected 22 samples from tephra fallout deposits from both the X century (12 samples) and Historic (10 samples) eruption cycles (Figure S2 from the Supporting Information). The average value of the calculated deposit densities (measured as the ratio mass/volume of the 22 samples) yields an average value of 745 kg/m^3.

Once all simulations were finished, probabilistic maps were produced in a post-processing stage (Fig. 4c) following the approach of Bonadonna (2006). According to this latter, the probability $P(N_{i,j})$ at each node $N_{i,j}$ (for the simulation output, same for the overestimation/underestimation maps) is determined by summing the number of times a certain thickness threshold (Thk) is reached and dividing it by the total number m of the simulations:

$$P\left(N_{i,j}\right) = \frac{\sum_{i=1}^{m} n_i}{m} \quad (4)$$

where

$$n_i = \begin{cases} 1, & if \ \left[\mathrm{Thk}\left(N_{i,j}\right) \geq threshold\right] \\ 0, & otherwise \end{cases} \quad (5)$$

In this study we have used six different thresholds (in mm, Fig. 4c), chosen to be comparable with existing hazard maps and hazard-related studies. Three maps were in the end produced ("Lower", "Natural" and "Upper"), defining a set of maps that quantify the uncertainty associated with the model. This procedure has been applied for all the six eruption types considered in this study (see section 3.3.2).

3.3.2 Maps and curves format

We focused on medium to large magnitude eruptions, i.e. those with VEIs 3 corresponding to sub-Plinian to Plinian eruptive styles (i.e. those for which the model performs better). For the two studied volcanoes, this corresponds to four eruption types for Cotopaxi (sub-Plinian/Plinian with rhyolitic magmas and sub-Plinian/Plinian with andesitic magmas) and two eruption types for Guagua Pichincha (sub-Plinian and Plinian). Different maps have therefore been produced for each eruption type and thickness threshold (see section 3.3.1). Moreover, for each volcano, the corresponding maps have been merged to produce a unique set of maps according to the procedure detailed in section 3.3.3. To limit the computational times, the computational domain of the simulations has been imposed equal to a square of 1.5°x1.5° centered on each volcano.

The resulting maps (produced through a post-processing procedure into the ArcGIS10© software) follow a similar format to those proposed by Biass and Bonadonna (2013), which are: i) probability maps (for the 10% and 50% isolines) corresponding to a thickness threshold; ii) isopach maps corresponding to a specific probability (10% and 50%). In order to simplify the resulting maps, for map type i) we plotted a colored band between upper and lower isolines that highlights the effects of the uncertainties of the numerical model (more details in the previous section) and in the probabilities of occurrence of the different eruption types considered (more details in the following section). Instead, for map type ii) we have shown only the upper isolines to present the worst result in a conservative approach. In addition, we derived hazard curves, which describe the probability of exceeding certain values of tephra accumulation for a given location Bonadonna, 2006(), at 10 sensitive sites within the city of Quito. Such sites have been chosen because they could be heavily affected by tephra fall and could cause major issues to population and authorities. These sites are (Fig. 5): Quito airport, Quito city center (UNESCO world heritage), Instituto Geofisico (IGEPN – Ecuador's center for both volcanic and seismic monitoring), five hospitals and two water treatment plants, all of them roughly distributed N-S along the city.

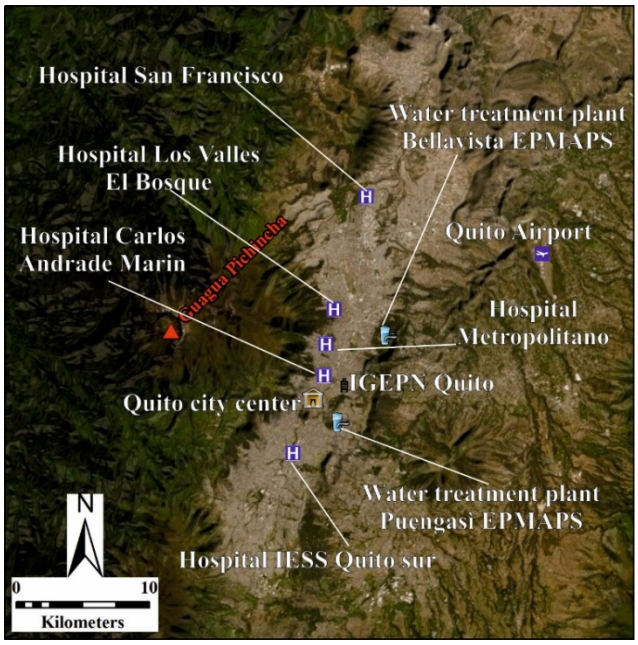

Figure 5. Sensitive sites within the capital city of Quito considered in this study. Service Layer Credits, source: Esri, DigitalGlobe, GeoEye, Earthstar Geographics, CNES/Airbus DS, USDA, USGS, AeroGRID, IGN and the GIS User Community.

3.3.3 Merging of the maps

On top of the algorithm described in the previous section, we implemented an additional procedure that combines the scenarios of sub-Plinian and Plinian eruption types, weighted according to their probability of occurrence (Fig. 6). The uncertainty distributions of these probabilities have been estimated in Tadini *et al.* (2021) and are reported in Fig. 2a for Cotopaxi and Fig. 2b for Guagua Pichincha, for both the next eruption and the next 100 years cases. While the former is used in our merging procedure, the second is considered when analyzing the maps related to single eruption types in terms of a comprehensive hazard assessment of the next 100 years, and it is not used in this section.

In more detail, in case of two eruption types a and b (Fig. 6), for each thickness threshold, the procedure illustrated in section 3.3.1 provides two sets of three output maps (Lower, Natural and Upper), each of them composed of a series of nodes (N) on a sampling grid. Each node N represents the probability of exceeding the considered thickness. During our merging procedure, we initially sampled m=1000 probabilities for each eruption type from the probability density functions of the corresponding eruption type of Fig. 2 (next eruption case), which were then normalized to sum to 100%. Such probabilities were then used

to derive m map sets, where the node of each map was the result of a weighted mean (with respect to the probability of occurrences) of the original nodes of each eruption type. Finally, the set of three maps for each thickness threshold related to the next eruption (conditional to the occurrence of either eruption a or b) was obtained by sampling, for each node of the grid:

- for the final Lower map, the 5^{th} percentile of the distribution of the m lower maps;
- for the final Natural map, the mean (E) of the distribution of the m natural maps;
- for the final Upper map, the 95^{th} percentile of the distribution of the m upper maps.

In this way we are able to show the full extent of the uncertainty linked to different eruption types (given by the 5^{th} and 95^{th} percentiles), with a mean value that ultimately represents the actual outputs of the model for each eruption type combined with mean values of eruption occurrences.

As already discussed, this merging procedure has been applied to combine four eruption types of Cotopaxi volcano (sub-Plinian andesitic/rhyolitic and Plinian rhyolitic/andesitic) and two eruption types for Guagua Pichincha volcano (sub-Plinian and Plinian). The same procedure has been used to combine the hazard curves of all the 10 sites.

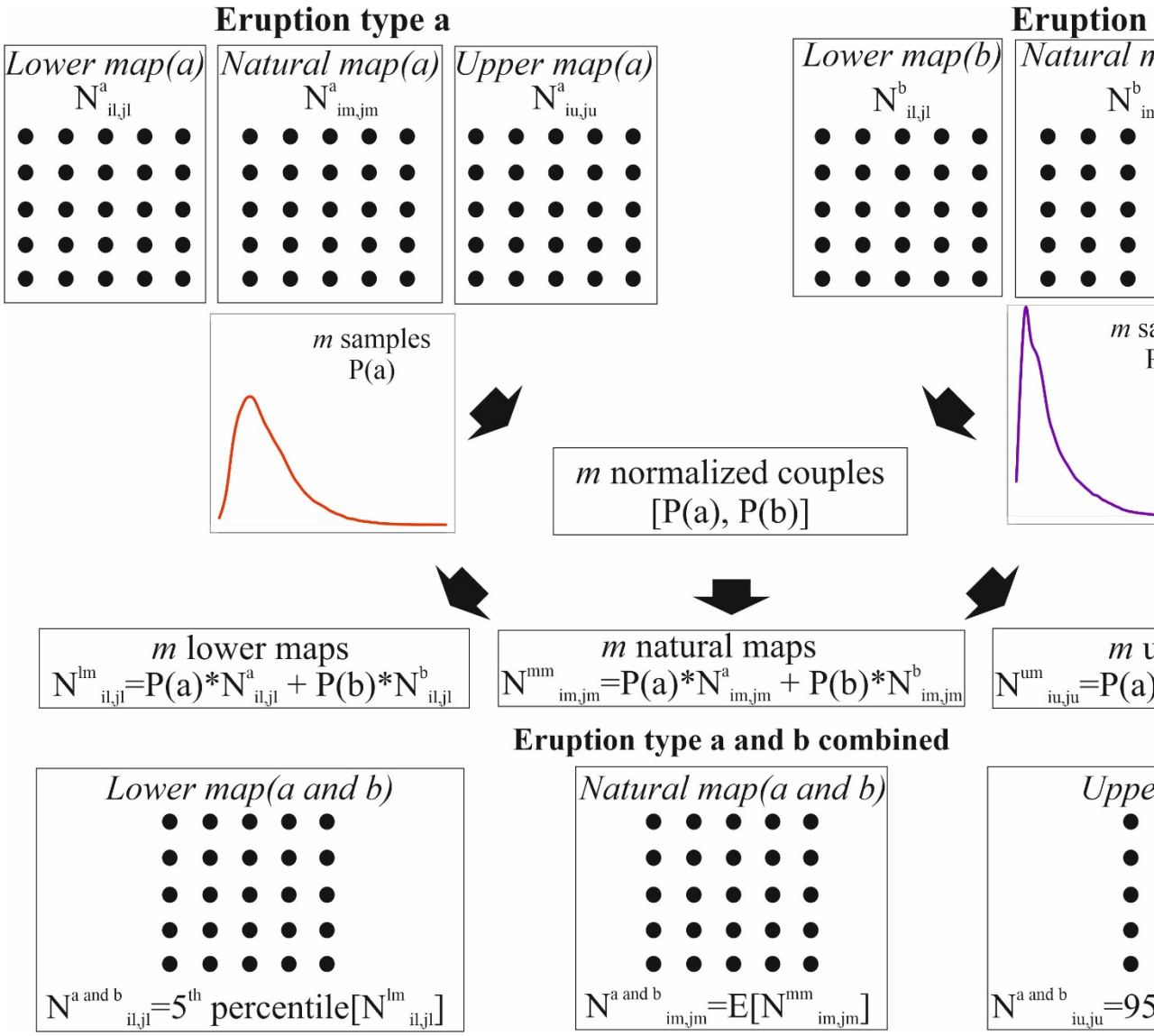

Figure 6. Sketch illustrating the procedure used for merging the set of maps of two eruption types (a and b).

4 Results and discussion

In the following sub-sections, we present and discuss separately the merged probabilistic and isopach maps and the hazard curves for both Cotopaxi (Figs. 7-9) and Guagua Pichincha (Figs. 10-12) volcanoes.We also report, in Tables 3-4, the areal extent covered and the people potentially affected by single isopach lines corresponding to 10% and 50% probabilities for both volcanoes. For the

number of people potentially affected, we have used data from the LandScan database Rose *et al.*, 2020(). We stress that for some isolines, the areas and the people potentially affected represent minimum values since some isolines extend further out of the computational domain. Additionally, we include in the supporting information the maps/curves for each single eruption type (Figs. S3-S57) and the calculated exceeding probability values for each accumulation threshold, each eruption type and each sensitive site related to the hazard curves (Tables S4-S6). Our results follow a "doubly stochastic" approach, made of two stages - first we varied the ESPs to produce "classical" hazard maps and curves, then we evaluated the effects of the uncertainties affecting both numerical model and eruption type probability of occurrence. Similar double-step procedures have been applied in pyroclastic density current hazard assessments Bevilacqua *et al.*, 2017, 2021Neri *et al.*, 2015Rutarindwa *et al.*, 2019(; ;), but not in the case of an ash fallout hazard assessment. In addition, previous studies did not evaluate the effects of the model uncertainty on the hazard assessments systematically.

4.1 Cotopaxi

At Cotopaxi, the amount of people potentially affected (especially considering the 50% isolines, see Table 3) isconsiderable (Figs. 7-8), since seven cities/towns are potentially affected by various tephra fall accumulations. Among them, three have $>$ 100,000 inhabitants (Quito, Ambato and Santo Domingo), one has $>$ 25,000 (Latacunga), two have $>$ 5,000 (Machachi and Tena) and one has $<$ 5,000 (Baeza). A striking feature of the maps presented is the drastic changes in people potentially affected within the Lower-Natural-Upper maps, . Considering for instance the 10% isolines (Table 3), for the 10 mm isopach the people potentially affected change from 350,000 (Lower) to almost 2 million (Natural). Concerning the maps themselves, the prevailing winds toward W imply that areas to this direction have higher probabilities of tephra accumulation, which could potentially cause severe issues for both building stability and infrastructures, such as the "Pan-American" highway see Figs. 7-8 and also Biass and Bonadonna, 2013().

Table 3 can be used for a partial comparison with the work of Biass and Bonadonna (2013), with which our paper shares similarities in the modelling strategy and product outputs, although they did not consider the uncertainties in the eruption type probabilities and in the numerical model results. With respect to the areas covered by their 1, 10, 100, 300 kg/m^2 (roughly comparable to our thickness thresholds) for the 50% probability, our data are generally lower. For example, in Biass and Bonadonna (2013) the area covered by the 1 kg/m^2 isomass for an eruption scenario VEI 3-5 for the next 100 years is 7,900 km^2, while our Upper (95$^{\text{th}}$ percentile) of the 1 mm is 7,000 km^2. The comparison between our results and those in Biass and Bonadonna (2013) is however complicated by the many methodological differences in i) the model employed, ii) the use of thickness thresholds, iii) the consideration of eruption types rather than single VEIs, and iv) the choice of focusing on the next eruption rather

than the next 100 years for combined eruption types (with differences in the estimation of probabilities of occurrence). Nevertheless, further improving the consistency between the elicited values of plume height, the empirical correlation formulas, and the numerical simulator output, within a fully fledged uncertainty assessment is a compelling task for additional research.

Considering the impact of tephra accumulation on airports, our maps indicate that two to five airports could be affected by a tephra accumulation of 1 mm with a probability of at least 10% (see Figs. 7 and 8). Among them, Quito international airport (Fig. 9) could have a tephra accumulation of 1 mm and 1 cm of, respectively, 6-24% and 1-11% (Tables S4 and S5 from the Supporting Information). Such values are in agreement with those proposed by Volentik and Houghton (2015), who calculated the same probabilities as, respectively, 14-20% and 2.5-6%.

Bebbington *et al.* (2008) estimated that an accumulation of 1-2 mm of ash could be sufficient for flashovers to occur along the normal electrical networks, and therefore to cause voltage fluctuations and power shutdown, as also shown by Lòpez *et al.* (2016) for Cotopaxi and Tungurahua volcanoes. For Cotopaxi, this accumulation could concern a minimum of three up to five power plants and a minimum of 364 up to 626 km, if we consider, respectively, the lower and upper 10% probability contours (Figs. 7-8).

Concerning the sensitive sites in Quito (Fig. 9), the probabilities for an accumulation of 1 cm (an average of the accumulation thresholds chosen) could be 3-18% for Quito city center (with possible consequences on the cultural heritage), 2-16% for IGEPN Quito (with possible impact on instrumentation and data transmission systems for volcanic and seismic monitoring), 2-22% for the five hospitals chosen (with possible problems on ventilation and power supply) and 2-20% for the water treatment plants (implying a possible contamination on water supply for the communities).

Thickness (mm)	**Cotopaxi 10% probability** *Area Covered (km^2)*	**Cotopaxi 10% probability** *Peop*
	Lower (5^{th} perc)	*Natural (Mean)*
1	13,305*	20,444*
3	9,137*	16,504*
10	4,134	11,615*
30	677	6,348
100	16	1,511
300	-	58
Thickness (mm)	**Cotopaxi 50% probability** *Area Covered (km^2)*	**Cotopaxi 50% probability** *Peop*
	Lower (5^{th} perc)	*Natural (Mean)*
1	1,612	4,230
3	433	2,316
10	14	650
30	-	37

Table 3. Area covered and number of people potentially affected by tephra falls characterized by isopach contours corresponding to 10% and 50% probabilities for next sub-Plinian/Plinian eruption at Cotopaxi volcano. Numbers with * indicate that the corresponding isopach extends out of the computational domain, and the number itself is therefore an underestimation.

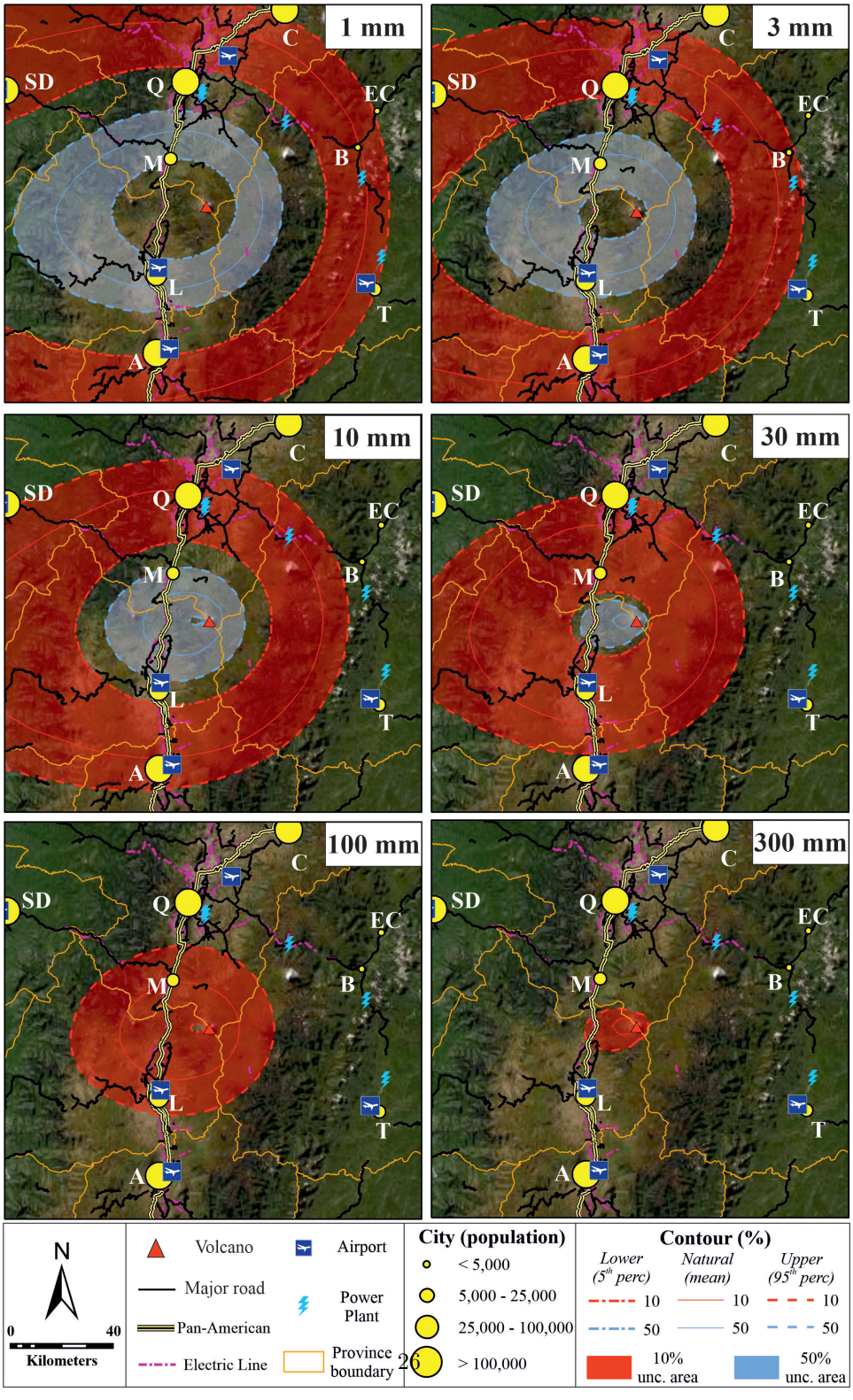
1 mm
3 mm
10 mm
30 mm
100 mm
300 mm
SD
Q
C
EC
B
M
L
T
A
N
0
40
Kilometers
Volcano
Major road
Pan-American
Electric Line
Airport
Power Plant
Province boundary
City (population)
< 5,000
5,000 - 25,000
25,000 - 100,000
> 100,000
Contour (%)
Lower (5th perc)
Natural (mean)
Upper (95th perc)
10
50
10% unc. area
50% unc. area

Figure 7: Probability maps (Cotopaxi volcano, red triangle) for different thickness accumulations in case the next eruption is sub-Plinian or Plinian. Uppercase letters are city names: A = Ambato, T = Tena, L =Latacunga, M = Machachi, B = Baeza, SD =Santo Domingo, Q =Quito, EC = El Chaco, C = Cayambe. Service Layer Credits, source: Esri, DigitalGlobe, GeoEye, Earthstar Geographics, CNES/Airbus DS, USDA, USGS, AeroGRID, IGN and the GIS User Community.

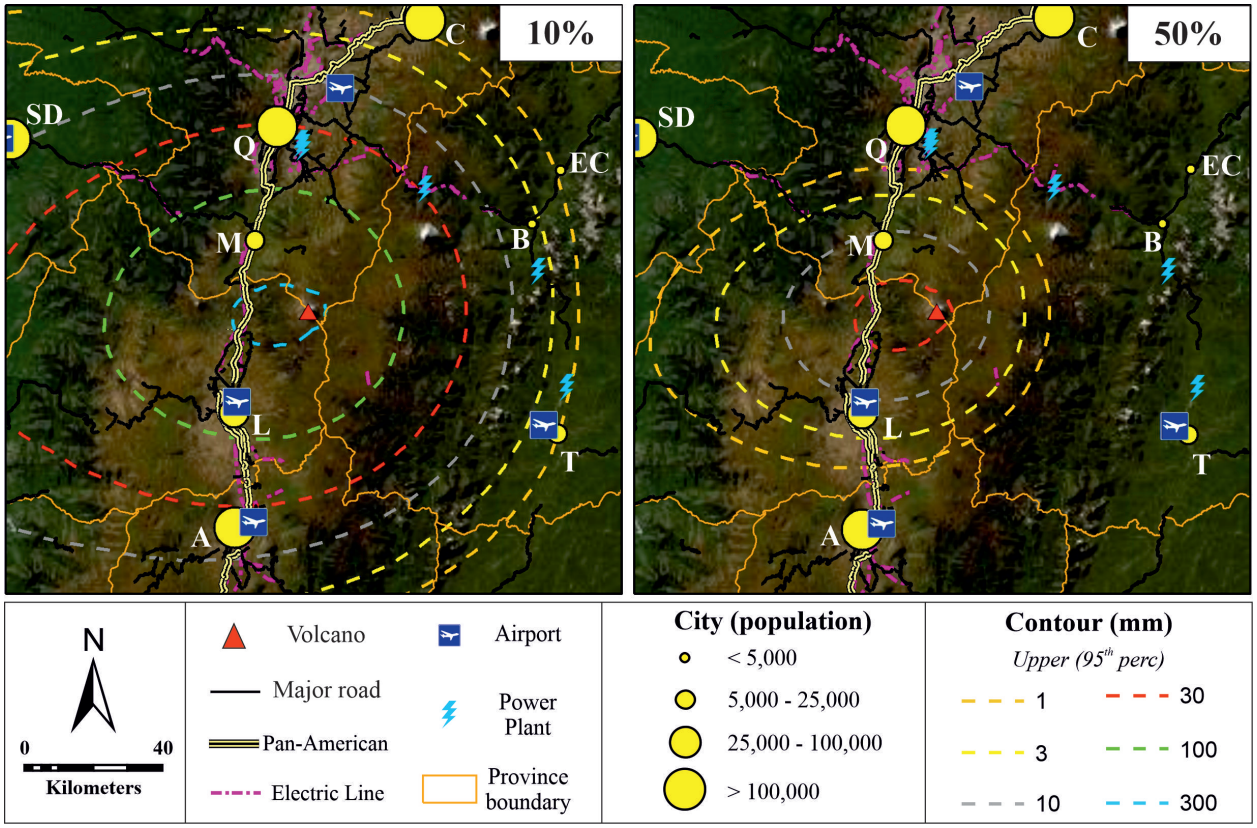

Figure 8: Isopach maps (Cotopaxi volcano, red triangle) for different probabilities in case the next eruption is sub-Plinian or Plinian. Uppercase letters are city names: A = Ambato, T = Tena, L =Latacunga, M = Machachi, B = Baeza, SD =Santo Domingo, Q =Quito, EC = El Chaco, C = Cayambe. Service Layer Credits, source: Esri, DigitalGlobe, GeoEye, Earthstar Geographics, CNES/Airbus DS, USDA, USGS, AeroGRID, IGN and the GIS User Community.

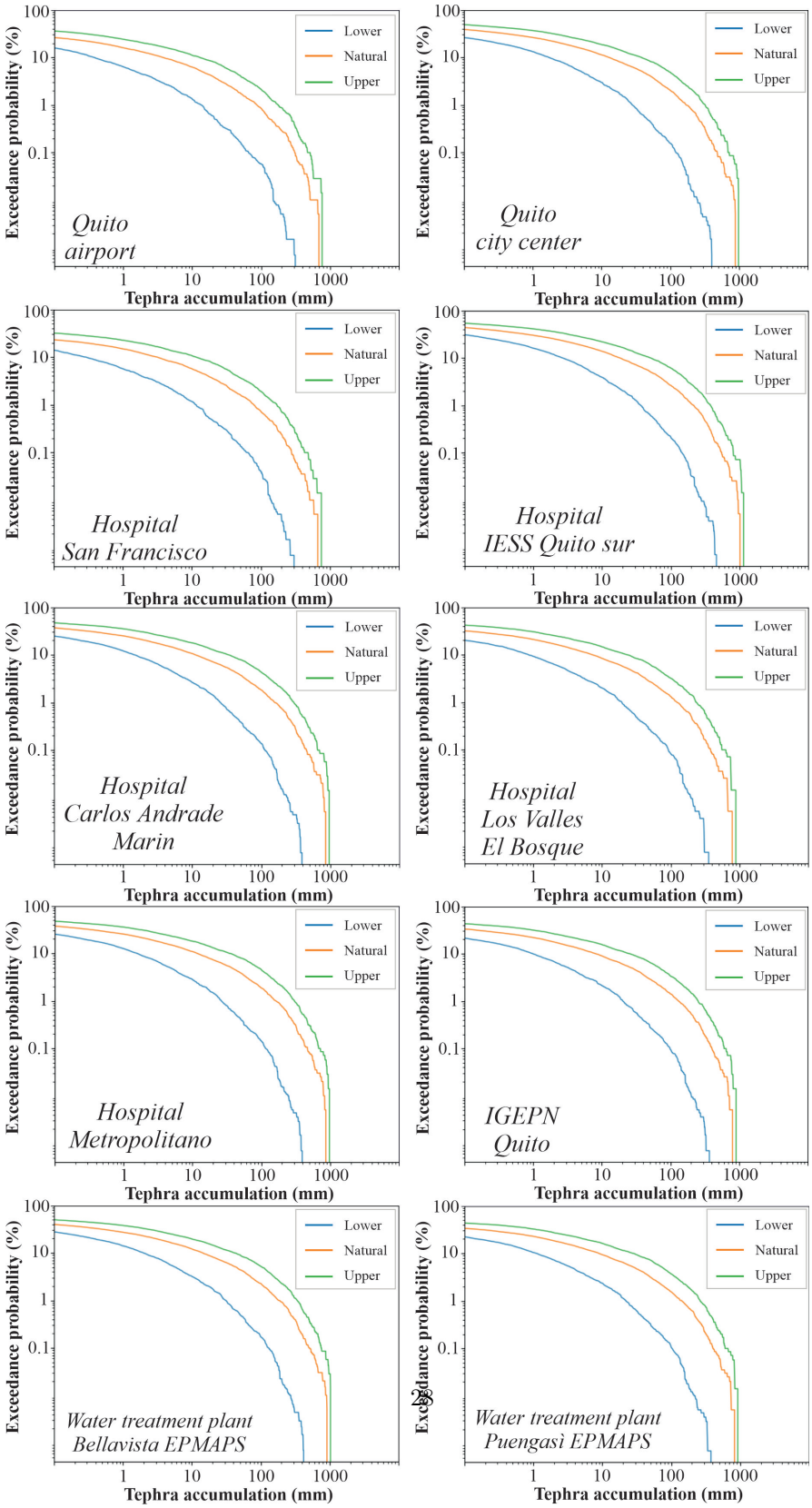
Exceedance probability (%)
100
10
1
0.1
Lower
Natural
Upper
Quito
airport
1
10
100
1000
Tephra accumulation (mm)
Quito
city center
Hospital
San Francisco
Hospital
IESS Quito sur
Hospital
Carlos Andrade
Marin
Hospital
Los Valles
El Bosque
Hospital
Metropolitano
IGEPN
Quito
Water treatment plant
Bellavista EPMAPS
Water treatment plant
Puengasì EPMAPS

Figure 9. Hazard curves for 10 sensitive sites in Quito in case the next eruption at Cotopaxi is sub-Plinian or Plinian.

4.2 Guagua Pichincha

For Guagua Pichincha volcano, due to the proximity with the highly populated city of Quito, even a small change in the location of an isoline can change significantly the amount of people potentially affected. For example, for the 30 mm isopach line with 10% probability (Figs. 10-11), the change in the area covered given by the Lower (5^{th} percentile) and Natural (Mean) maps is only 600 km^2 (Table 4), but the amount of people potentially involved changes from 1,200 to more than 2.7 million. Similar effects are evident also for the 100 mm (10% probability) and 3-10 mm (50% probability). The drastic change in people potentially affected is also linked to the fact that the main direction of wind blowing is toward W (see Figure S1 from the supporting information). This is consequently the main direction of isolines elongation, and since the amount of people living in this area is low (due to the presence of the rain forest), the small upwind changes of isoline areas to the E (where Quito is located) are the major causes for the drastic changes in the number of people potentially affected. In general, considering all the isolines and their uncertainties, seven cities/towns are potentially involved with various tephra fall accumulation, four of which with $>$ 100,000 inhabitants (Quito, Ibarra, Cayambe and Santo Domingo), one with $>$ 25,000 (Otavalo), one with $>$ 5,000 (Machachi) and one with $<$ 5,000 (Puerto Quito).

The uncertainty illustrated by the Lower-Natural-Upper maps is also particularly evident with respect to the airports potentially involved. If we focus for example on the isopach 1 mm, only two airports are included within the Lower (5^{th} percentile) isopach, while four are included if we consider the Upper (95^{th} percentile). For comparison, the Vulcanian 1999 eruption of Guagua Pichincha volcano has caused an accumulation of 3-5 mm of ash within the old location of Quito airport, and the subsequent closure of the airport for eight days Guffanti *et al.*, 2009(). Concerning the new Quito airport, our study provides a specific hazard curve for this site (Fig. 12) with specific exceeding probabilities (Tables and S6 from the supporting information). Our probabilities for the 1 mm (26-50%) and 1 cm (8-27%) accumulation are higher than those provided by Volentik and Houghton (2015) (17-20% and 7-8% for the 1 mm and 1 cm, respectively). This is due to the different range of parameters used and the different models employed.

Considering the already mentioned threshold of 1-2 mm of ash that could cause electrical flashovers Bebbington *et al.*, 2008Lòpez *et al.*, 2016(;) and the maps of Fig. 11, two power plants have 50% probability to have accumulation of 1-3 mm, while other two have 10% probability for the same accumulation. Electric lines concerned by an accumulation of 1 mm cover a total of at least 420 to 536 km considering, respectively, the lower and upper isoline of the 10% (Fig. 10) For comparison, during the 1999 eruption of Guagua Pichincha that caused $<$ 5 mm accumulation of ash in Quito, the local thermal power stations stopped

their activity as a precautionary measure d'Ercole and Metzger, 2000().

Specifically for the city of Quito, a sub-Plinian to Plinian eruption could lead to ash accumulation of 1 cm with probabilities for the analyzed sites of (Fig. 12 and Tables S4 and S6 from the supporting information) i) 15-50% for the five hospitals, ii) 19-50% for city center, iii) 15-42% for IGEPN Quito and iv) 16-48% for the two water treatment plants. With respect to the latter, we recall that, during the 1999 eruption of Guagua Pichincha, a treatment plant in Quito had to be closed due to possible water contamination d'Ercole and Metzger, 2000().

Thickness (mm)	**Guagua Pichincha 10% probability** *Area Covered (km^2)*	**Guagua Pichincha 10%**
	Lower (5^{th} perc)	*Natural (Mean)*
1	12,145*	18,683*
3	11,687*	14,791*
10	8,804	9,862*
30	4,073	4,678
100	6	571
300	-	26
Thickness (mm)	**Guagua Pichincha 50% probability** *Area Covered (km^2)*	**Guagua Pichincha 50%**
	Lower (5^{th} perc)	*Natural (Mean)*
1	1,374	3,368
3	395	1,757
10	18	417
30	-	25

Table 4. Area covered and number of people potentially affected by tephra falls characterized by isopach contours corresponding to 10% and 50% probabilities for next sub-Plinian/Plinian eruption at Guagua Pichincha volcano. Numbers with * indicate that the corresponding isopach extends out of the computational domain, and the number itself is therefore an underestimation.

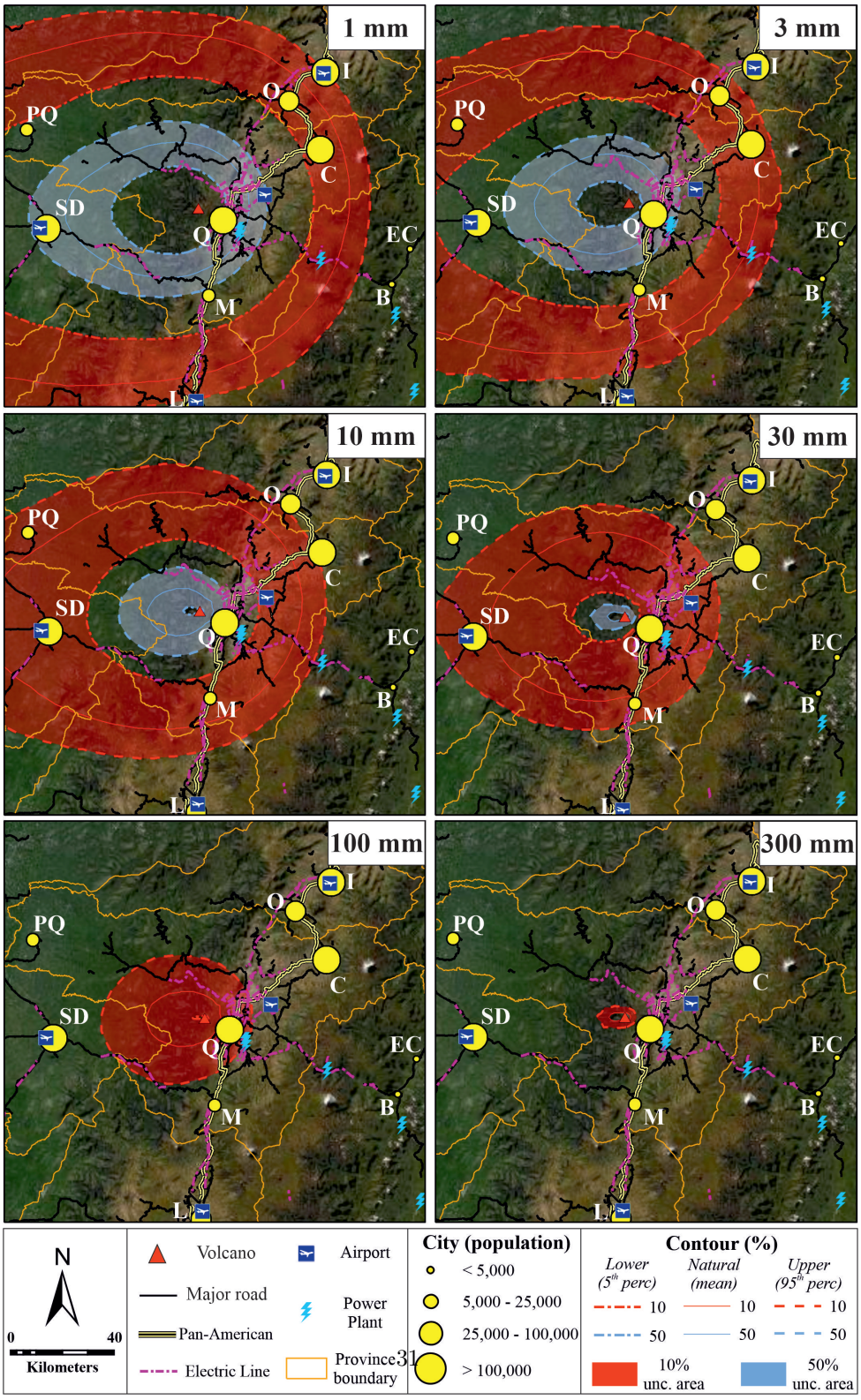
1 mm
3 mm
10 mm
30 mm
100 mm
300 mm
I
O
PQ
C
SD
Q
EC
B
M
L
N
0
40
Kilometers
Volcano
Airport
Major road
Power Plant
Pan-American
Electric Line
Province boundary
City (population)
< 5,000
5,000 - 25,000
25,000 - 100,000
> 100,000
Contour (%)
Lower (5th perc)
Natural (mean)
Upper (95th perc)
10
50
10% unc. area
50% unc. area

Figure 10: Probability maps (Guagua Pichincha volcano, red triangle) for different thickness accumulations in case the next eruption is sub-Plinian or Plinian. Uppercase letters are city names: L = Latacunga, M = Machachi, B = Baeza, SD = Santo Domingo, Q = Quito, EC = El Chaco, C = Cayambe, PQ = Puerto Quito, O = Otavalo, I = Ibarra. Service Layer Credits, source: Esri, DigitalGlobe, GeoEye, Earthstar Geographics, CNES/Airbus DS, USDA, USGS, AeroGRID, IGN and the GIS User Community.

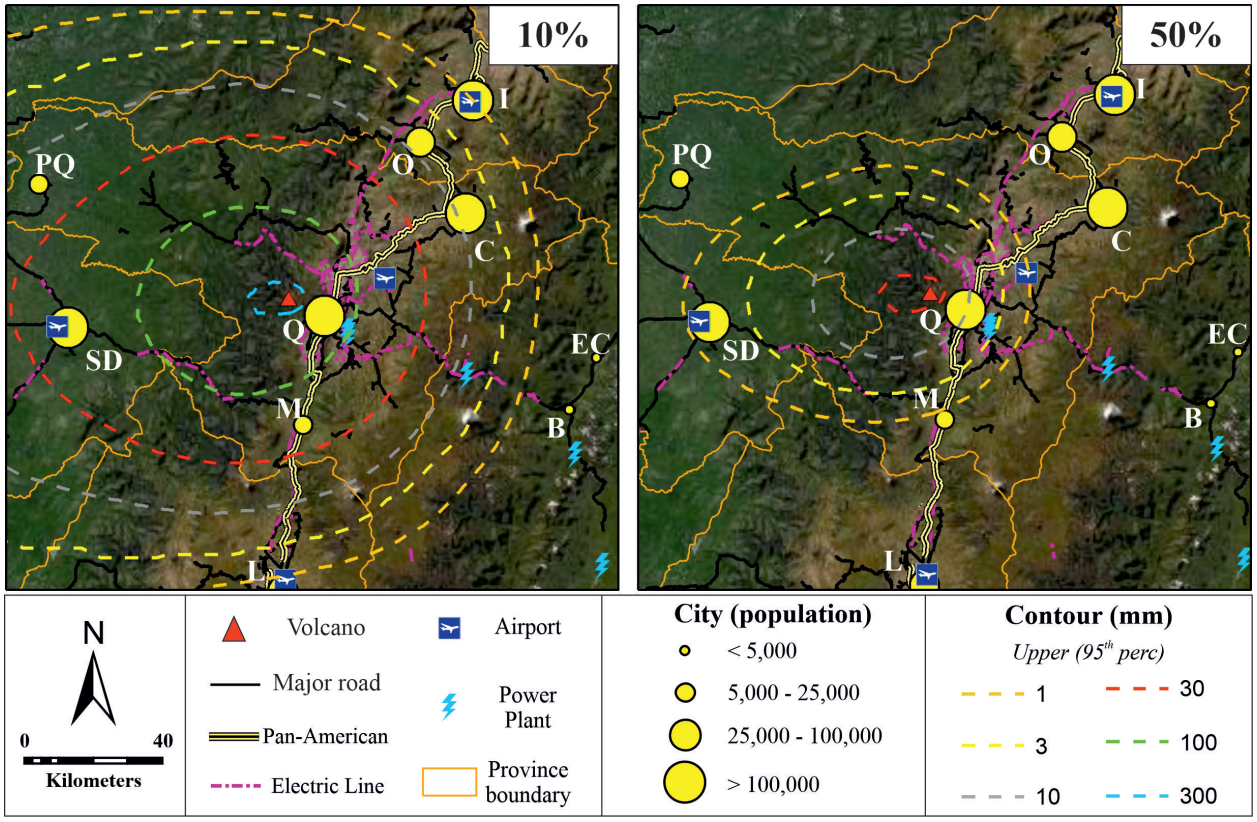

Figure 11: Isopach maps (Guagua Pichincha volcano, red triangle) for different probabilities in case the next eruption is sub-Plinian or Plinian. Uppercase letters are city names: L =Latacunga, M = Machachi, B = Baeza, SD = Santo Domingo, Q = Quito, EC = El Chaco, C = Cayambe, PQ = Puerto Quito, O = Otavalo, I = Ibarra. Service Layer Credits, source: Esri, DigitalGlobe, GeoEye, Earthstar Geographics, CNES/Airbus DS, USDA, USGS, AeroGRID, IGN and the GIS User Community.

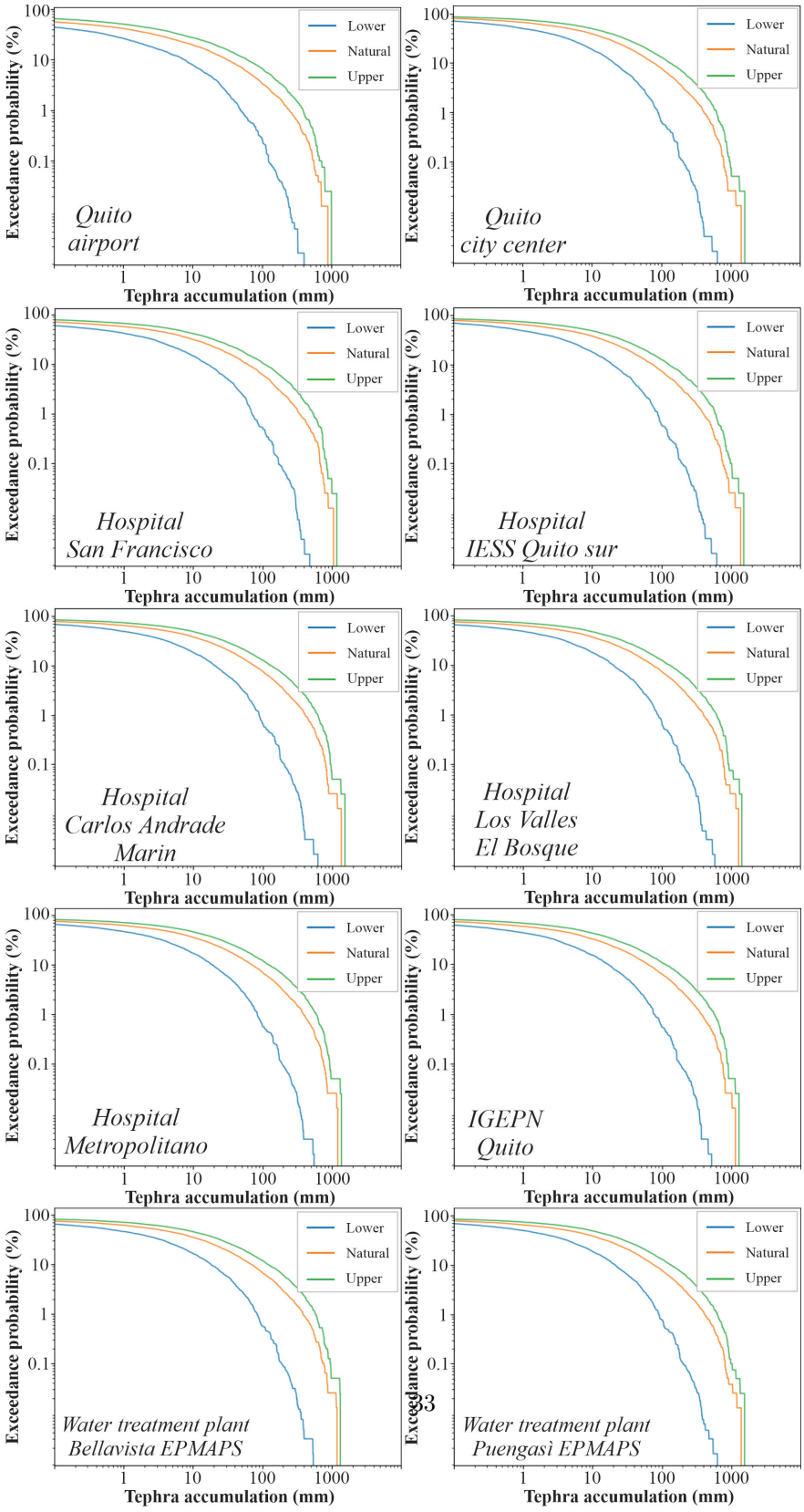
Exceedance probability (%)
Tephra accumulation (mm)
Lower
Natural
Upper
Quito airport
Quito city center
Hospital San Francisco
Hospital IESS Quito sur
Hospital Carlos Andrade Marin
Hospital Los Valles El Bosque
Hospital Metropolitano
IGEPN Quito
Water treatment plant Bellavista EPMAPS
Water treatment plant Puengasì EPMAPS

Figure 12. Hazard curves for 10 sensitive sites in Quito in case the next eruption at Guagua Pichincha is sub-Plinian or Plinian.

5 Conclusions

This paper presents a tephra fallout hazard assessment for Cotopaxi and Guagua Pichincha volcanoes and an evaluation of the exposure of different sites and infrastructures in the region, with a specific focus on the consequences for the city of Quito. The results include probabilistic maps (for a fixed tephra accumulation and a fixed probability) and hazard curves for 10 sensitive sites in the city of Quito (airport, hospitals, city center, Instituto Geofisico, water treatment plants), related to the specific case that the next eruption at both volcanoes could be either sub-Plinian or Plinian (VEI 3-5). Our new uncertainty quantification procedure has introduced, for all the eruption types and for both volcanoes, set of maps in which each isoline produced from the model output ("Natural") is corrected by producing two additional isolines that take into account model underestimation ("Upper") and overestimation ("Lower"). For both volcanoes, the impacted area, the number of people and the sensitive sites affected could vary significantly if these three isolines are considered. Apart from hazard implications discussed in the previous sections, in our study:

- we have employed a coupling between a plume model (PLUME-MoM) and a tephra transport and dispersal model (HYSPLIT). HYSPLIT is currently used by several Volcanic Ash Advisory Centers (VAACs) and, to the best of our knowledge, has never been used so far to produce isopach tephra fallout hazard maps. Further investigation with HYSPLIT is advisable in order to reduce its computational times and therefore consider larger computational domains and/or more refined computational grids.

- as sampling strategy, we chose to derive (for each eruption) sets of eruptive source parameters (duration, total mass of tephra fallout and plume height) physically consistent with real eruptions. We used the relations of Mastin *et al.* (2009) to calculate from one (or two) parameters sampled the remaining two (or one). This introduced correlations between the ESPs, but, as shown in section 3.3.1, introduced some variations in the original sampling distributions. While such new distributions are within physically coherent ranges, other existing relations e.g., Sparks *et al.*, 1997() could be employed to evaluate their effect of this recalculation.

- We performed the uncertainty quantification in two stages - first varying eruptive source parameters to produce "classical" hazard maps and curves, then evaluating the effects of the uncertainties affecting both numerical model and eruption type probability of occurrence. This "doubly stochastic" approach increases the complexity of the final products, but the effects of the considered sources of uncertainty are significant and should not be averaged or neglected. In fact, even small shifts in the position of isolines can imply a significant change in the amount of people potentially affected by a given tephra accumulation, which has a direct implication in both

emergency and long-term planning.

Appendix: total grain-size distribution

Following Costa *et al.* (2016a), total-grain size distribution is here considered to be composed of two log-normal distributions (i.e. Gaussian in Φ scale) with the form

$$f_{bi-Gauss}(\Phi) = p\frac{1}{\sigma_1\sqrt{2\pi}}\exp\left[-\frac{(\Phi-\mu_1)}{2{\sigma_1}^2}\right] + (1-p)\frac{1}{\sigma_2\sqrt{2\pi}}\exp\left[-\frac{(\Phi-\mu_2)}{2{\sigma_2}^2}\right] \quad (6)$$

where μ_1, μ_2 and σ_1, σ_2 are respectively the means and standard deviations of the two Gaussian distributions in distributions in Φ units, while p is the weight of each sub-population. Empirical values to calculate these parameters have been proposed by the same authors and have been adapted to our study in the following form

$$\sigma_1 \approx 0.67 + 0.07\ H$$

$$\mu_1 + 3\sigma_1 \approx 0.96 + 0.20H$$

$$\mu_2 - \mu_1 \approx 1.62\left(\mathrm{Log}_{10}\eta\right)^{0.66}$$

$$\sigma_2 \approx 1.46$$

$$p = 1.61exp\left(-0.31\mathrm{Log}_{10}\eta\right)$$

with H the plume height (km) and η the magma dynamic viscosity (Pa s)

Acknowledgments

The simulations have been performed on the cluster of the Laboratoire de Mathématiques Blaise Pascal and on the supercomputer facilities of the Mésocentre at Clermont Auvergne University. We thank Damien Ferney for technical assistance. This research was financed by the French government IDEX-ISITE initiative 16-IDEX-0001 (CAP 20-25), the French Research Institute for Sustainable Development (IRD) in the context of the Laboratoire Mixte International "Séismes et Volcans dans les Andes du Nord", and the CNRS Tellus programme. This work was also partly funded by the ClerVolc project - Programme 1 "Detection and characterization of volcanic plumes and ash clouds" funded by the French government 'Laboratory of Excellence' initiative. This is Clervolc contribution number XXX.

The authors have no competing interests to declare.

Data supporting the analyses and conclusions presented in this study could be found in a repository in the Figshare community with the following DOI: https://figshare.com/s/d039d9c741040b70c88c

References

Alpízar Segura, Y., M. Fernández Arce, C. Ramírez Umaña, and D. Arroyo Alpízar (2019), Hazard Map of Rincón de la Vieja Volcano, Costa Rica: Qualitative Integration of Computer Simulations and Geological Data, *Anuario do Instituto de Geociencias*, *42*(3), doi:http://dx.doi.org/10.11137/2019_3_474_488.Andújar, J., C. Martel, M. Pichavant, P. Samaniego, B. Scaillet, and I. Molina (2017), Structure of the plumbing system at Tungurahua volcano, Ecuador: insights from phase equilibrium experiments on July–August 2006 eruption products, *Journal of Petrology*, *58*(7), 1249-1278, doi:https://doi.org/10.1093/petrology/egx054.Annen, C., and J. J. Wagner (2003), The impact of volcanic eruptions during the 1990s, *Natural Hazards Review*, *4*(4), 169-175, doi:https://doi.org/10.1061/(ASCE)1527-6988(2003)4:4(169).Armienti, P., G. Macedonio, and M. T. Pareschi (1988), A numerical model for simulation of tephra transport and deposition: Applications to May 18, 1980, Mount St. Helens eruption, *Journal of Geophysical Research: Solid Earth*, *93*(B6), 6463-6476, doi:https://doi.org/10.1029/JB093iB06p06463.Aspinall, W. P. (2006), Structured elicitation of expert judgment for probabilistic hazard and risk assessment in volcanic eruptions, *Statistics in volcanology*, *1*, 15-30.Aspinall, W. P., A. Bevilacqua, A. Costa, H. Inakura, S. Mahony, A. Neri, and R. S. J. Sparks (2019), Probabilistic reconstruction (or forecasting) of distal runouts of large magnitude ignimbrite PDC flows sensitive to topography using mass-dependent inversion models, paper presented at AGU Fall Meeting 2019, San Francisco, CA, USA.Barberi, F., M. Ghigliotti, G. Macedonio, H. Orellana, M. T. Pareschi, and M. Rosi (1992), Volcanic hazard assessment of Guagua Pichincha (Ecuador) based on past behaviour and numerical models, *J. Volcanol. Geoth. Res.*, *49*(1-2), 53-68, doi:https://doi.org/10.1016/0377-0273(92)90004-W.Barberi, F., G. Macedonio, M. T. Pareschi, and R. Santacroce (1990), Mapping the tephra fallout risk: an example from Vesuvius, Italy, *Nature*, *344*(6262), 142-144.Barsotti, S., D. I. Di Rienzo, T. Thordarson, B. B. Björnsson, and S. Karlsdóttir (2018), Assessing impact to infrastructures due to tephra fallout from Öræfajökull volcano (Iceland) by using a scenario-based approach and a numerical model, *Frontiers in Earth Science*, *6*, 196, doi:https://doi.org/10.3389/feart.2018.00196.Barsotti, S., and A. Neri (2008), The VOL-CALPUFF model for atmospheric ash dispersal: 2. Application to the weak Mount Etna plume of July 2001, *Journal of Geophysical Research: Solid Earth*, *113*(B3), doi:https://doi.org/10.1029/2006JB004624.Barsotti, S., A. Neri, and J. S. Scire (2008), The VOL-CALPUFF model for atmospheric ash dispersal: 1. Approach and physical formulation, *Journal of Geophysical Research: Solid Earth*, *113*(B3), doi:https://doi.org/10.1029/2006JB004623.Baxter, P. J. (1990), Medical effects of volcanic eruptions, *Bulletin of Volcanology*, *52*(7), 532-544, doi:https://doi.org/10.1007/BF00301534.Baxter, P. J., and C. J. Horwell (2015), Impacts of eruptions on human health, in *The encyclopedia of volcanoes*, edited by H. Sigurdsson, B. F. Houghton, S. R. McNutt, H. Rymer

and J. Stix, pp. 1035-1047, Elsevier, doi:https://doi.org/10.1016/B978-0-12-385938-9.00060-2.Bebbington, M. S., S. J. Cronin, I. Chapman, and M. B. Turner (2008), Quantifying volcanic ash fall hazard to electricity infrastructure, *Journal of Volcanology and Geothermal Research*, *177*(4), 1055-1062, doi:https://doi.org/10.1016/j.jvolgeores.2008.07.023.Bernard, B., J. Battaglia, A. Proaño, S. Hidalgo, F. Vásconez, S. Hernandez, and M. C. Ruiz (2016), Relationship between volcanic ash fallouts and seismic tremor: quantitative assessment of the 2015 eruptive period at Cotopaxi volcano, Ecuador, *Bull. Volc.*, *78*(11), doi:10.1007/s00445-016-1077-5.Bevilacqua, A., A. Aravena, A. Neri, E. Gutiérrez, D. Escobar, M. Schliz, et al. (2021), Thematic vent opening probability maps and hazard assessment of small-scale pyroclastic density currents in the San Salvador volcanic complex (El Salvador) and Nejapa-Chiltepe volcanic complex (Nicaragua), *Natural Hazards and Earth System Sciences*, *21*(5), 1639-1665, doi:https://doi.org/10.5194/nhess-21-1639-2021.Bevilacqua, A., A. Bertagnini, M. Pompilio, P. Landi, P. Del Carlo, A. Di Roberto, et al. (2020), Major explosions and paroxysms at Stromboli (Italy): a new historical catalog and temporal models of occurrence with uncertainty quantification, *Scientific Reports*, *10*, doi:https://doi.org/10.1038/s41598-020-74301-8.Bevilacqua, A., M. I. Bursik, A. K. Patra, B. E. Pitman, Q. Yang, R. Sangani, and S. Kobs-Nawotniak (2018), Late Quaternary eruption record and probability of future volcanic eruptions in the Long Valley volcanic region (CA, USA), *Journal of Geophysical Research: Solid Earth*, *123*(7), 5466-5494, doi:https://doi.org/10.1029/2018JB015644.Bevilacqua, A., F. Flandoli, A. Neri, R. Isaia, and S. Vitale (2016), Temporal models for the episodic volcanism of Campi Flegrei caldera (Italy) with uncertainty quantification, *Journal of Geophysical Research: Solid Earth*, *121*(11), 7821-7845, doi:https://doi.org/10.1002/2016JB013171.Bevilacqua, A., R. Isaia, A. Neri, S. Vitale, W. P. Aspinall, M. Bisson, et al. (2015), Quantifying volcanic hazard at Campi Flegrei caldera (Italy) with uncertainty assessment: I. Vent opening maps, *Journal of Geophysical Research: Solid Earth*, *120*, 2309-2329, doi:https://doi.org/10.1002/2014JB011775.Bevilacqua, A., A. Neri, M. Bisson, T. Esposti Ongaro, F. Flandoli, R. Isaia, et al. (2017), The effects of vent location, event scale, and time forecasts on pyroclastic density current hazard maps at Campi Flegrei caldera (Italy), *Frontiers in Earth Science*, *5*, 72, doi:https://doi.org/10.3389/feart.2017.00072.Bevilacqua, A., A. K. Patra, M. I. Bursik, E. B. Pitman, J. L. Macías, R. Saucedo, and D. Hyman (2019), Probabilistic forecasting of plausible debris flows from Nevado de Colima (Mexico) using data from the Atenquique debris flow, 1955, *Natural Hazard and Earth System Sciences*, *19*(4), doi:https://doi.org/10.5194/nhess-19-791-2019.Biass, S., and C. Bonadonna (2011), A quantitative uncertainty assessment of eruptive parameters derived from tephra deposits: the example of two large eruptions of Cotopaxi volcano, Ecuador, *Bulletin of Volcanology*, *73*(1), 73-90.Biass, S., and C. Bonadonna (2013), A fast GIS-based risk assessment for tephra fallout: the example of Cotopaxi volcano, Ecuador, *Natural Hazards*, *65*(1), 477-495, doi:https://doi.org/10.1007/s11069-012-0378-z.Biass, S., C. Frischknecht, and C. Bonadonna (2013), A fast GIS-based

risk assessment for tephra fallout: the example of Cotopaxi volcano, Ecuador - Part II: vulnerability and risk assessment, *Natural hazards*, *65*(1), 497-521, doi:https://doi.org/10.1007/s11069-012-0457-1.Biass, S., C. Scaini, C. Bonadonna, A. Folch, K. Smith, and A. Höskuldsson (2014), A multi-scale risk assessment for tephra fallout and airborne concentration from multiple Icelandic volcanoes-Part 1: Hazard assessment, *Natural Hazards and Earth System Sciences*, *14*(8), 2265, doi:10.5194/nhess-14-2265-2014.Blake, D. M., T. M. Wilson, J. W. Cole, N. I. Deligne, and J. M. Lindsay (2017), Impact of volcanic ash on road and airfield surface skid resistance, *Sustainability*, *9*(8), 1389, doi:https://doi.org/10.3390/su9081389.Blong, R. J. (1996), Volcanic hazards risk assessment, in *Monitoring and mitigation of volcano hazards*, edited by R. Scarpa and R. I. Tilling, pp. 675-698, Springer, Berlin.Bonadonna, C. (2006), Probabilistic modelling of tephra dispersion, in *Statistics in Volcanology*, edited by H. M. Mader, S. G. Coles, C. B. Connor and L. J. Connor, pp. 243-259, Geological Society, London.Bonadonna, C., C. B. Connor, B. F. Houghton, L. J. Connor, M. Byrne, A. Laing, and T. K. Hincks (2005), Probabilistic modeling of tephra dispersal: Hazard assessment of a multiphase rhyolitic eruption at Tarawera, New Zealand, *Journal of Geophysical Research: Solid Earth*, *110*(B3), doi:https://doi.org/10.1029/2003JB00289.Bonadonna, C., and J. C. Phillips (2003), Sedimentation from strong volcanic plumes, *Journal of Geophysical Research: Solid Earth*, *108*(B7), doi:https://doi.org/10.1029/2002JB002034.Bonadonna, C., M. Pistolesi, R. Cioni, W. Degruyter, M. Elissondo, and V. Baumann (2015), Dynamics of wind-affected volcanic plumes: The example of the 2011 Cordón Caulle eruption, Chile, *Journal of Geophysical Research: Solid Earth*, *120*(4), 2242-2261.Bonasia, R., L. Capra, A. Costa, G. Macedonio, and R. Saucedo (2011), Tephra fallout hazard assessment for a Plinian eruption scenario at Volcán de Colima (Mexico), *Journal of Volcanology and Geothermal Research*, *203*(1-2), 12-22, doi:https://doi.org/10.1016/j.jvolgeores.2011.03.006.Brown, S. K., S. F. Jenkins, R. S. J. Sparks, H. Odbert, and M. R. Auker (2017), Volcanic fatalities database: analysis of volcanic threat with distance and victim classification, *Journal of Applied Volcanology*, *6*(1), 1-20, doi:https://doi.org/10.1186/s13617-017-0067-4.Budd, L., S. Griggs, D. Howarth, and S. Ison (2011), A fiasco of volcanic proportions? Eyjafjallajökull and the closure of European airspace, *Mobilities*, *6*(1), 31-40, doi:https://doi.org/10.1080/17450101.2011.532650.Bursik, M. I. (2001), Effect of wind on the rise height of volcanic plumes, *Geophysical Research Letters*, *28*(18), 3621-3624, doi:https://doi.org/10.1029/2001GL013393.Bursik, M. I., M. Jones, S. Carn, K. Dean, A. K. Patra, M. Pavolonis, et al. (2012), Estimation and propagation of volcanic source parameter uncertainty in an ash transport and dispersal model: application to the Eyjafjallajokull plume of 14–16 April 2010, *Bulletin of volcanology*, *74*(10), 2321-2338, doi:https://doi.org/10.1007/s00445-012-0665-2.Bursik, M. I., S. E. Kobs, A. Burns, O. A. Braitseva, L. I. Bazanova, I. V. Melekestsev, et al. (2009), Volcanic plumes and wind: Jetstream interaction examples and implications for air traffic, *Journal of Volcanology and Geothermal Research*, *186*(1-2), 60-67, doi:https://doi.org/10.1016/j.jvolgeores.2009.01.021.Capra, L., G. Norini, G.

Groppelli, J. L. Macías, and J. L. Arce (2008), Volcanic hazard zonation of the Nevado de Toluca volcano, México, *Journal of Volcanology and Geothermal Research*, *176*(4), 469-484, doi:https://doi.org/10.1016/j.jvolgeores.2008.04.016.Cioni, R., A. Longo, G. Macedonio, R. Santacroce, A. Sbrana, R. Sulpizio, and D. Andronico (2003), Assessing pyroclastic fall hazard through field data and numerical simulations: example from Vesuvius, *Journal of Geophysical Research: Solid Earth (1978–2012)*, *108*(B2), 2063.Cooke, R. M. (1991), Experts in uncertainty: opinion and subjective probability in science.Costa, A., F. Dell'Erba, M. A. Di Vito, R. Isaia, G. Macedonio, G. Orsi, and T. Pfeiffer (2009), Tephra fallout hazard assessment at the Campi Flegrei caldera (Italy), *Bulletin of Volcanology*, *71*(3), 259, doi:https://doi.org/10.1007/s00445-008-0220-3.Costa, A., G. Macedonio, and A. Folch (2006), A three-dimensional Eulerian model for transport and deposition of volcanic ashes, *Earth and Planetary Science Letters*, *241*(3-4), 634-647, doi:https://doi.org/10.1016/j.epsl.2005.11.019.Costa, A., L. Pioli, and C. Bonadonna (2016a), Assessing tephra total grain-size distribution: Insights from field data analysis, *Earth and Planetary Science Letters*, *443*, 90-107, doi:https://doi.org/10.1016/j.epsl.2016.02.040.Costa, A., Y. J. Suzuki, M. Cerminara, B. J. Devenish, T. Esposti Ongaro, M. Herzog, et al. (2016b), Results of the eruptive column model intercomparison study, *Journal of Volcanology and Geothermal Research*, *326*, 2-25, doi:https://doi.org/10.1016/j.jvolgeores.2016.01.017.d'Ercole, R., and P. Metzger (2000), La vulnérabilité de Quito (Equateur) face à l'activité du Guagua Pichincha. Les premières leçons d'une crise volcanique durable, *Cahiers Savoisiens de Géographie*, *1*, 39-52, doi:https://hal.archives-ouvertes.fr/hal-01196431.de' Michieli Vitturi, M., and F. Pardini (2021), PLUME-MoM-TSM 1.0.0: a volcanic column and umbrella cloud spreading model, *Geoscientific Model Development*, *14*(3), 1345–1377, doi:https://doi.org/10.5194/gmd-14-1345-2021.de'Michieli Vitturi, M., A. Neri, and S. Barsotti (2015), PLUME-MoM 1.0: A new integral model of volcanic plumes based on the method of moments, *Geoscientific Model Development*, *8*(8), 2447.Ecuatoriana, C. R. (2020), Plan de acción temprana por dispersión de ceniza volcánica. Proyecto Preparación basada en Pronósticos*Rep*.Flandoli, F., E. Giorgi, W. P. Aspinall, and A. Neri (2011), Comparison of a new expert elicitation model with the Classical Model, equal weights and single experts, using a cross-validation technique, *Reliability Engineering & System Safety*, *96*(10), 1292-1310, doi:https://doi.org/10.1016/j.ress.2011.05.012.Folch, A., A. Costa, and S. Basart (2012), Validation of the FALL3D ash dispersion model using observations of the 2010 Eyjafjallajökull volcanic ash clouds, *Atmospheric Environment*, *48*, 165-183, doi:https://doi.org/10.1016/j.atmosenv.2011.06.072.Folch, A., A. Costa, and G. Macedonio (2009), FALL3D: A computational model for transport and deposition of volcanic ash, *Computers & Geosciences*, *35*(6), 1334-1342, doi:https://doi.org/10.1016/j.cageo.2008.08.008.Folch, A., L. Mingari, N. Gutierrez, M. Hanzich, G. Macedonio, and A. Costa (2020), FALL3D-8.0: a computational model for atmospheric transport and deposition of particles, aerosols and radionuclides–Part 1: Model physics and numerics, *Geoscientific Model Development*, *13*(3), 1431-1458, doi:https://doi.org/10.5194/gmd-13-

1431-2020.Folch, A., and R. Sulpizio (2010), Evaluating long-range volcanic ash hazard using supercomputing facilities: application to Somma-Vesuvius (Italy), and consequences for civil aviation over the Central Mediterranean Area, *Bulletin of Volcanology*, *72*(9), 1039-1059, doi:https://doi.org/10.1007/s00445-010-0386-3.Ganser, G. H. (1993), A rational approach to drag prediction of spherical and nonspherical particles, *Powder technology*, *77*(2), 143-152, doi:https://doi.org/10.1016/0032-5910(93)80051-B.Garcia-Aristizabal, A., H. Kumagai, P. Samaniego, P. Mothes, H. Yepes, and M. Monzier (2007), Seismic, petrologic, and geodetic analyses of the 1999 dome-forming eruption of Guagua Pichincha volcano, Ecuador, *J. Volcanol. Geoth. Res.*, *161*(4), 333-351, doi:https://doi.org/10.1016/j.jvolgeores.2006.12.007.Gaunt, H. E., B. Bernard, S. Hidalgo, A. Proaño, H. M. Wright, P. Mothes, et al. (2016), Juvenile magma recognition and eruptive dynamics inferred from the analysis of ash time series: The 2015 reawakening of Cotopaxi volcano, *Journal of Volcanology and Geothermal Research*, *328*, 134-146, doi:https://doi.org/10.1016/j.jvolgeores.2016.10.013.Guffanti, M., G. C. Mayberry, T. J. Casadevall, and R. Wunderman (2009), Volcanic hazards to airports, *Natural hazards*, *51*(2), 287-302, doi:https://doi.org/10.1007/s11069-008-9254-2.Hall, M. L., P. Mothes, D. Andrade, P. Samaniego, and H. Yepes (2004a), Mapa regional de peligros volcánicos potenciales del volcán Cotopaxi-Zona Sur, IG-EPN, Quito, Ecuador.Hall, M. L., P. Mothes, P. Samaniego, H. Yepes, and D. Andrade (2004b), Mapa Regional de Peligros Volcánicos Potenciales del Volcán Cotopaxi Zona Norte, IG-EPN, Quito, Ecuador.Hall, M. L., and P. A. Mothes (2008), The rhyolitic–andesitic eruptive history of Cotopaxi volcano, Ecuador, *Bull. Volc.*, *70*(6), 675-702, doi:https://doi.org/10.1007/s00445-007-0161-2.Hall, M. L., and C. G. M. von Hillebrandt (1988a), Mapa de los peligros volcanicos potenciales asociados con el volcan Cotopaxi: zona norte and zona sur, IG-EPN, Quito, Ecuador.Hall, M. L., and C. G. M. von Hillebrandt (1988b), Mapa de los peligros volcanicos potenciales asociados con el volcan Guagua Pichincha-Provincia de Pichincha, IG-EPN, Quito, Ecuador.Hidalgo, S., J. Battaglia, S. Arellano, D. Sierra, B. Bernard, R. Parra, et al. (2018), Evolution of the 2015 Cotopaxi eruption revealed by combined geochemical and seismic observations, *Geochemistry, Geophysics, Geosystems*, *19*(7), 2087-2108, doi:https://doi.org/10.1029/2018GC007514.Hurst, T., and W. Smith (2004), A Monte Carlo methodology for modelling ashfall hazards, *Journal of volcanology and geothermal research*, *138*(3-4), 393-403, doi:https://doi.org/10.1016/j.jvolgeores.2004.08.001.IG-EPN, IGM, and IRD (2019), Mapa de Peligros Volcánicos Potenciales del Volcán Guagua Pichincha 3ra. Edición, Quito - Ecuador, Quito - Ecuador.Kalnay, E., M. Kanamitsu, R. Kistler, W. Collins, D. Deaven, L. Gandin, et al. (1996), The NCEP/NCAR 40-Year Reanalysis Project, *Bull. Am. Met. Soc.*, *77*(3), 437-472, doi:10.1175/1520-0477(1996)077<0437:tnyrp>2.0.co;2.Lòpez, A., J. Ramírez, F. Vásconez, B. Bernard, F. Valencia, S. Hidalgo, et al. (2016), Volcanic ash impacts on the dielectric strength of HVAC Outdoor Suspension Insulators: the case of Cotopaxi and Tungurahua volcanoes (Ecuador), paper presented at Cities on Volcanoes 9, Puerto Varas, Chile, 20-25/11/2016.Macedonio,

G., and A. Costa (2012), Brief Communication" Rain effect on the load of tephra deposits", *Natural Hazards and Earth System Sciences*, *12*(4), 1229-1233, doi:https://doi.org/10.5194/nhess-12-1229-2012.Macedonio, G., A. Costa, and A. Longo (2005), A computer model for volcanic ash fallout and assessment of subsequent hazard, *Computers & Geosciences*, *31*(7), 837-845, doi:https://doi.org/10.1016/j.cageo.2005.01.013.Macedonio, G., A. Costa, S. Scollo, and A. Neri (2016), Effects of eruption source parameter variation and meteorological dataset on tephra fallout hazard assessment: example from Vesuvius (Italy), *Journal of Applied Volcanology*, *5*(1), 1.Macedonio, G., M. T. Pareschi, and R. Santacroce (1988), A numerical simulation of the Plinian fall phase of 79 AD eruption of Vesuvius, *Journal of Geophysical Research: Solid Earth*, *93*(B12), 14817-14827.Madankan, R., S. Pouget, P. Singla, M. I. Bursik, J. Dehn, M. Jones, et al. (2014), Computation of probabilistic hazard maps and source parameter estimation for volcanic ash transport and dispersion, *Journal of Computational Physics*, *271*, 39-59, doi:https://doi.org/10.1016/j.jcp.2013.11.032.Martel, C., J. Andújar, P. Mothes, B. Scaillet, M. Pichavant, and I. Molina (2018), Storage conditions of the mafic and silicic magmas at Cotopaxi, Ecuador, *Journal of Volcanology and Geothermal Research*, *354*, 74-86.Marzocchi, W., L. Sandri, and J. Selva (2008), BET_EF: a probabilistic tool for long-and short-term eruption forecasting, *Bulletin of Volcanology*, *70*(5), 623-632, doi:https://doi.org/10.1007/s00445-007-0157-y.Marzocchi, W., L. Sandri, and J. Selva (2010), BET_VH: a probabilistic tool for long-term volcanic hazard assessment, *Bulletin of Volcanology*, *72*(6), 705-716, doi:https://doi.org/10.1007/s00445-010-0357-8.Mastin, L. G., M. Guffanti, R. Servranckx, P. Webley, S. Barsotti, K. Dean, et al. (2009), A multidisciplinary effort to assign realistic source parameters to models of volcanic ash-cloud transport and dispersion during eruptions, *Journal of Volcanology and Geothermal Research*, *186*(1-2), 10-21, doi:https://doi.org/10.1016/j.jvolgeores.2009.01.008.Miller, C. D., D. R. Mullineaux, and M. L. Hall (1978), Reconnaissance Map of Potential Volcanic Hazards from Cotopaxi Volcano, Ecuador: Mapa de Reconocimiento de Riesgos Volganicos Potenciales Del Volcan Cotopaxi, Ecuador, US Geological Survey.Mothes, P. A., P. Espin, M. L. Hall, F. Vasconez, D. Sierra, and D. Andrade (2016a), Mapa regional de amenazas volcánicas potenciales del volcán Cotopaxi, zona Norte, Quito.Mothes, P. A., P. Espin, M. L. Hall, F. Vasconez, D. Sierra, and D. Andrade (2016b), Mapa regional de amenazas volcánicas potenciales del volcán Cotopaxi, zona Sur, Quito.Neri, A., W. P. Aspinall, R. Cioni, A. Bertagnini, P. J. Baxter, G. Zuccaro, et al. (2008), Developing an event tree for probabilistic hazard and risk assessment at Vesuvius, *Journal of Volcanology and Geothermal Research*, *178*(3), 397-415, doi:https://doi.org/10.1016/j.jvolgeores.2008.05.014.Neri, A., A. Bevilacqua, T. Esposti Ongaro, R. Isaia, W. P. Aspinall, M. Bisson, et al. (2015), Quantifying volcanic hazard at Campi Flegrei caldera (Italy) with uncertainty assessment: II. Pyroclastic density current invasion maps, *Journal of Geophysical Research: Solid Earth*, doi:https://doi.org/10.1002/2014JB011776.NOAA (2004), Global Data Assimilation System (GDAS1) Archive Information, edited,

doi:https://www.ready.noaa.gov/gdas1.php.Orsi, G., M. A. Di Vito, and R. Isaia (2004), Volcanic hazard assessment at the restless Campi Flegrei caldera, *Bulletin of Volcanology*, *66*(6), 514-530, doi:https://doi.org/10.1007/s00445-003-0336-4.Pardini, F., S. Corradini, A. Costa, T. Esposti Ongaro, L. Merucci, A. Neri, and D. Stelitano (2020), Ensemble-Based Data Assimilation of Volcanic Ash Clouds from Satellite Observations: Application to the 24 December 2018 Mt. Etna Explosive Eruption, *Atmosphere*, *11*(4), 359, doi:https://doi.org/10.3390/atmos11040359.Patra, A. K., A. Bevilacqua, A. Akhavan-Safaei, E. B. Pitman, M. I. Bursik, and D. Hyman (2020), Comparative analysis of the structures and outcomes of geophysical flow models and modeling assumptions using uncertainty quantification, *Frontiers in Earth Science*, doi:10.3389/feart.2020.00275.Patra, A. K., A. Bevilacqua, and A. A. Safei (2018), Analyzing Complex Models using Data and Statistics, paper presented at International Conference on Computational Science, Springer.Pistolesi, M., M. Rosi, R. Cioni, K. V. Cashman, A. Rossotti, and E. Aguilera (2011), Physical volcanology of the post–twelfth-century activity at Cotopaxi volcano, Ecuador: Behavior of an andesitic central volcano, *Geol. Soc. Am. Bull.*, *123*(5-6), 1193-1215, doi:https://doi.org/10.1130/B30301.1.Pouget, S., M. I. Bursik, P. Singla, and T. Singh (2016), Sensitivity analysis of a one-dimensional model of a volcanic plume with particle fallout and collapse behavior, *Journal of Volcanology and Geothermal Research*, *326*, 43-53, doi:https://doi.org/10.1016/j.jvolgeores.2016.02.018.Prata, A. T., L. Mingari, A. Folch, G. Macedonio, and A. Costa (2021), FALL3D-8.0: a computational model for atmospheric transport and deposition of particles, aerosols and radionuclides–Part 2: model validation, *Geoscientific Model Development*, *14*(1), 409-436, doi:https://doi.org/10.5194/gmd-14-409-2021.Riley, C. M., W. I. Rose, and G. J. S. Bluth (2003), Quantitative shape measurements of distal volcanic ash, *Journal of Geophysical Research: Solid Earth*, *108*(B10), doi:https://doi.org/10.1029/2001JB000818.Robin, C., P. Samaniego, J. L. Le Pennec, M. Fornari, P. Mothes, and J. Van Der Plicht (2010), New radiometric and petrological constraints on the evolution of the Pichincha volcanic complex (Ecuador), *Bulletin of volcanology*, *72*(9), 1109-1129, doi:https://doi.org/10.1007/s00445-010-0389-0.Robin, C., P. Samaniego, J. L. Le Pennec, P. Mothes, and J. van der Plicht (2008), Late Holocene phases of dome growth and Plinian activity at Guagua Pichincha volcano (Ecuador), *Journal of Volcanology and Geothermal Research*, *176*(1), 7-15, doi:https://doi.org/10.1016/j.jvolgeores.2007.10.008.Rose, A. N., J. J. McKee, K. M. Sims, E. A. Bright, A. E. Reith, and M. L. Urban (2020), LandScan 2019, edited, Oak Ridge National Laboratory, Oak Ridge, TN, doi:https://landscan.ornl.gov/.Rutarindwa, R., E. T. Spiller, A. Bevilacqua, M. I. Bursik, and A. K. Patra (2019), Dynamic probabilistic hazard mapping in the Long Valley Volcanic Region CA: integrating vent opening maps and statistical surrogates of physical models of pyroclastic density currents, *J. Geophys. Res.-Sol. Ea.*Samaniego, P., C. Robin, G. Chazot, E. Bourdon, and J. Cotten (2010), Evolving metasomatic agent in the Northern Andean subduction zone, deduced from magma composition of the long-lived Pichincha

volcanic complex (Ecuador), *Contributions to Mineralogy and Petrology*, *160*(2), 239-260, doi:https://doi.org/10.1007/s00410-009-0475-5.Sandri, L., A. Costa, J. Selva, R. Tonini, G. Macedonio, A. Folch, and R. Sulpizio (2016), Beyond eruptive scenarios: assessing tephra fallout hazard from Neapolitan volcanoes, *Scientific reports*, *6*(1), 1-13, doi:https://doi.org/10.1038/srep24271.Scaini, C., A. Folch, and M. Navarro (2012), Tephra hazard assessment at Concepción Volcano, Nicaragua, *Journal of volcanology and geothermal research*, *219*, 41-51, doi:https://doi.org/10.1016/j.jvolgeores.2012.01.007.Schwaiger, H. F., R. P. Denlinger, and L. G. Mastin (2012), Ash3d: A finite-volume, conservative numerical model for ash transport and tephra deposition, *Journal of Geophysical Research: Solid Earth*, *117*(B4), doi:https://doi.org/10.1029/2011JB008968.Scollo, S., S. Tarantola, C. Bonadonna, M. Coltelli, and A. Saltelli (2008), Sensitivity analysis and uncertainty estimation for tephra dispersal models, *Journal of Geophysical Research: Solid Earth*, *113*(B6), doi:https://doi.org/10.1029/2006JB004864.Sparks, R. S. J., M. I. Bursik, S. N. Carey, J. S. Gilbert, L. S. Glaze, H. Sigurdsson, and A. W. Woods (1997), *Volcanic plumes*, Wiley.Spence, R. J. S., I. Kelman, P. J. Baxter, G. Zuccaro, and S. Petrazzuoli (2005), Residential building and occupant vulnerability to tephra fall, *Natural Hazards and Earth System Sciences*, *5*(4), 477-494, doi:https://doi.org/10.5194/nhess-5-477-2005.Spera, F. J. (2000), Physical properties of magma, in *Encyclopedia on Volcanoes*, edited by H. Sigurdsson, B. F. Houghton, S. R. McNutt, H. Rymer and J. Stix, Academic Press, San Diego, CA.Stefanescu, E. R., A. K. Patra, M. I. Bursik, R. Madankan, S. Pouget, M. Jones, et al. (2014), Temporal, probabilistic mapping of ash clouds using wind field stochastic variability and uncertain eruption source parameters: Example of the 14 A pril 2010 E yjafjallajökull eruption, *Journal of Advances in Modeling Earth Systems*, *6*(4), 1173-1184, doi:https://doi.org/10.1002/2014MS000332.Stein, A. F., R. R. Draxler, G. D. Rolph, B. J. B. Stunder, M. D. Cohen, and F. Ngan (2015), NOAA's HYSPLIT atmospheric transport and dispersion modeling system, *Bulletin of the American Meteorological Society*, *96*(12), 2059-2077.Tadini, A., A. Bevilacqua, A. Neri, R. Cioni, W. P. Aspinall, M. Bisson, et al. (2017a), Assessing future vent opening locations at the Somma-Vesuvio volcanic complex: 2. Probability maps of the caldera for a future Plinian/sub-Plinian event with uncertainty quantification, *Journal of Geophysical Research: Solid Earth*, *122*(6), 4357-4376, doi:10.1002/2016JB013860.Tadini, A., M. Bisson, A. Neri, R. Cioni, A. Bevilacqua, and W. P. Aspinall (2017b), Assessing future vent opening locations at the Somma-Vesuvio volcanic complex: 1. A new information geo-database with uncertainty characterizations, *Journal of Geophysical Research: Solid Earth*, *122*(6), 4336-4356, doi:10.1002/2016JB013858.Tadini, A., O. Roche, P. Samaniego, N. Azzaoui, A. Bevilacqua, A. Guillin, et al. (2021), Eruption type probability and eruption source parameters at Cotopaxi and Guagua Pichincha volcanoes (Ecuador) with uncertainty quantification, *Bullettin of Volcanology*, *83*(35), doi:https://doi.org/10.1007/s00445-021-01458-z.Tadini, A., O. Roche, P. Samaniego, A. Guillin, N. Azzaoui, M. Gouhier, et al. (2020), Quantifying the uncertainty of a coupled plume and tephra dispersal model: PLUME-MOM/HYSPLIT simulations applied to

Andean volcanoes, *Journal of Geophysical Research: Solid Earth*, *125*(2), doi:https://doi.org/10.1029/2019JB018390.Tsuji, T., M. Ikeda, H. Kishimoto, K. Fujita, N. Nishizaka, and K. Onishi (2017), Tephra Fallout Hazard Assessment for VEI5 Plinian Eruption at Kuju Volcano, Japan, Using TEPHRA2, paper presented at IOP Conference Series: Earth and Environmental Science, IOP Publishing.Tsunematsu, K., and C. Bonadonna (2015), Grain-size features of two large eruptions from Cotopaxi volcano (Ecuador) and implications for the calculation of the total grain-size distribution, *Bulletin of Volcanology*, *77*(7), 64, doi:https://doi.org/10.1007/s00445-015-0949-4.Vasconez, F., D. Sierra, M. Almeida, D. Andrade, J. M. Marrero, P. A. Mothes, et al. (2017), Mapa preliminar de amenazas potenciales del volcán Cotopaxi—Zona oriental, IG-EPN, Quito, Ecuador.Vázquez, R., R. Bonasia, A. Folch, J. L. Arce, and J. L. Macías (2019), Tephra fallout hazard assessment at Tacaná volcano (Mexico), *Journal of South American Earth Sciences*, *91*, 253-259, doi:https://doi.org/10.1016/j.jsames.2019.02.013.Volentik, A. C. M., and B. F. Houghton (2015), Tephra fallout hazards at Quito International Airport (Ecuador), *Bulletin of Volcanology*, *77*(6), 50, doi:https://doi.org/10.1007/s00445-015-0923-1.Wilson, G., T. M. Wilson, N. I. Deligne, and J. W. Cole (2014), Volcanic hazard impacts to critical infrastructure: A review, *Journal of Volcanology and Geothermal Research*, *286*, 148-182, doi:https://doi.org/10.1016/j.jvolgeores.2014.08.030.Wilson, T. M., C. Stewart, V. Sword-Daniels, G. S. Leonard, D. M. Johnston, J. W. Cole, et al. (2012), Volcanic ash impacts on critical infrastructure, *Physics and Chemistry of the Earth, Parts A/B/C*, *45*, 5-23, doi:https://doi.org/10.1016/j.pce.2011.06.006.Wolf, T. (1904), *Crónica de los fenómenos volcánicos y terremotos en el Ecuador con algunas noticias sobre otros países de la América Central y Meridional desde 1535 hasta 1797*, Imprenta de la Universidad Central de Quito, Quito, doi:http://www.dspace.uce.edu.ec/handle/25000/14200.Wright, H. M. N., K. V. Cashman, M. Rosi, and R. Cioni (2007), Breadcrust bombs as indicators of Vulcanian eruption dynamics at Guagua Pichincha volcano, Ecuador, *Bulletin of Volcanology*, *69*(3), 281-300, doi:https://doi.org/10.1007/s00445-006-0073-6.Yang, Q., E. B. Pitman, M. I. Bursik, and S. F. Jenkins (2021), Tephra deposit inversion by coupling Tephra2 with the Metropolis-Hastings algorithm: algorithm introduction and demonstration with synthetic datasets, *Journal of Applied Volcanology*, *10*(1), 1-24, doi:https://doi.org/10.1186/s13617-020-00101-4.Yang, Q., E. B. Pitman, E. T. Spiller, M. I. Bursik, and A. Bevilacqua (2020), Novel statistical emulator construction for volcanic ash transport model Ash3d with physically motivated measures, *Proceedings of the Royal Society A*, *476*(2242), 20200161, doi:https://doi.org/10.1098/rspa.2020.0161. References from the Supporting Information

Tadini, A., O. Roche, P. Samaniego, N. Azzaoui, A. Bevilacqua, A. Guillin, et al. (2021), Eruption type probability and eruption source parameters at Cotopaxi and Guagua Pichincha volcanoes (Ecuador) with uncertainty quantification, *Bullettin of Volcanology*, *83*(35), doi:https://doi.org/10.1007/s00445-021-01458-z.

Journal of Geophysical Research: Solid Earth

Supporting Information for

Tephra fallout probabilistic hazard maps for Cotopaxi and Guagua Pichincha volcanoes (Ecuador) with uncertainty quantification

A. Tadini[1], N. Azzaoui[2], O. Roche[1], P. Samaniego[1,3], B. Bernard[3], A. Bevilacqua[4], S. Hidalgo[3], A. Guillin[2], M. Gouhier[1]

[1]Université Clermont Auvergne, Laboratoire Magmas et Volcans, 6 Avenue Blaise Pascal, 63178 Aubière, France.

[2]Université Clermont Auvergne, Laboratoire de Mathématiques Blaise Pascal, 3 place Vasarely, 63178 Aubière, France.

[3]Escuela Politécnica Nacional, Instituto Geofísico, Ladrón de Guevara E11-253 y Andalucía, Quito, Ecuador.

[4]Istituto Nazionale di Geofisica e Vulcanologia, Sezione di Pisa, via Cesare Battisti 53, 56125 Pisa, Italy.

Contents of this file

Additional Supporting Information (Files uploaded separately)

Tables S4 to S6

Introduction

This supporting information provides:

- Tables S1 and S2, which collects the raw percentiles for, respectively, eruption type probabilities (for both the next eruption and the next 100 years) and eruption source parameters as derived from the elicitation of Tadini et al. (2021);
- Table S3, which lists all the other parameters (and their uncertainty ranges) used for the simulations;
- Figure S1, which provides an example of wind directions and intensities for the whole meteorological dataset divided per month above Cotopaxi volcano at a specific pressure level;
- Figure S2, which indicates the locations of the stratigraphic sections and the calculated values of deposit density for Guagua Pichincha volcano;
- Figures S3 to S57 which collect the probabilistic maps, the isopach maps and the hazard curves related to single eruption types of, respectively, Cotopaxi (S3-S39) and Guagua Pichincha (S40-S57) volcanoes Such maps and curves should be used in conjunction with their probability of occurrences within the next 100 years, which are reported in Fig. 2 of the main document. For each thickness value/probability value, three maps are provided ("Lower", "Natural" and "Upper"), reflecting the model uncertainty discussed in the main document. Each contour of the maps is in % (for probabilistic maps) or in mm (for isopach maps).;
- Caption for Table S4, which reports all the exceeding probabilities for the 10 sensitive sites within Quito.

TABLES

Volcano	Variable	% - 5th/Median/95th		
Cotopaxi	*sub-Plinian Rhyolitic (NE)*	< 0.1	**3.7**	19
	Plinian Rhyolitic (NE)	< 0.1	**2.7**	15
	sub-Plinian Andesitic (NE)	0.4	**9.5**	33
	Plinian Andesitic (NE)	< 0.1	**4.2**	23
	sub-Plinian Rhyolitic (N100)	< 0.1	**7.3**	40
	Plinian Rhyolitic (N100)	< 0.1	**6.7**	41
	sub-Plinian Andesitic (N100)	< 0.1	**28**	75
	Plinian Andesitic (N100)	< 0.1	**14**	43
Guagua Pichincha	*sub-Plinian (NE)*	1.8	**18**	55
	Plinian (NE)	0.3	**9.9**	46
	sub-Plinian (N100)	2.1	**25**	63
	Plinian (N100)	1.0	**17**	66

Table S1. 5th, Median and 95th percentiles for eruption type occurrences for the next eruption (NE) and next 100 years (N100) time frames for all eruption types (Tadini et al., 2021).

Volcano	Variable	5th/Median/95th		
Cotopaxi	*Mean duration sub-Plinian Rhyolitic (minutes)*	15	**170**	6300
	Total mass tephra sub-Plinian Rhyolitic (10^9 kg)	2.4	**53**	760
	Average plume height sub-Plinian Rhyolitic (km)	5.6	**16**	25
	Mean duration Plinian Rhyolitic (minutes)	27	**340**	13000
	Total mass tephra Plinian Rhyolitic (10^9 kg)	8.8	**410**	7600
	Average plume height Plinian Rhyolitic (km)	10	**24**	40
	Mean duration sub-Plinian Andesitic (minutes)	9	**75**	9400
	Total mass tephra sub-Plinian Andesitic (10^9 kg)	1.2	**34**	430
	Average plume height sub-Plinian Andesitic (km)	6.6	**18**	25
	Mean duration Plinian Andesitic (minutes)	11	**180**	19000
	Total mass tephra Plinian Andesitic (10^9 kg)	11	**220**	4200
	Average plume height Plinian Andesitic (km)	13	**25**	35
Guagua Pichincha	*Mean duration sub-Plinian (minutes)*	9	**88**	6400
	Total mass tephra sub-Plinian (10^9 kg)	0.4	**28**	660
	Average plume height sub-Plinian (km)	6.9	**17**	25
	Mean duration Plinian (minutes)	11	**190**	13000
	Total mass tephra Plinian (10^9 kg)	1.6	**170**	3600
	Average plume height Plinian (km)	13	**24**	34

Table S2. 5th, Median and 95th percentiles for eruption source parameters (mean duration, total fallout mass and average plume height) for all eruption types (Tadini et al., 2021).

Volcano	Magma type	Parameters								
		Magma density (kg/m^3)	Magma water mass fraction (%)	Magma viscosity (Pa*s)	Particle density				Particle shape factor	Deposit density (kg/m^3)
					Φ_1	ρ_1	Φ_2	ρ_2		
Cotopaxi	*Rhyolitic*	2110	6 / 8	3.3 / 7.3	-4 / -1	440 / 500	5 / 7	2300 / 2670	0.6 / 0.7	560
	Andesitic	2340	5 / 6	2.8 / 7.9	-1	1000 / 1487	2 / 7	2478 / 2561	0.7 / 0.8	825
Guagua Pichincha	*Dacitic*	2220	5 / 6	4.6 / 6.9	-4 / -1	665 / 993	7	2400	0.7 / 0.8	745

Table S3. List of parameters (with their uncertainty ranges) used for the simulations for each eruption type.

Captions for Table S4 to S6

Table S4. Calculated exceeding probabilities for each thickness threshold (1, 3, 10, 30, 100 and 300 mm) for all the 10 sensitive sites within Quito and for the merged sub-Plinian and Plinian eruptions for both Cotopaxi and Guagua Pichincha volcanoes.

Table S5. Calculated exceeding probabilities for each thickness threshold (1, 3, 10, 30, 100 and 300 mm) for all the 10 sensitive sites within Quito and for all the eruption types of Cotopaxi volcano.

Table S6. Calculated exceeding probabilities for each thickness threshold (1, 3, 10, 30, 100 and 300 mm) for all the 10 sensitive sites within Quito and for all the eruption types of Guagua Pichincha volcano.

FIGURES

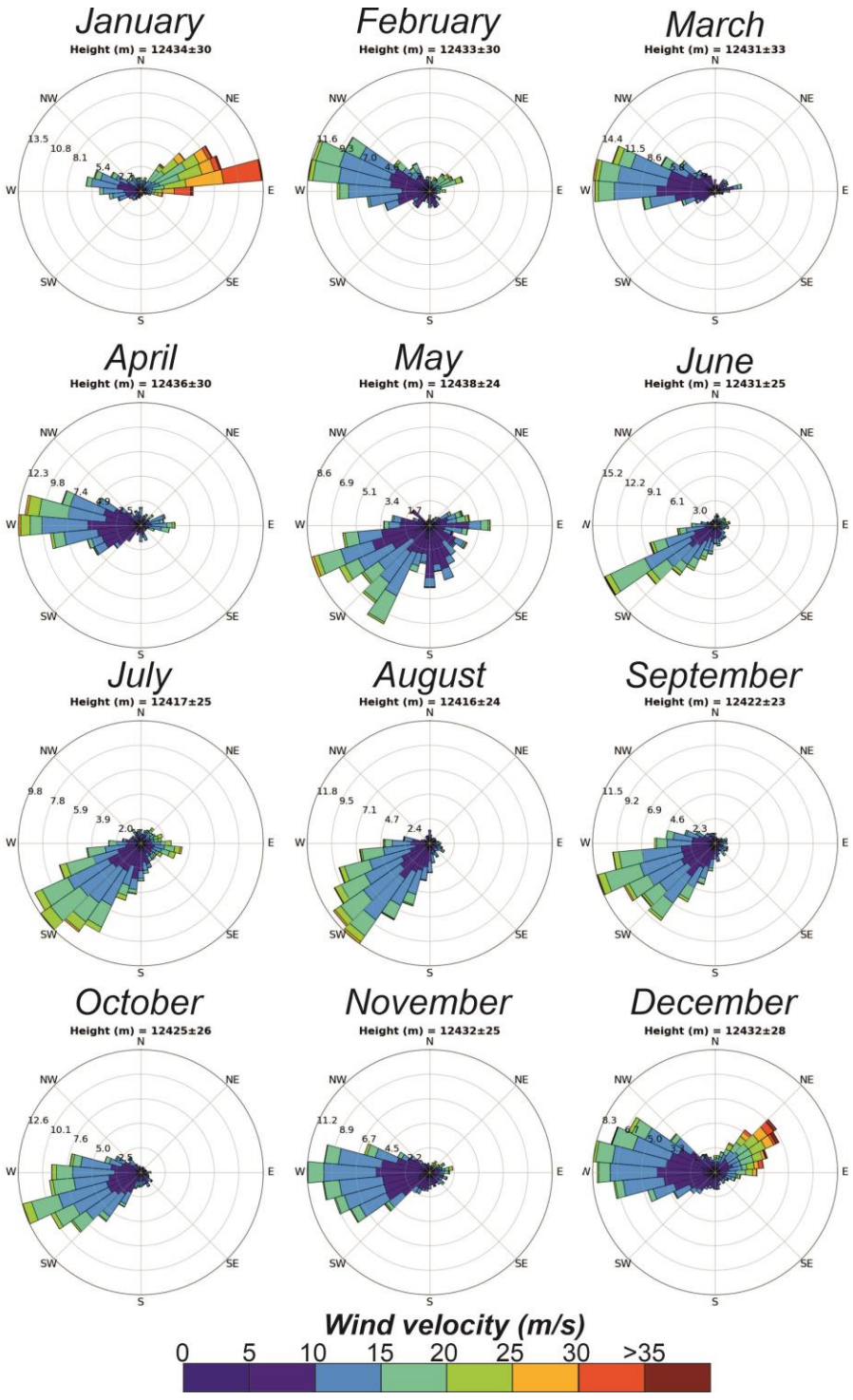

Figure S1. Wind directions and speeds for the whole GDAS dataset and for each month at the pressure level of 200 hPa (heights provided are average values ± standard deviations) above Cotopaxi volcano. Numbers on concentric circles are percentages.

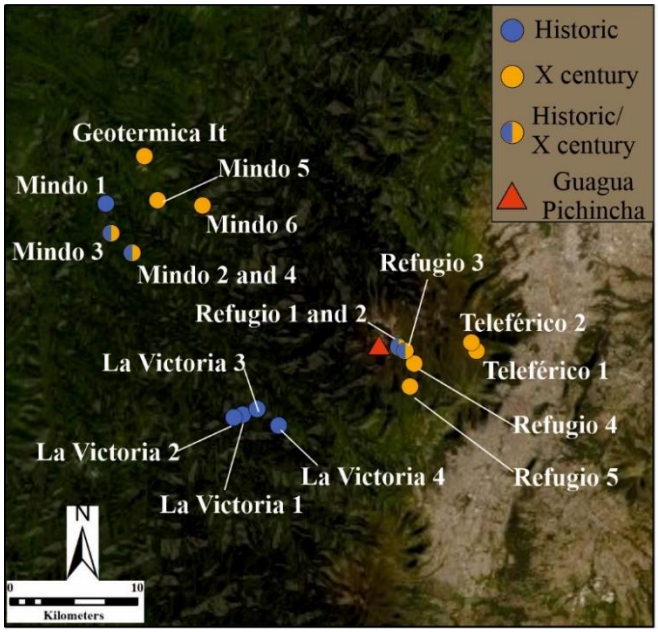

Section name	Deposit density X century (kg/m^3)	Deposit density Historic (kg/m^3)
Refugio 1	-	662
Refugio 2	532	668
Refugio 3	555	725
Refugio 4	589	-
Refugio 5	702	-
La Victoria 1	-	839
La Victoria 2	-	651
La Victoria 3	-	700
La Victoria 4	-	530
Mindo 1	-	876
Mindo 2	879	881
Mindo 3	883	831
Mindo 4	937	-
Mindo 5	903	-
Mindo 6	917	-
Geotermica It	754	-
Teleferico 1	719	-
Teleferico 2	671	-

Figure S2. Sample location and calculated deposit densities for both the X century and the Historic eruption cycles of Guagua Pichincha volcano. Service Layer Credits, source: Esri, DigitalGlobe, GeoEye, Earthstar Geographics, CNES/Airbus DS, USDA, USGS, AeroGRID, IGN and the GIS User Community.

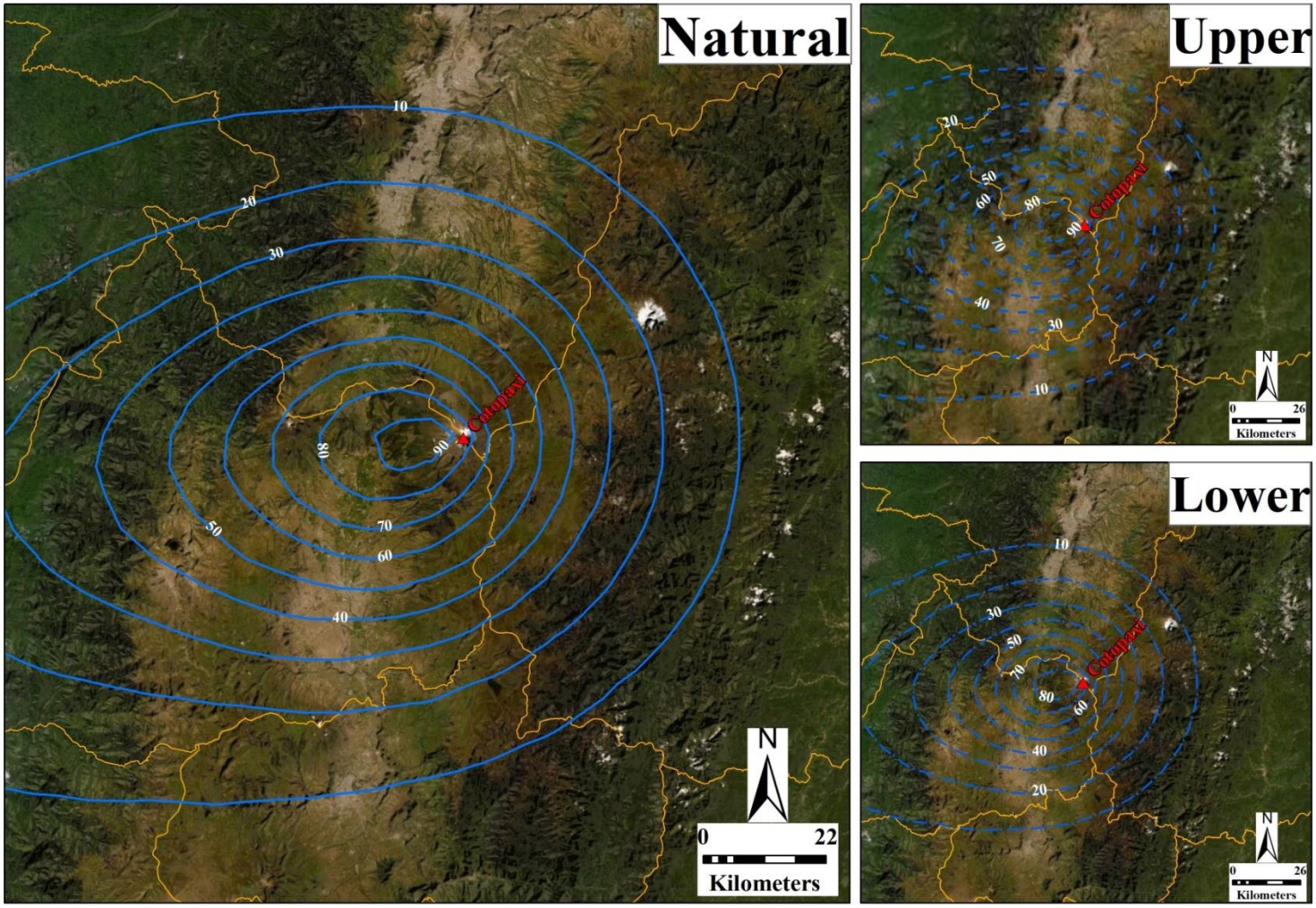

Figure S3. Cotopaxi volcano, sub-Plinian rhyolitic eruption – Probabilistic map (1 mm)

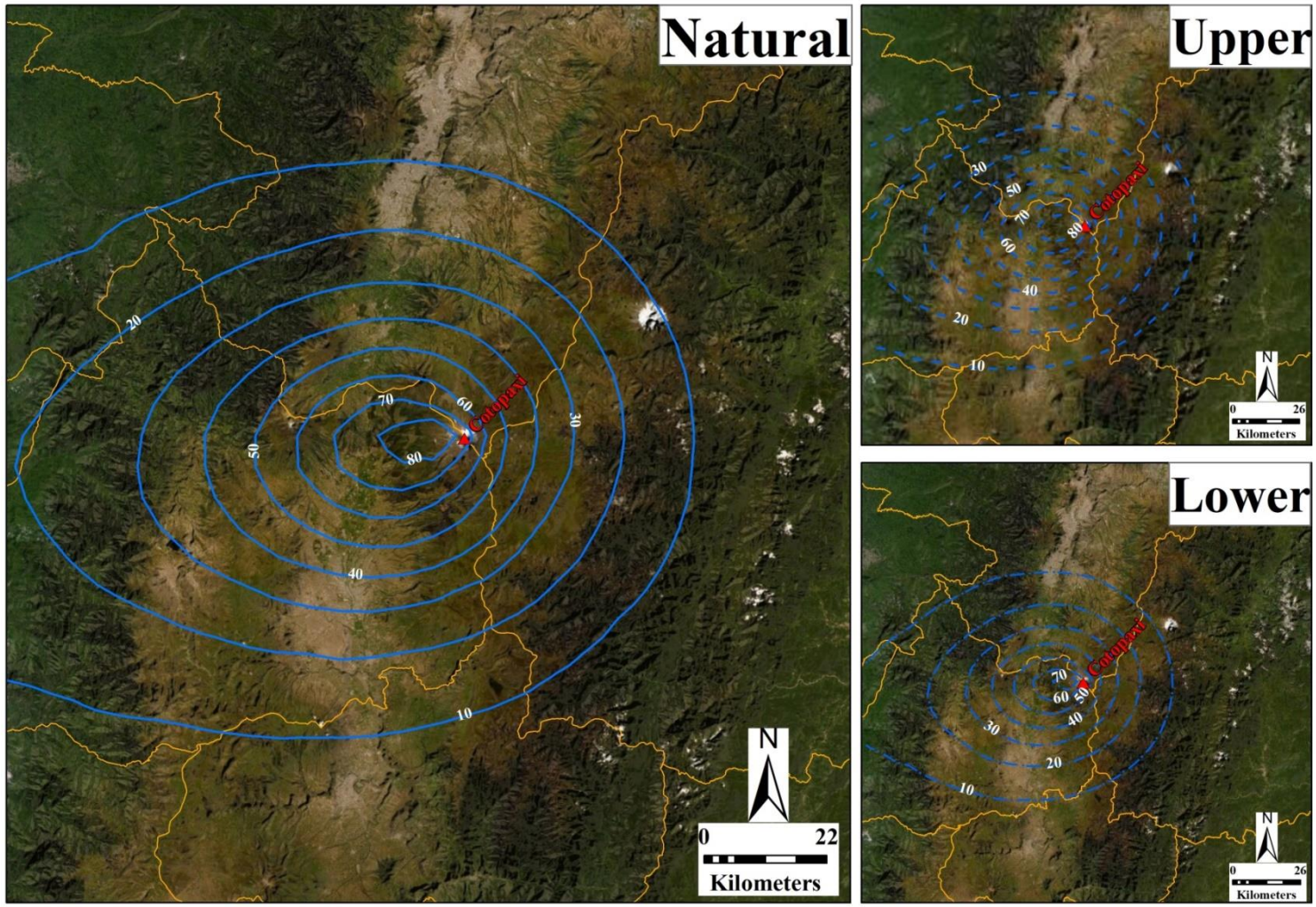

Figure S4. Cotopaxi volcano, sub-Plinian rhyolitic eruption – Probabilistic map (3 mm)

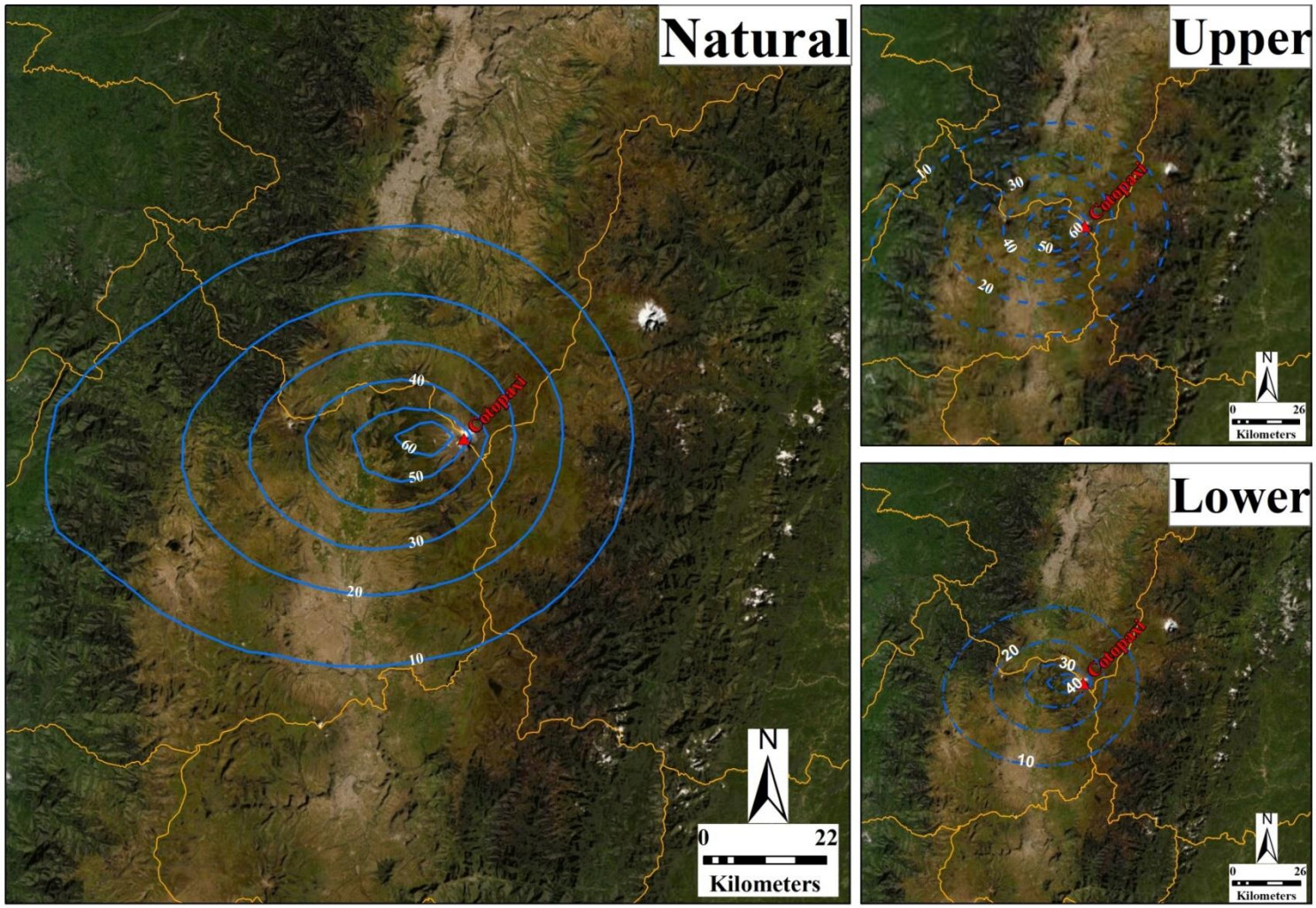

Figure S5. Cotopaxi volcano, sub-Plinian rhyolitic eruption – Probabilistic map (10 mm)

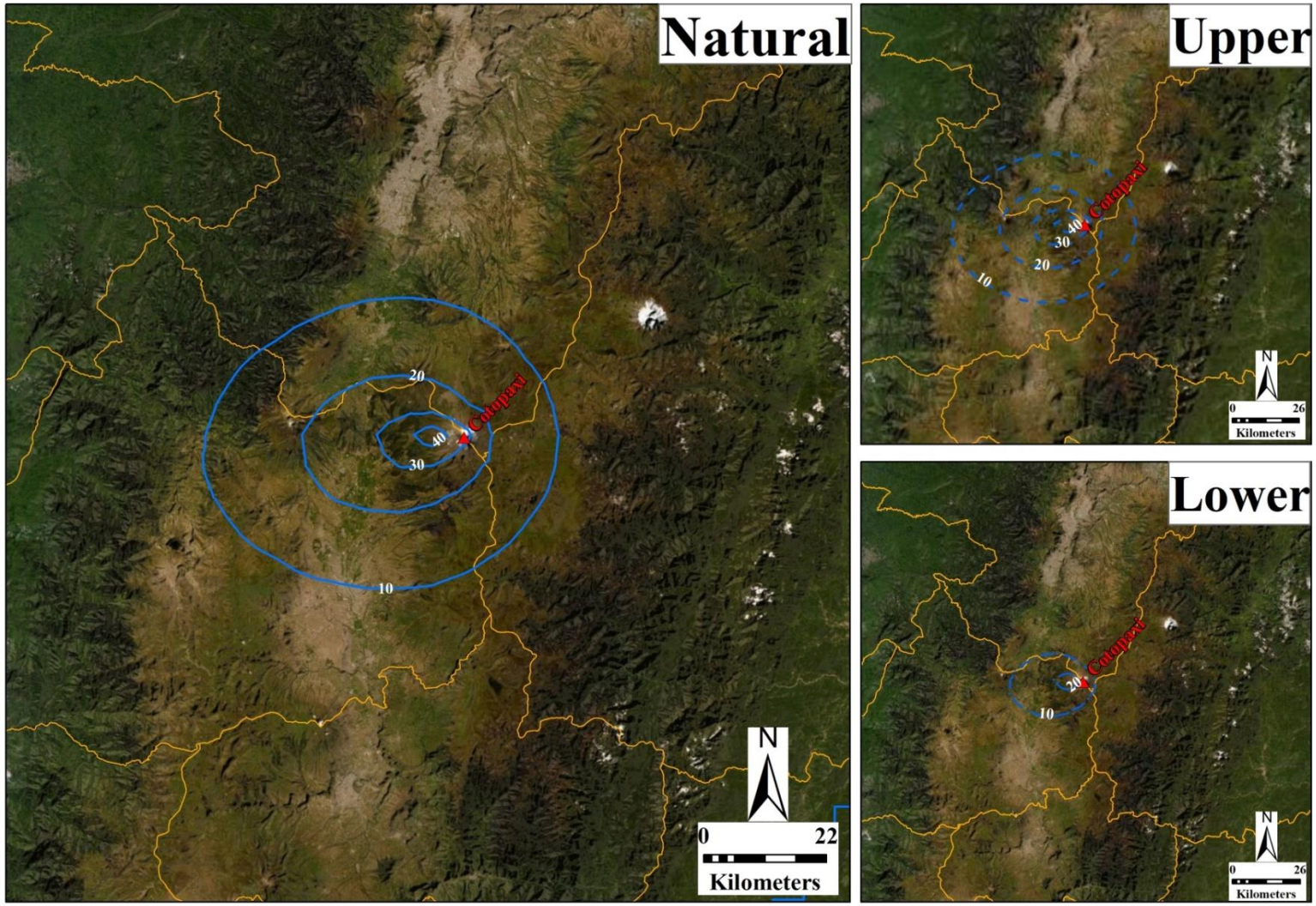

Figure S6. Cotopaxi volcano, **s**ub-Plinian rhyolitic eruption – Probabilistic map (30 mm)

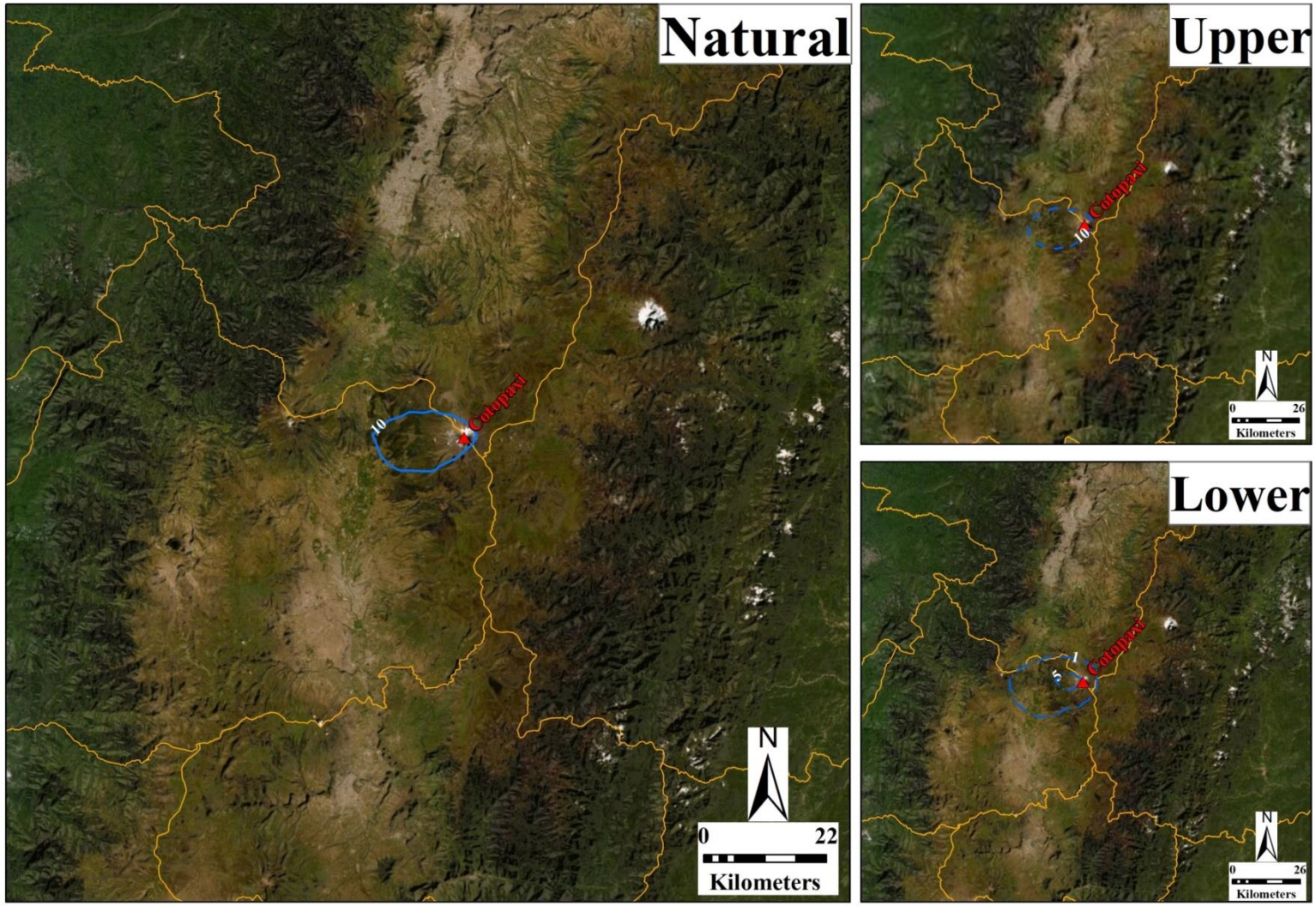

Figure S7. Cotopaxi volcano, sub-Plinian rhyolitic eruption – Probabilistic map (100 mm)

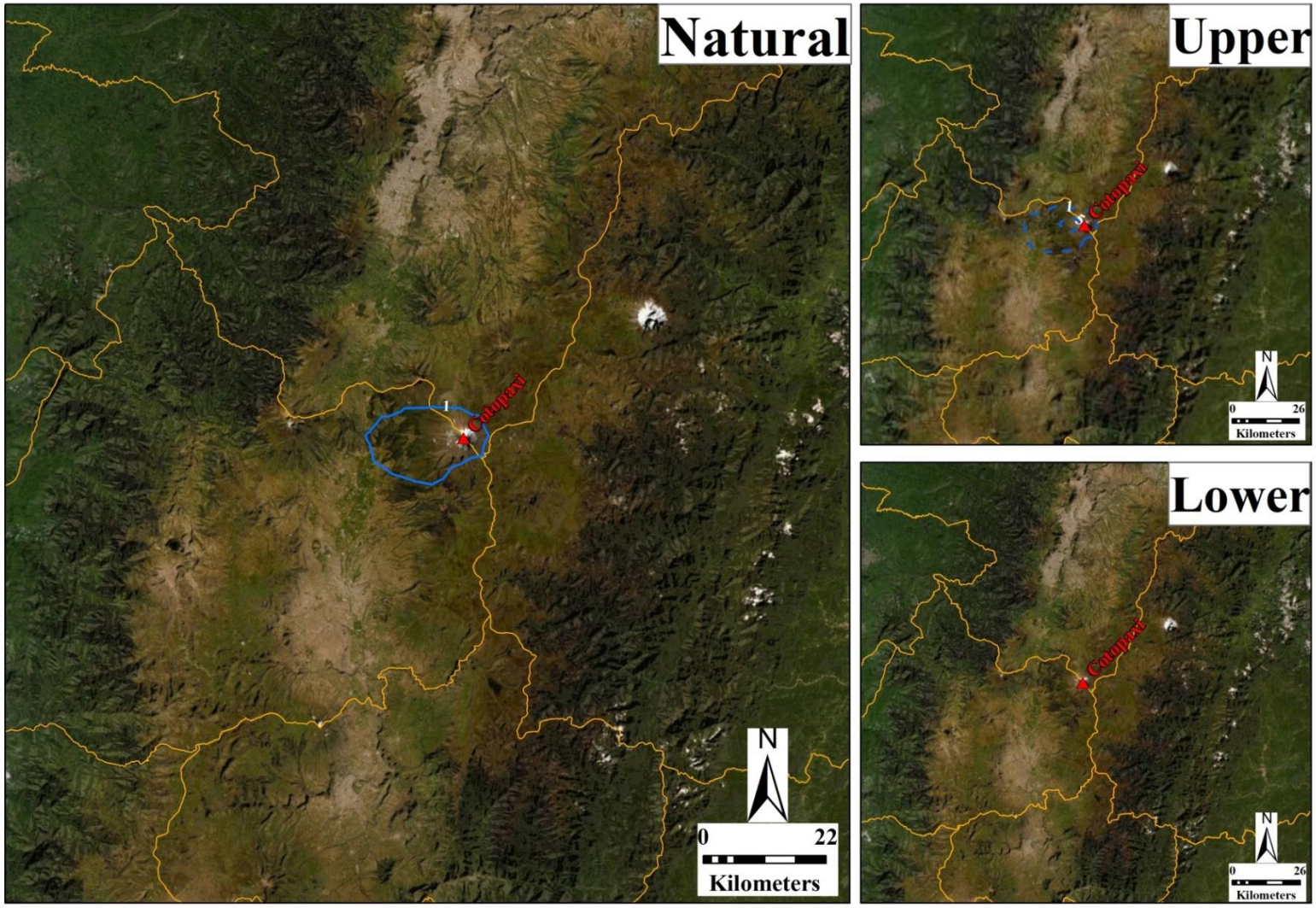

Figure S8. Cotopaxi volcano, sub-Plinian rhyolitic eruption – Probabilistic map (300 mm)

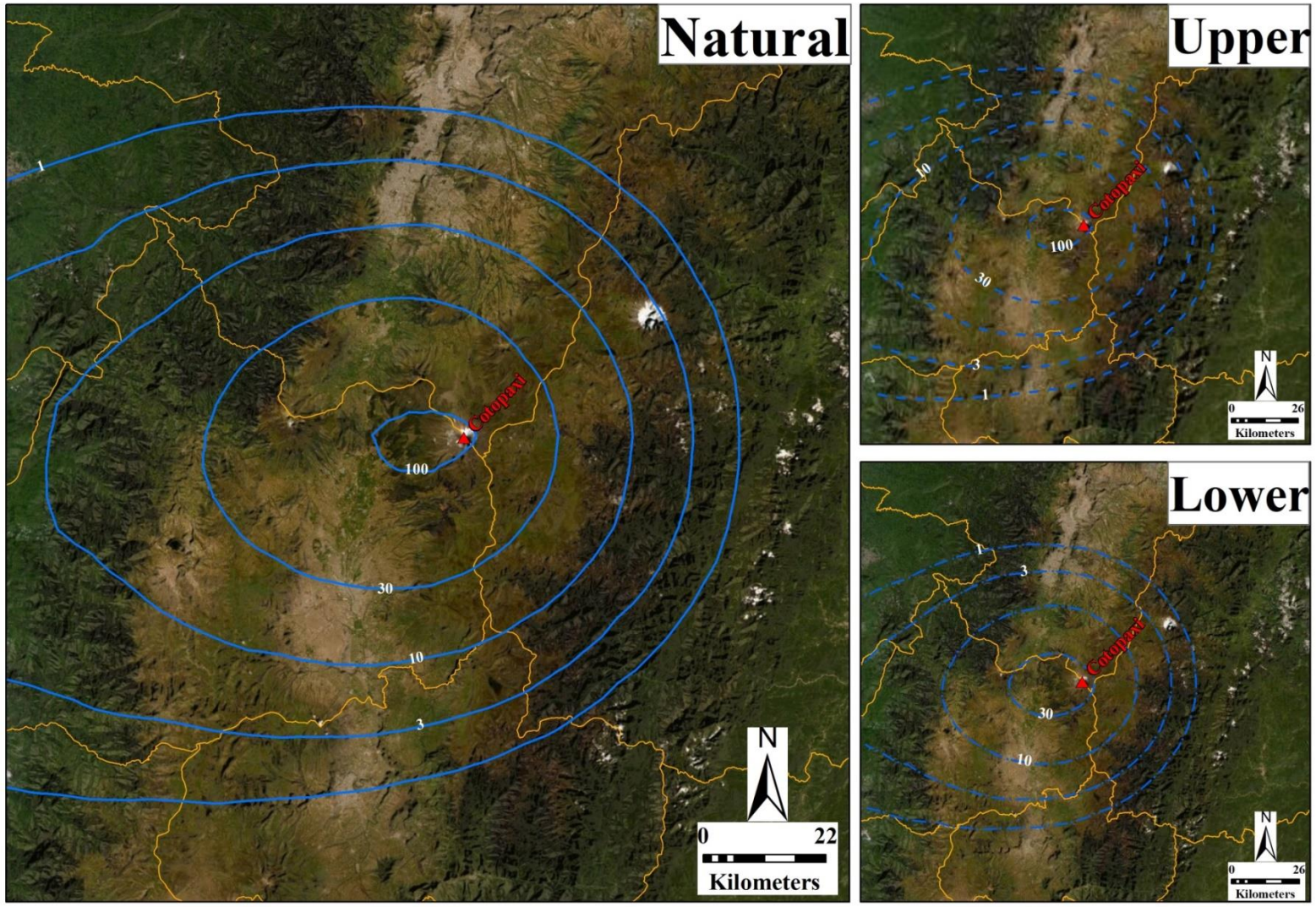

Figure S9. Cotopaxi volcano, sub-Plinian rhyolitic eruption – Isopach map (10 %)

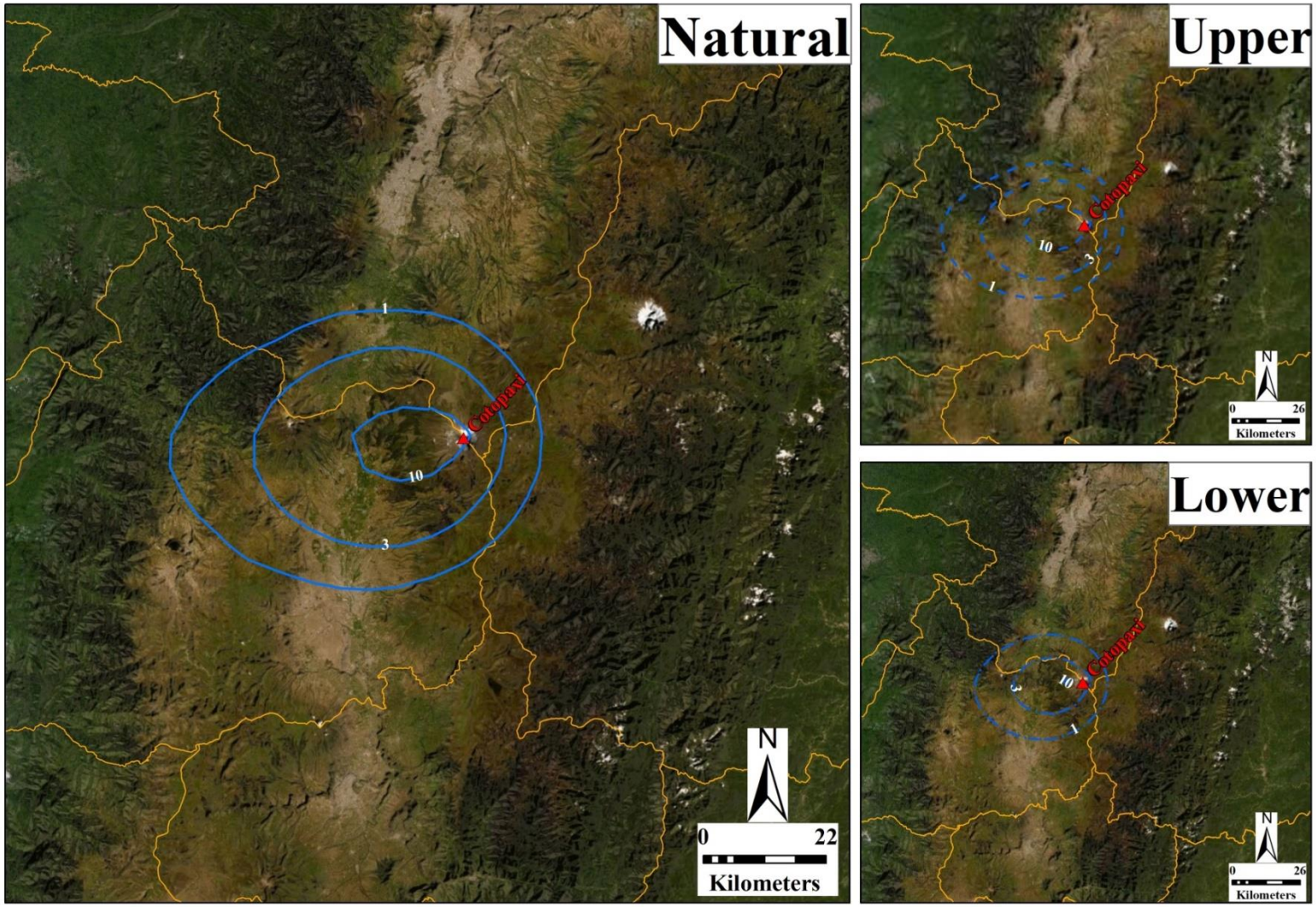

Figure S10. Cotopaxi volcano, sub-Plinian rhyolitic eruption – Isopach map (50 %)

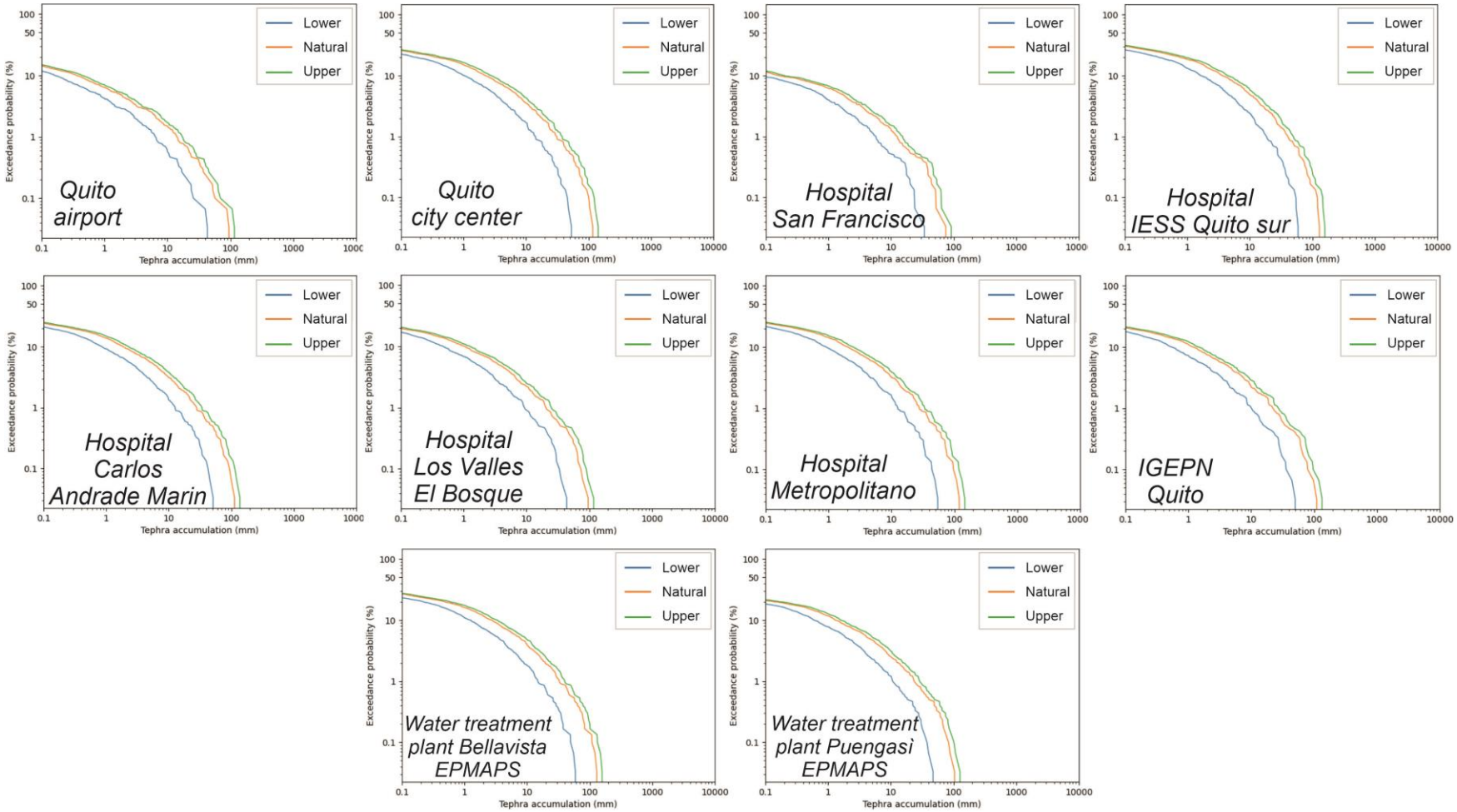

Figure S11. Cotopaxi volcano, sub-Plinian rhyolitic eruption – Hazard curves

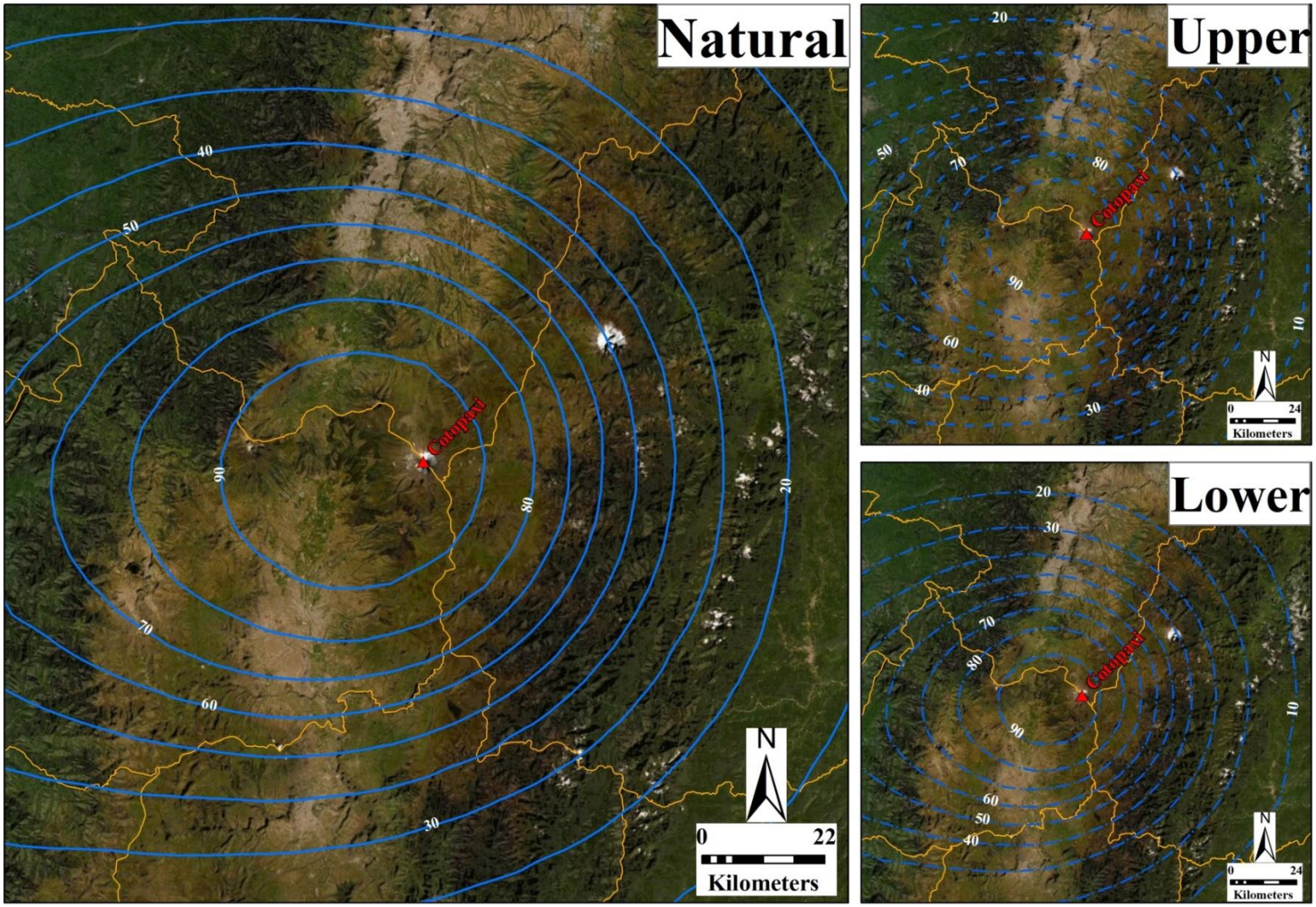

Figure S12. Cotopaxi volcano, Plinian rhyolitic eruption – Probabilistic map (1 mm)

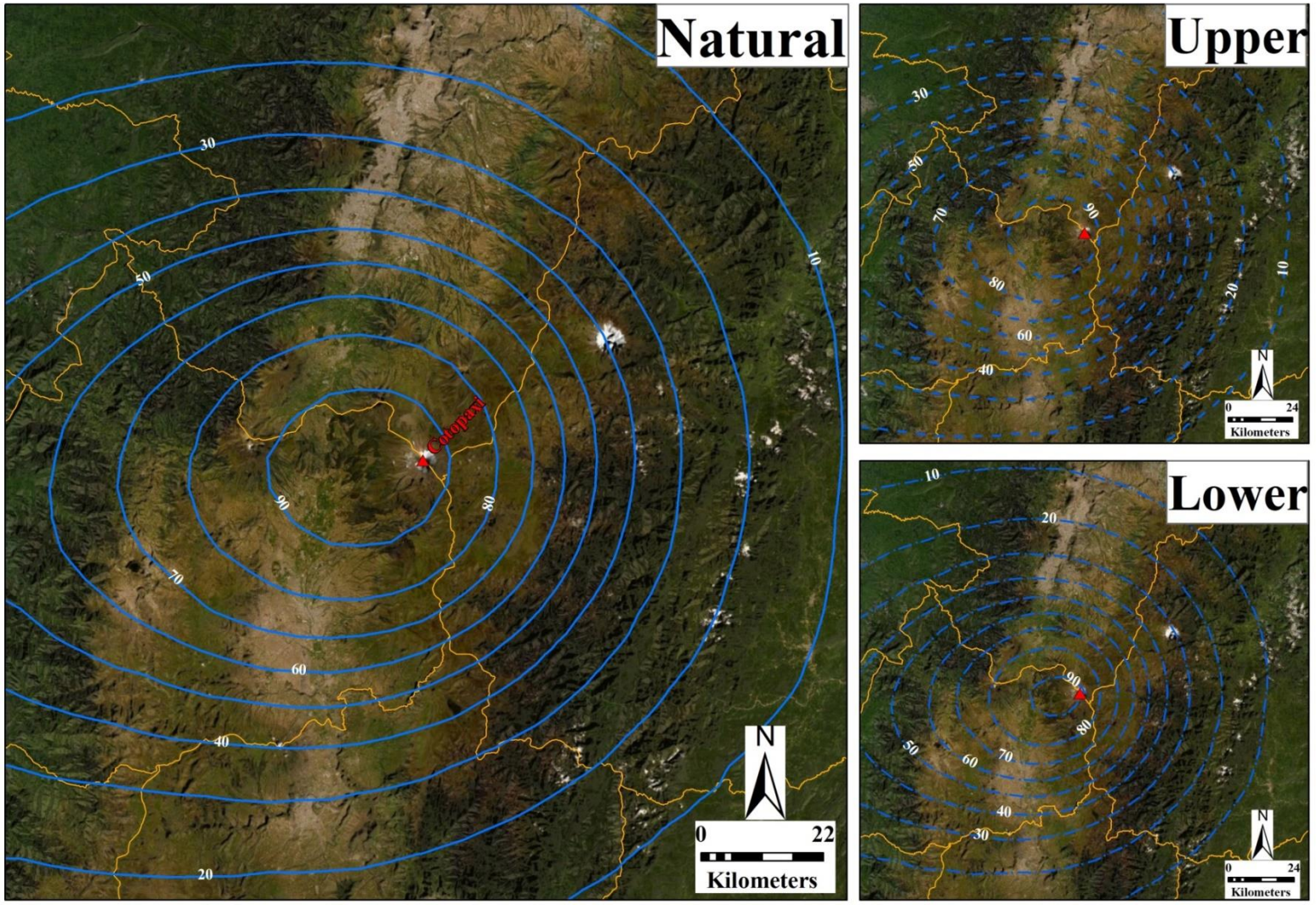

Figure S13. Cotopaxi volcano, Plinian rhyolitic eruption – Probabilistic map (3 mm)

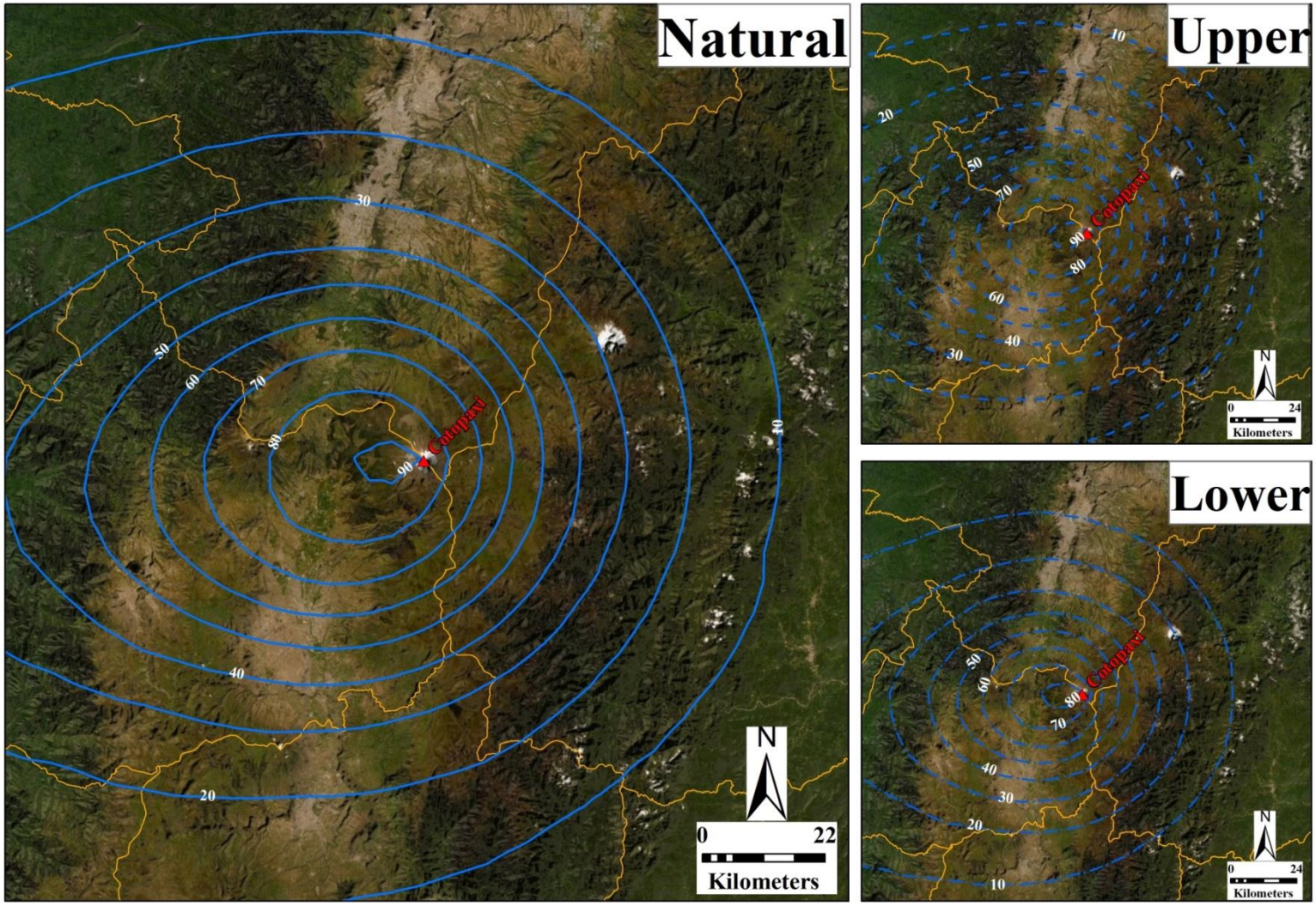

Figure S14. Cotopaxi volcano, Plinian rhyolitic eruption – Probabilistic map (10 mm)

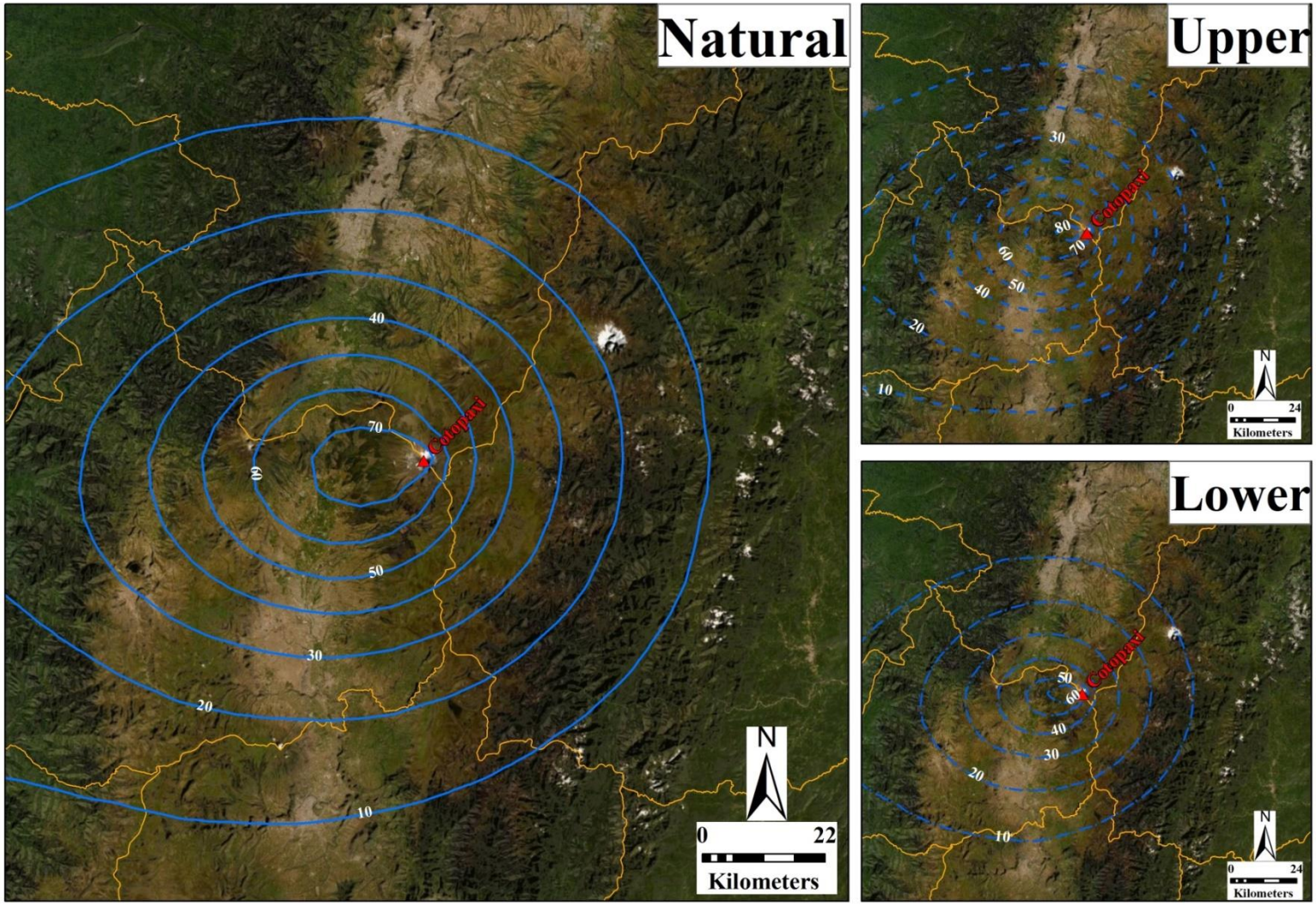

Figure S15. Cotopaxi volcano, Plinian rhyolitic eruption – Probabilistic map (30 mm)

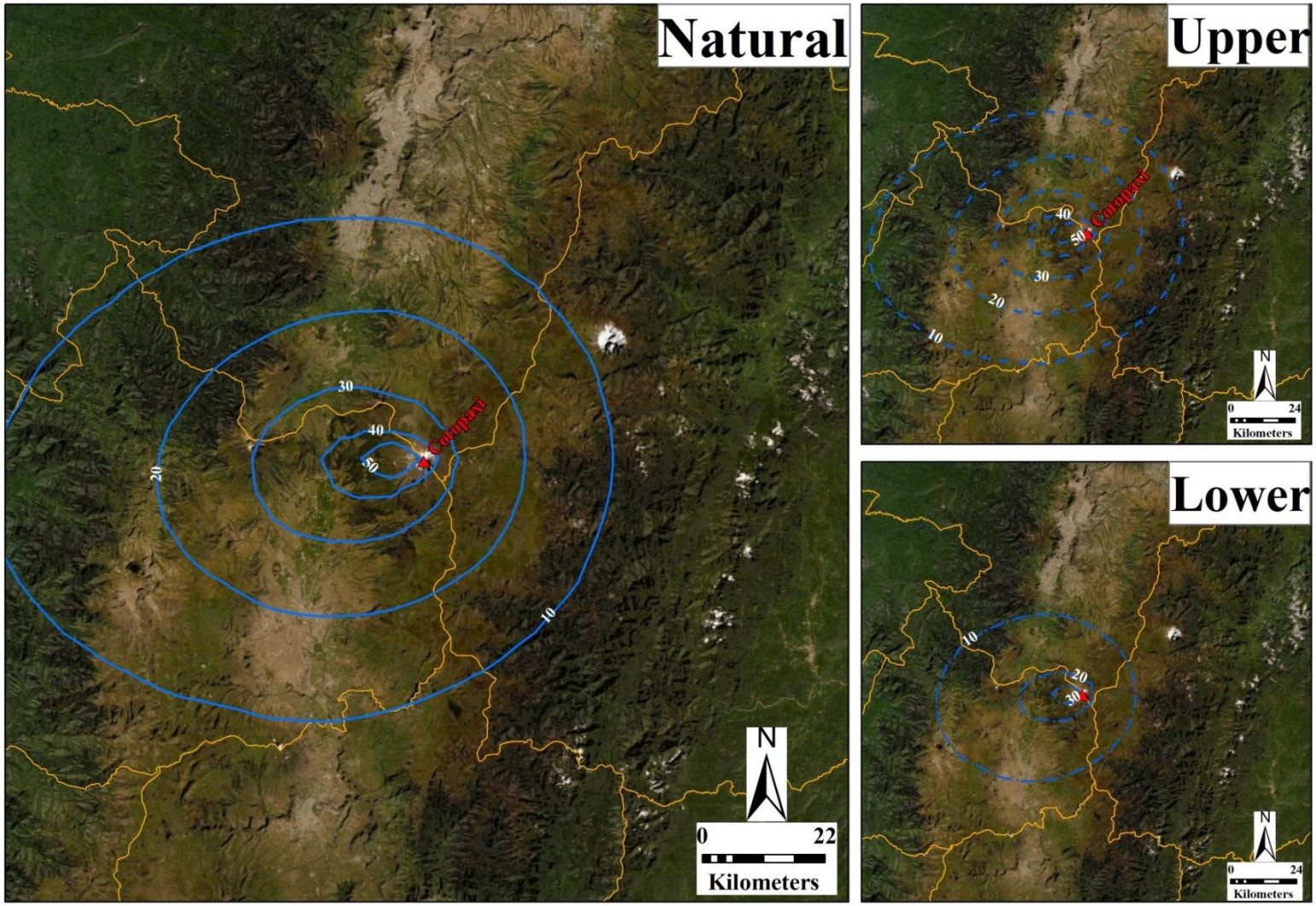

Figure S16. Cotopaxi volcano, Plinian rhyolitic eruption – Probabilistic map (100 mm)

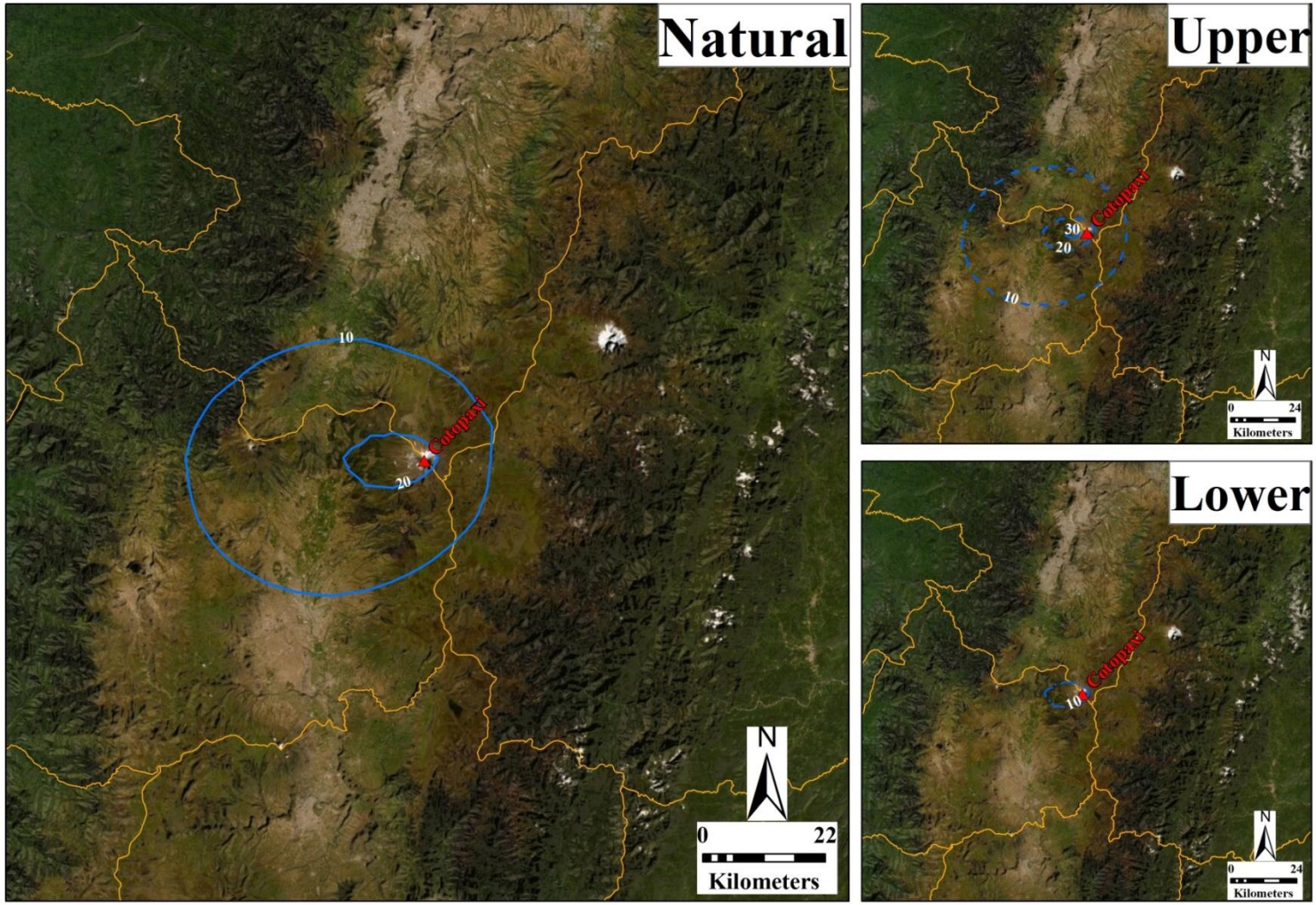

Figure S17. Cotopaxi volcano, Plinian rhyolitic eruption – Probabilistic map (300 mm)

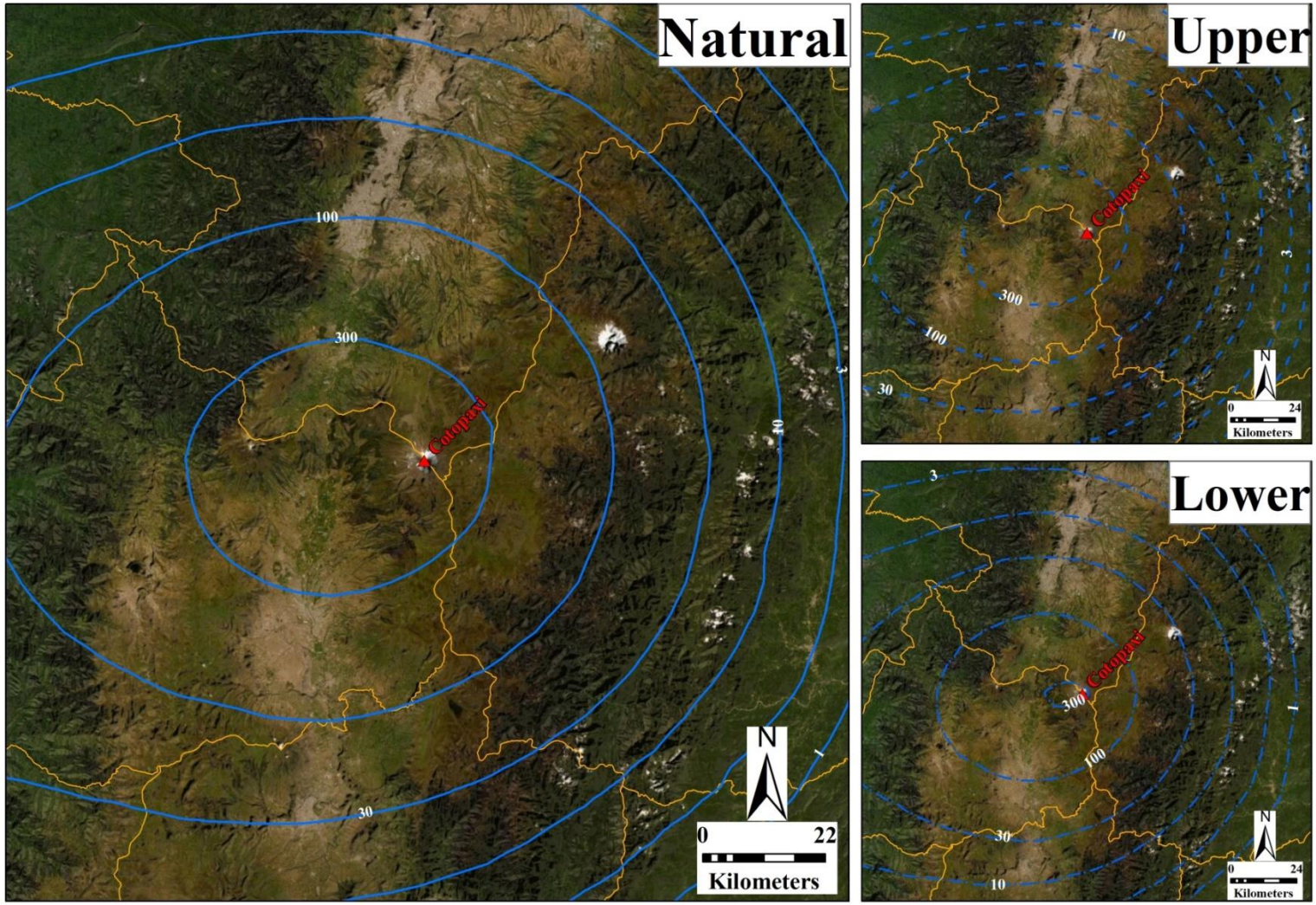

Figure S18. Cotopaxi volcano, Plinian rhyolitic eruption – Isopach map (10 %)

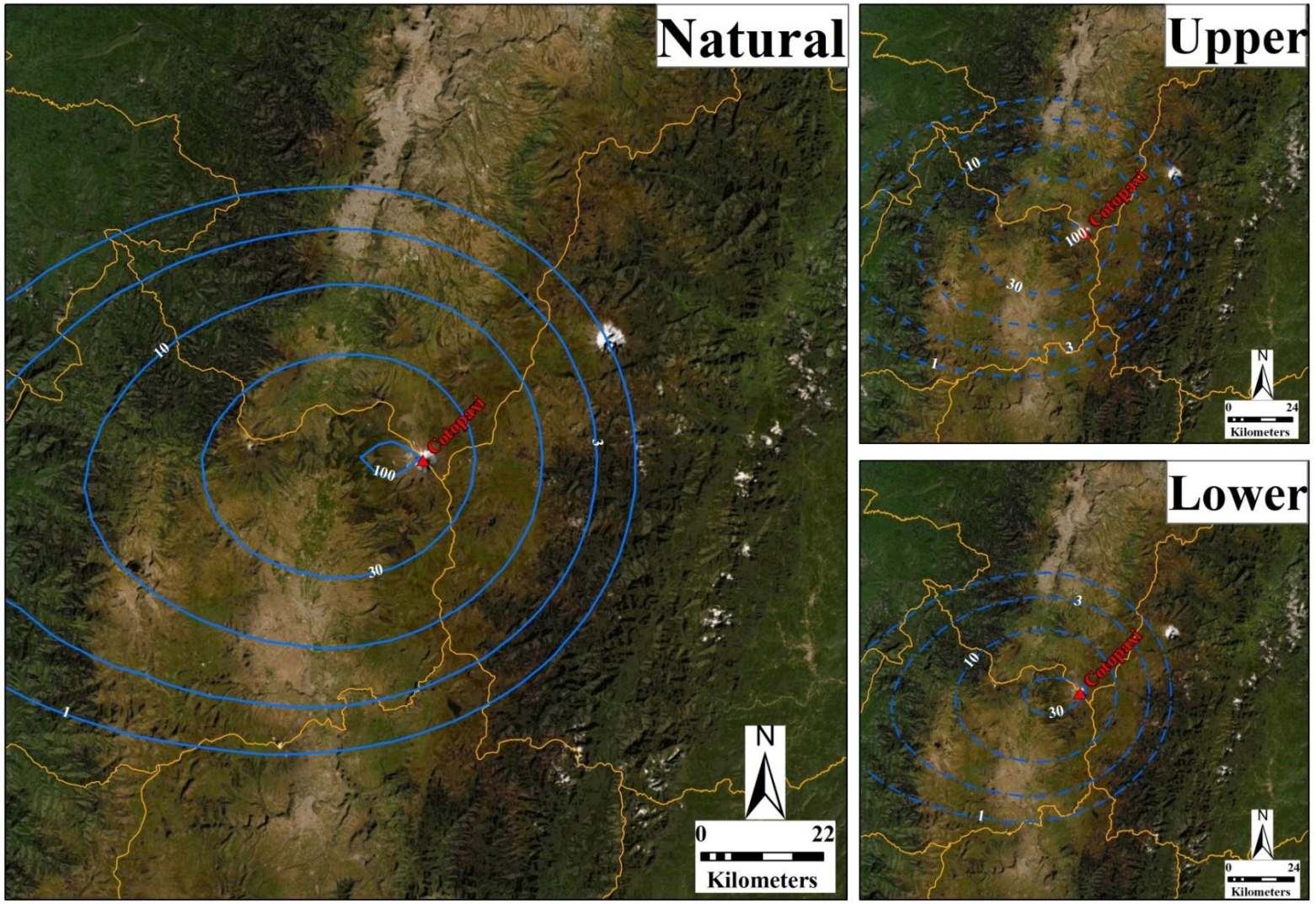

Figure S19. Cotopaxi volcano, Plinian rhyolitic eruption – Probabilistic map (50 %)

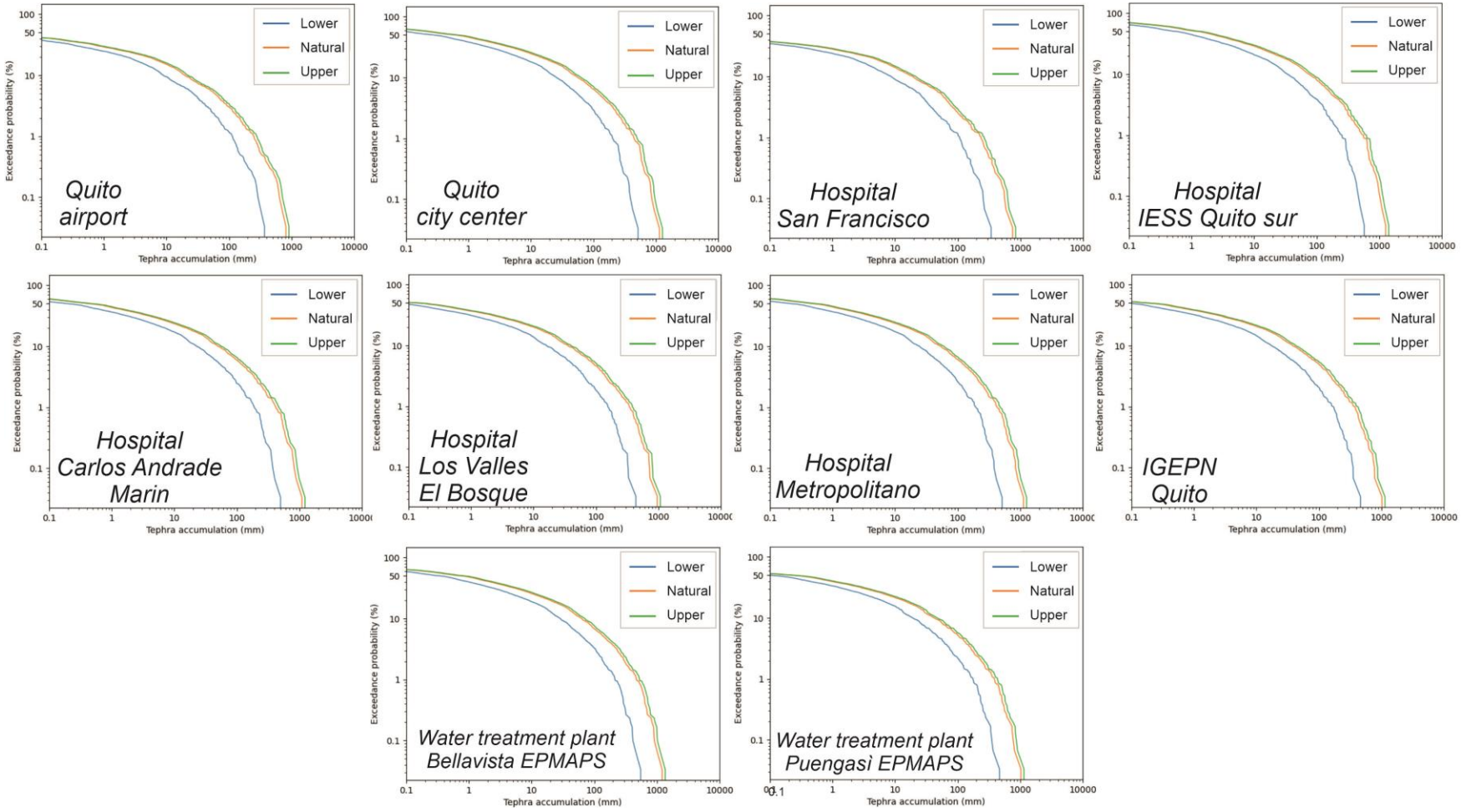

Figure S20. Cotopaxi volcano, Plinian rhyolitic eruption – Hazard curves

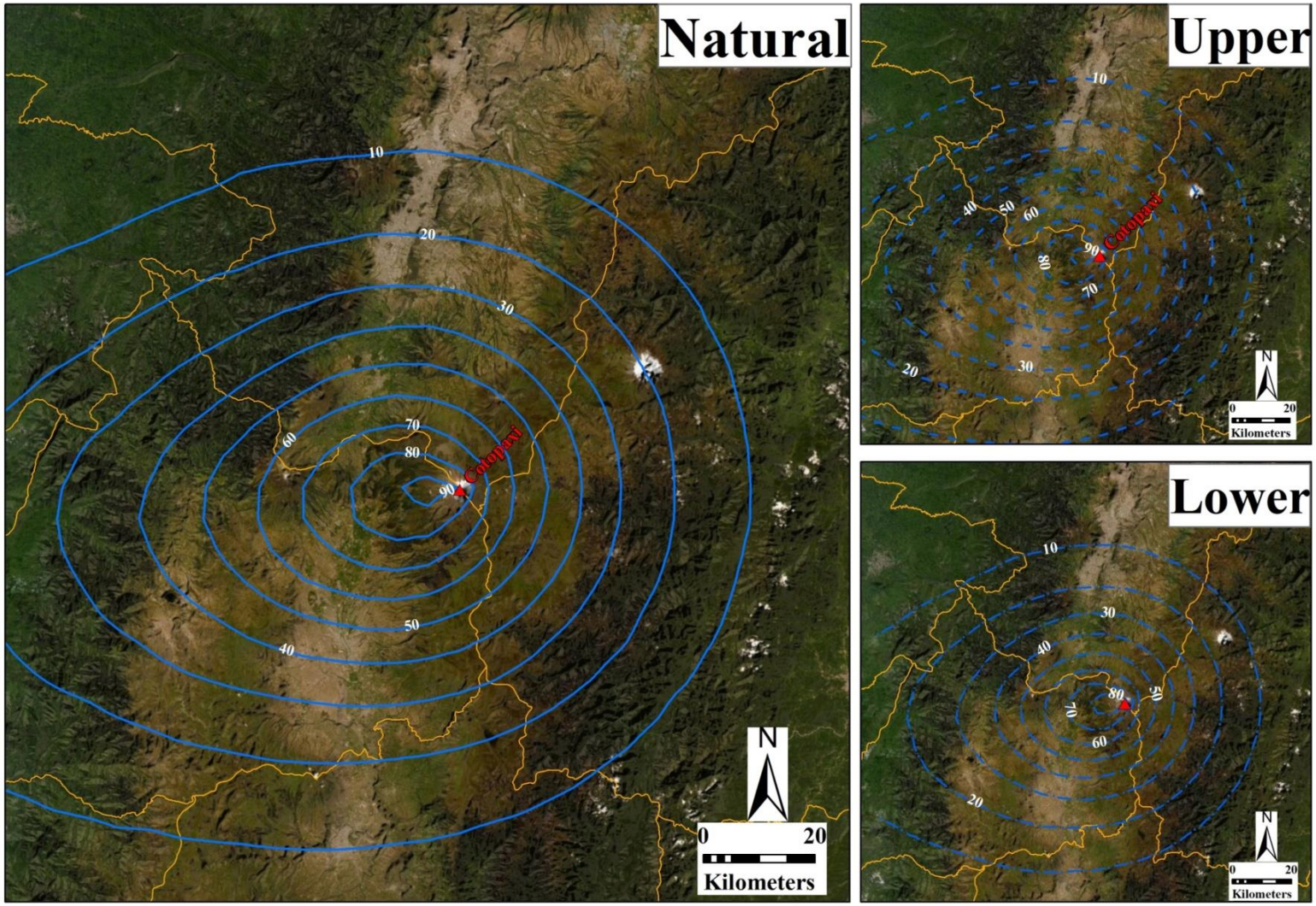

Figure S21. Cotopaxi volcano, sub-Plinian andesitic eruption – Probabilistic map (1 mm)

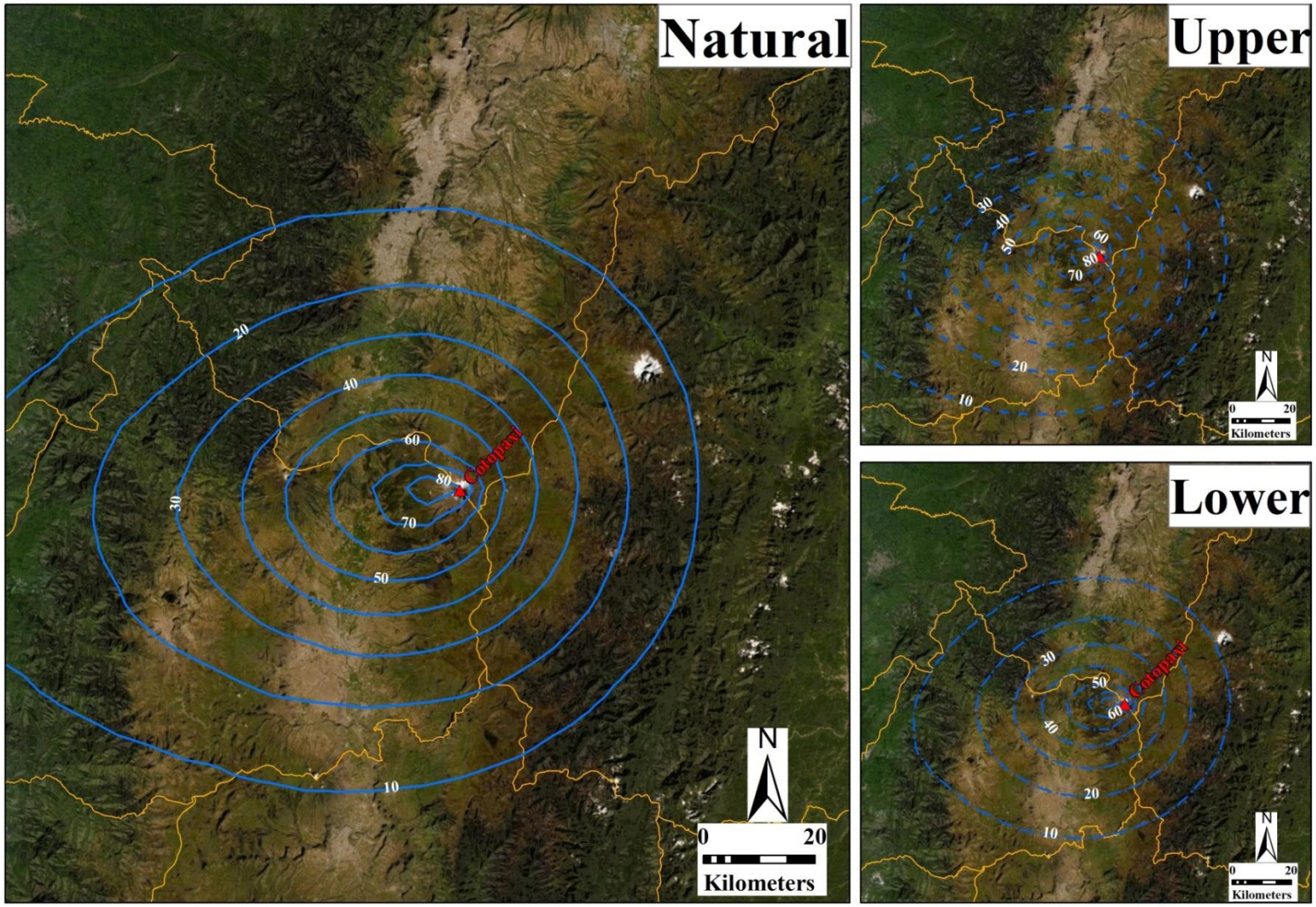

Figure S22. Cotopaxi volcano, sub-Plinian andesitic eruption – Probabilistic map (3 mm)

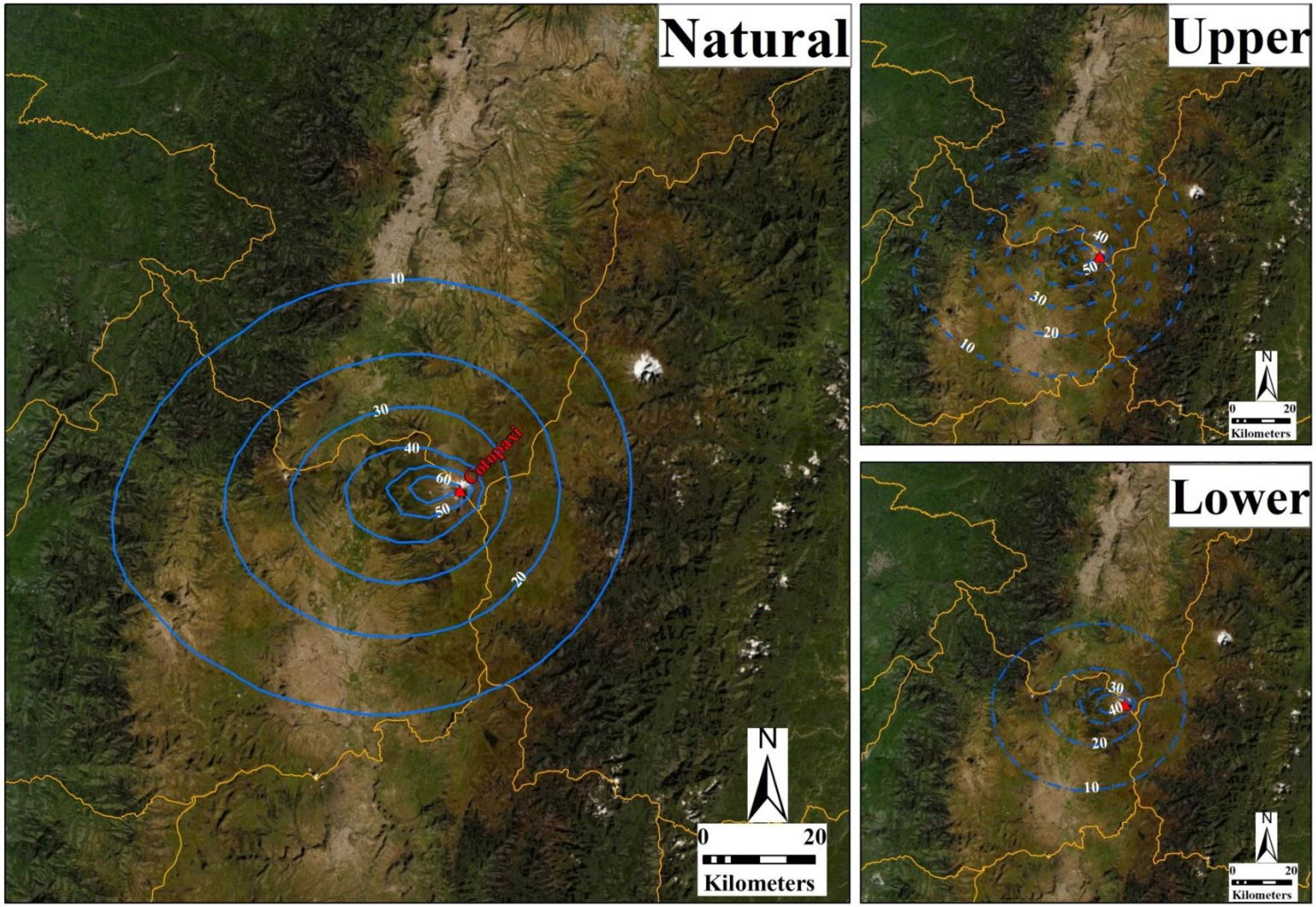

Figure S23. Cotopaxi volcano, sub-Plinian andesitic eruption – Probabilistic map (10 mm)

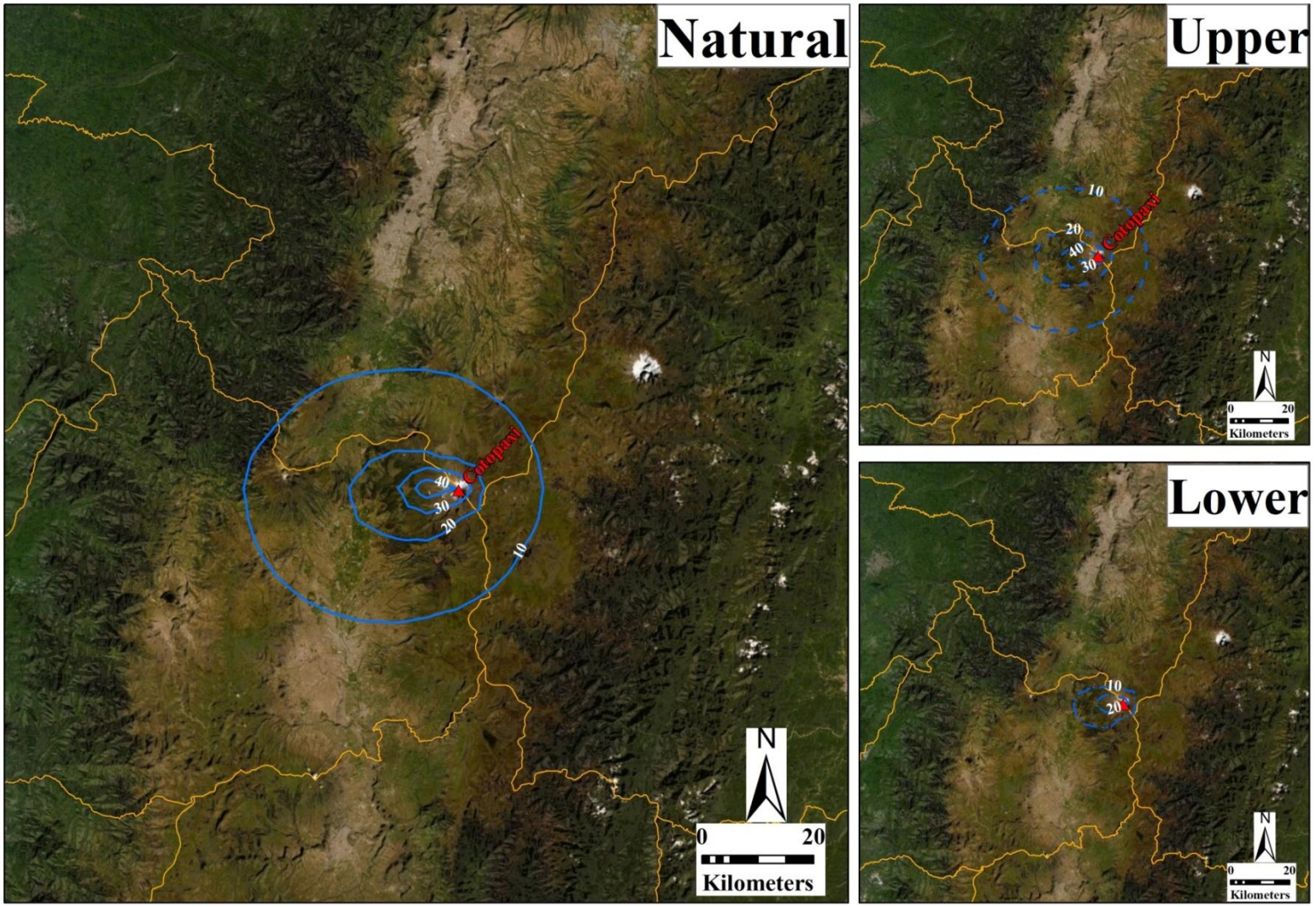

Figure S24. Cotopaxi volcano, sub-Plinian andesitic eruption – Probabilistic map (30 mm)

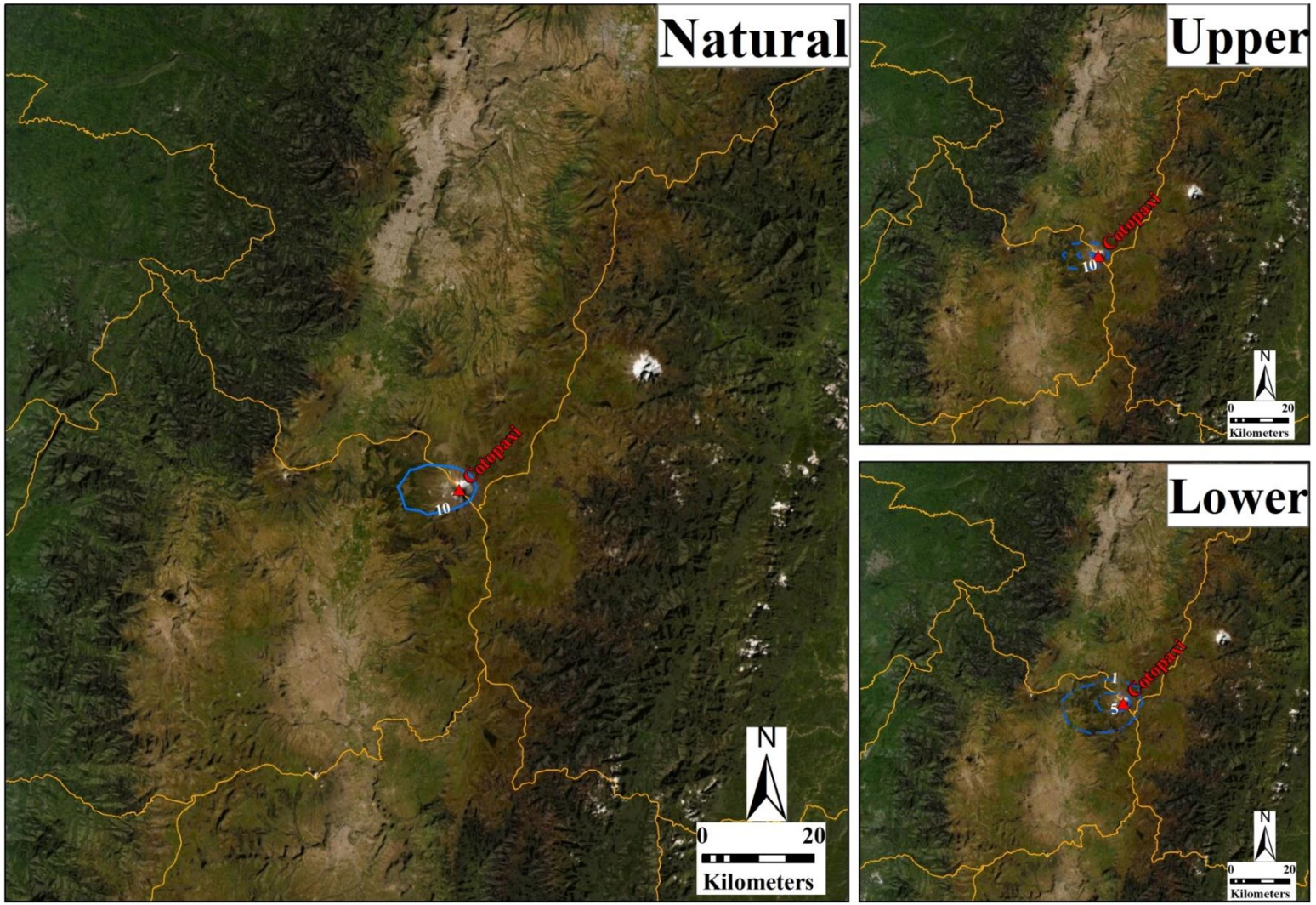

Figure S25. Cotopaxi volcano, sub-Plinian andesitic eruption – Probabilistic map (100 mm)

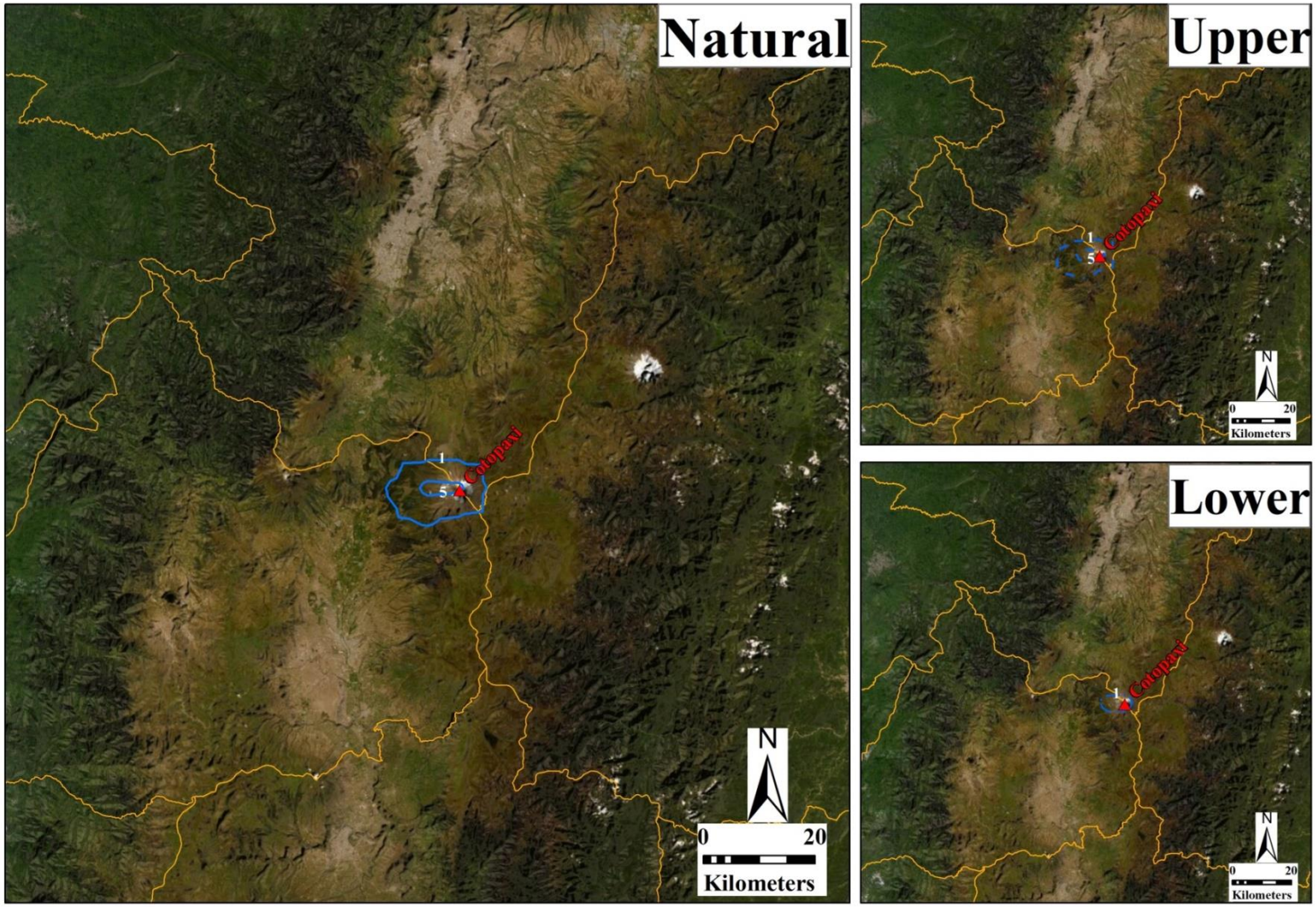

Figure S26. Cotopaxi volcano, sub-Plinian andesitic eruption – Probabilistic map (300 mm)

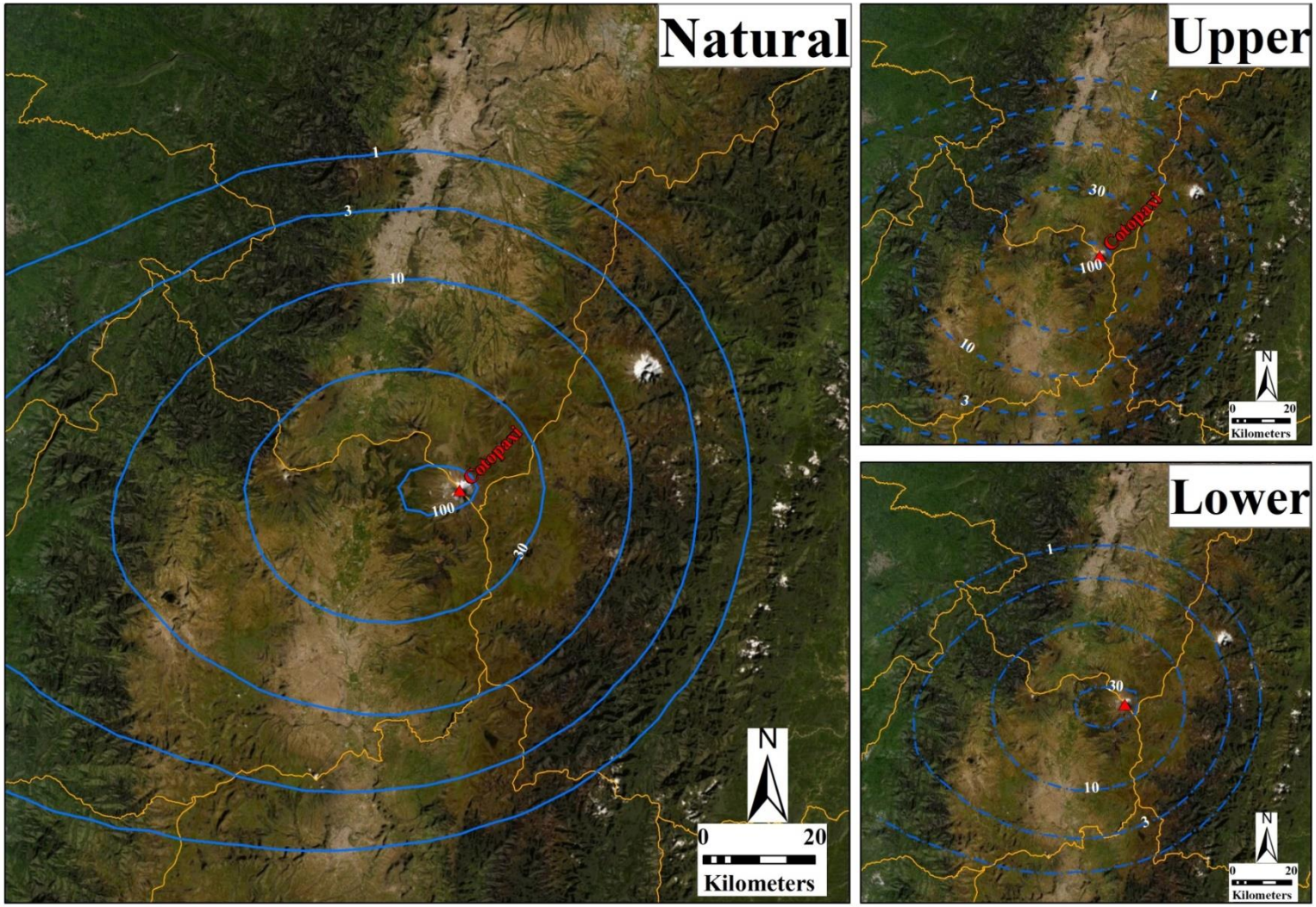

Figure S28. Cotopaxi volcano, sub-Plinian andesitic eruption – Isopach map (10 %)

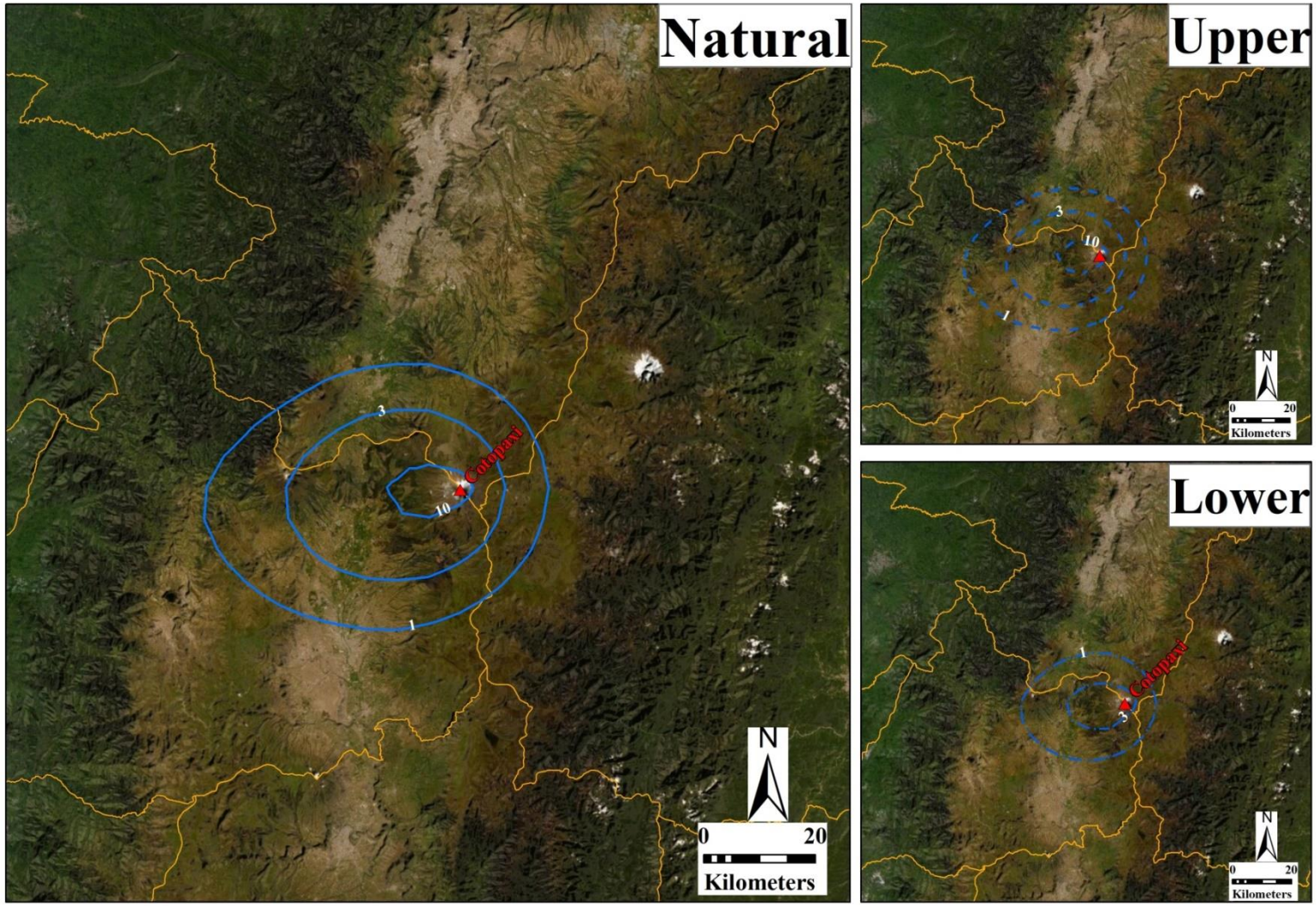

Figure S29. Cotopaxi volcano, sub-Plinian andesitic eruption – Probabilistic map (50 %)

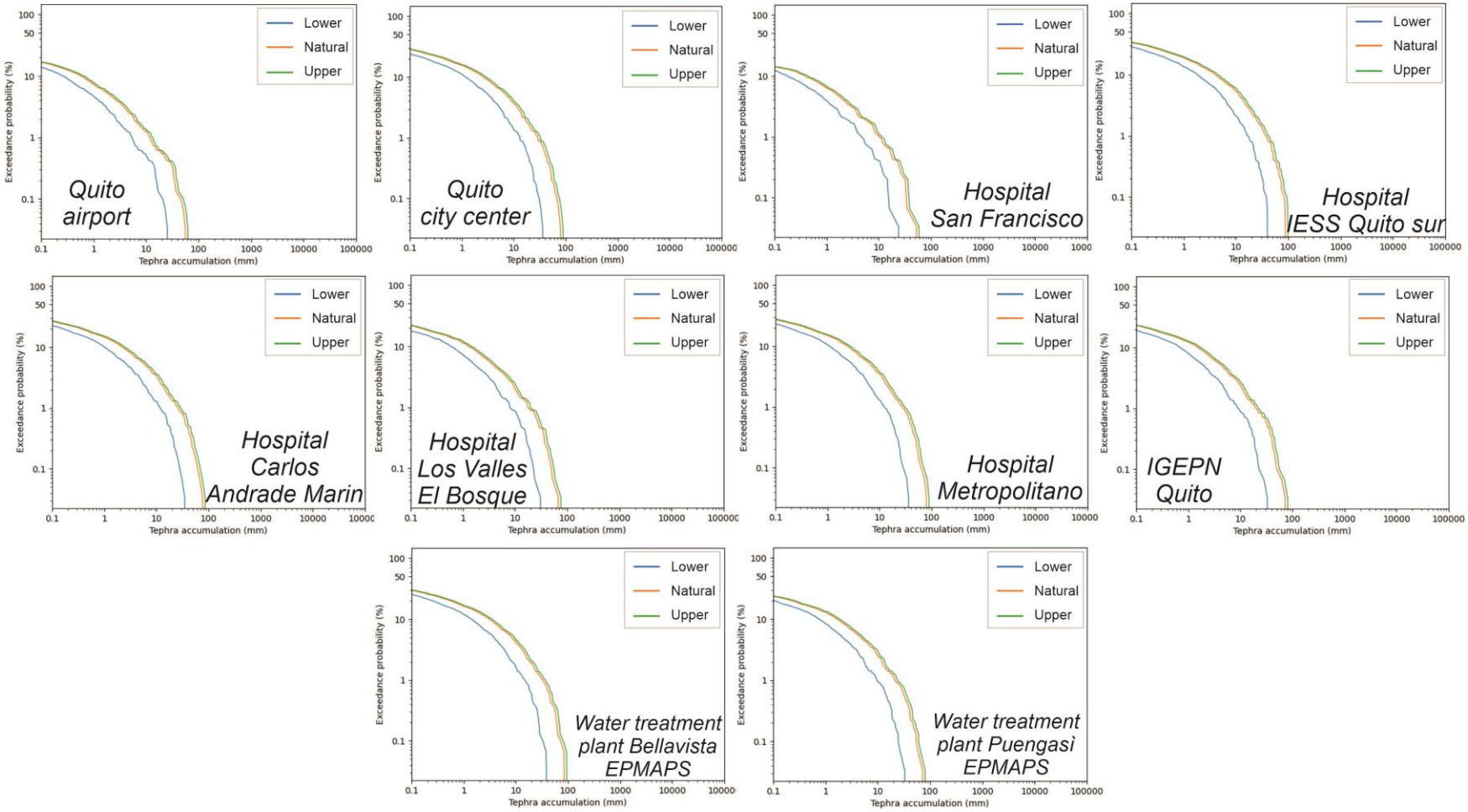

Figure S30. Cotopaxi eruption, sub-Plinian andesitic eruption – Hazard curves

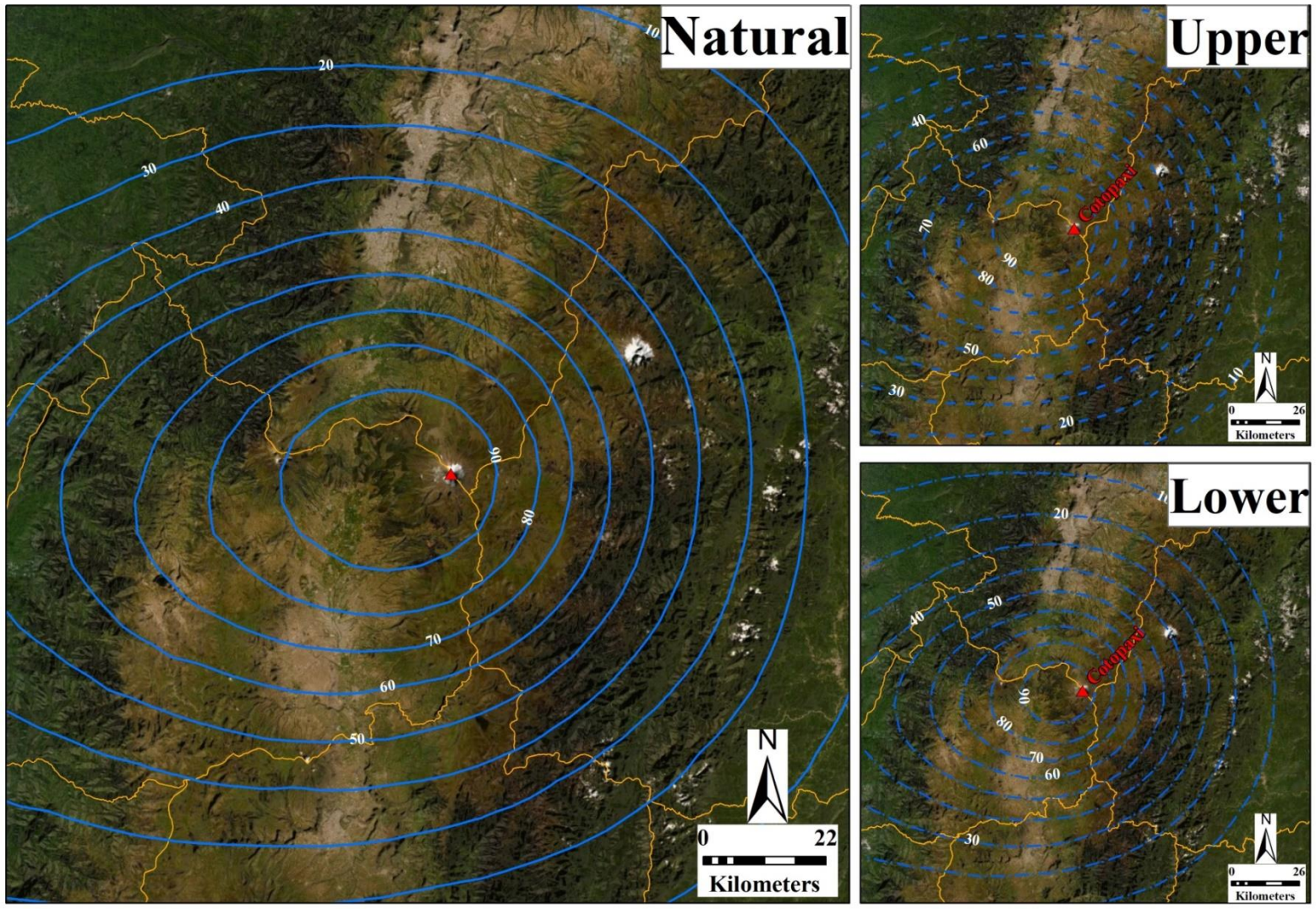

Figure S31. Cotopaxi volcano, Plinian andesitic eruption – Probabilistic map (1 mm)

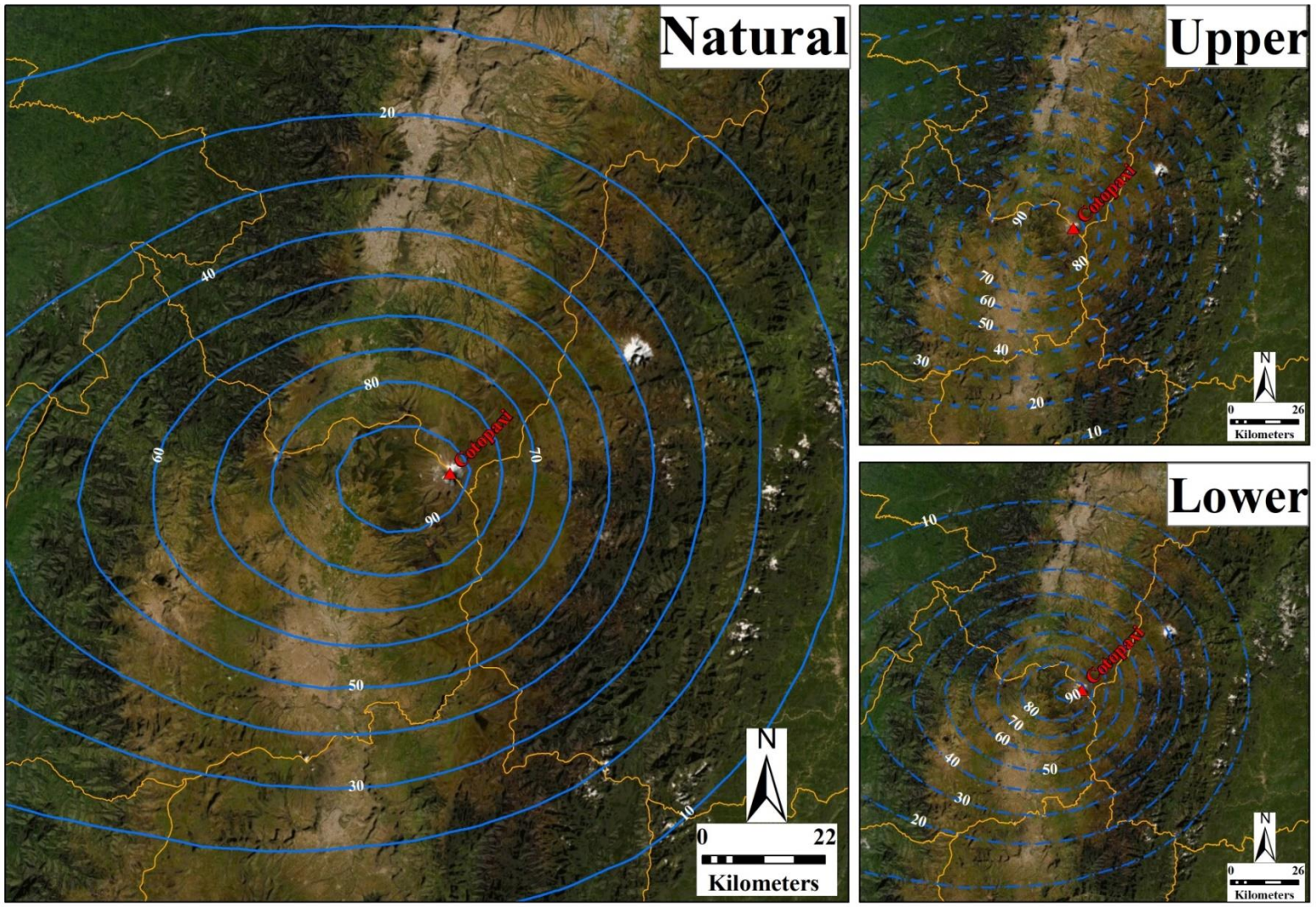

Figure S32. Cotopaxi volcano, Plinian andesitic eruption – Probabilistic map (3 mm)

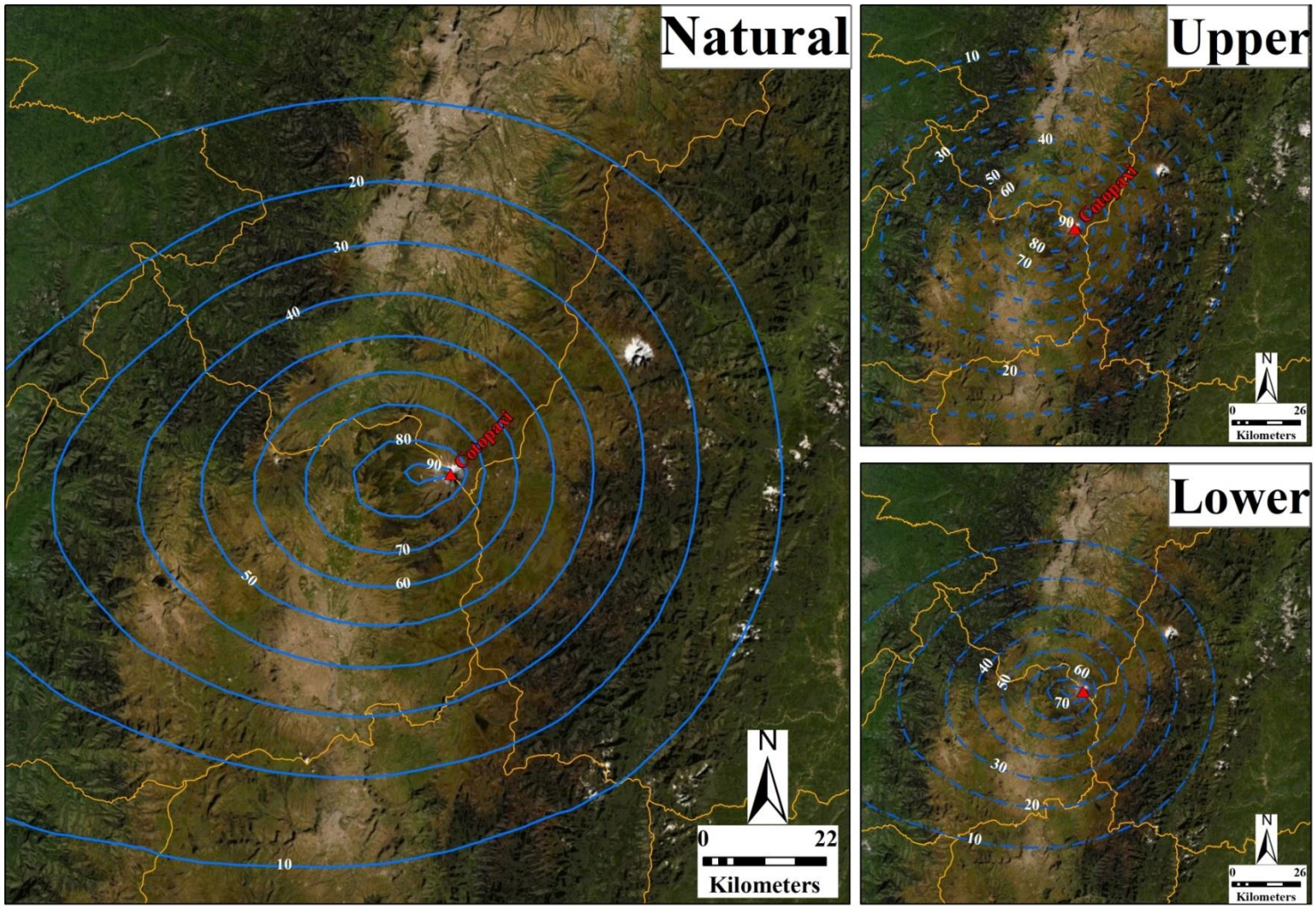

Figure S33. Cotopaxi volcano, Plinian andesitic eruption – Probabilistic map (10 mm)

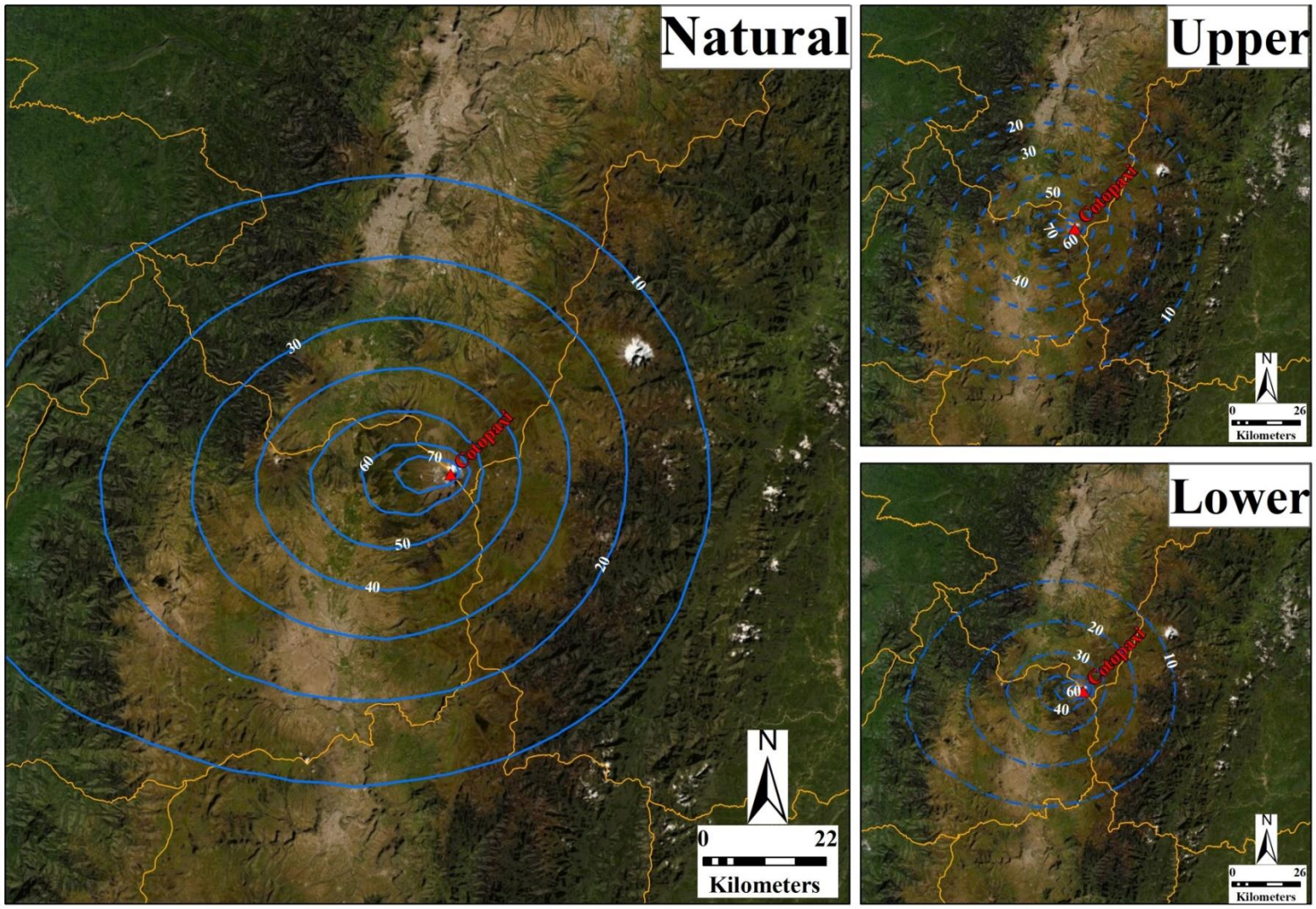

Figure S34. Cotopaxi volcano, Plinian andesitic eruption – Probabilistic map (30 mm)

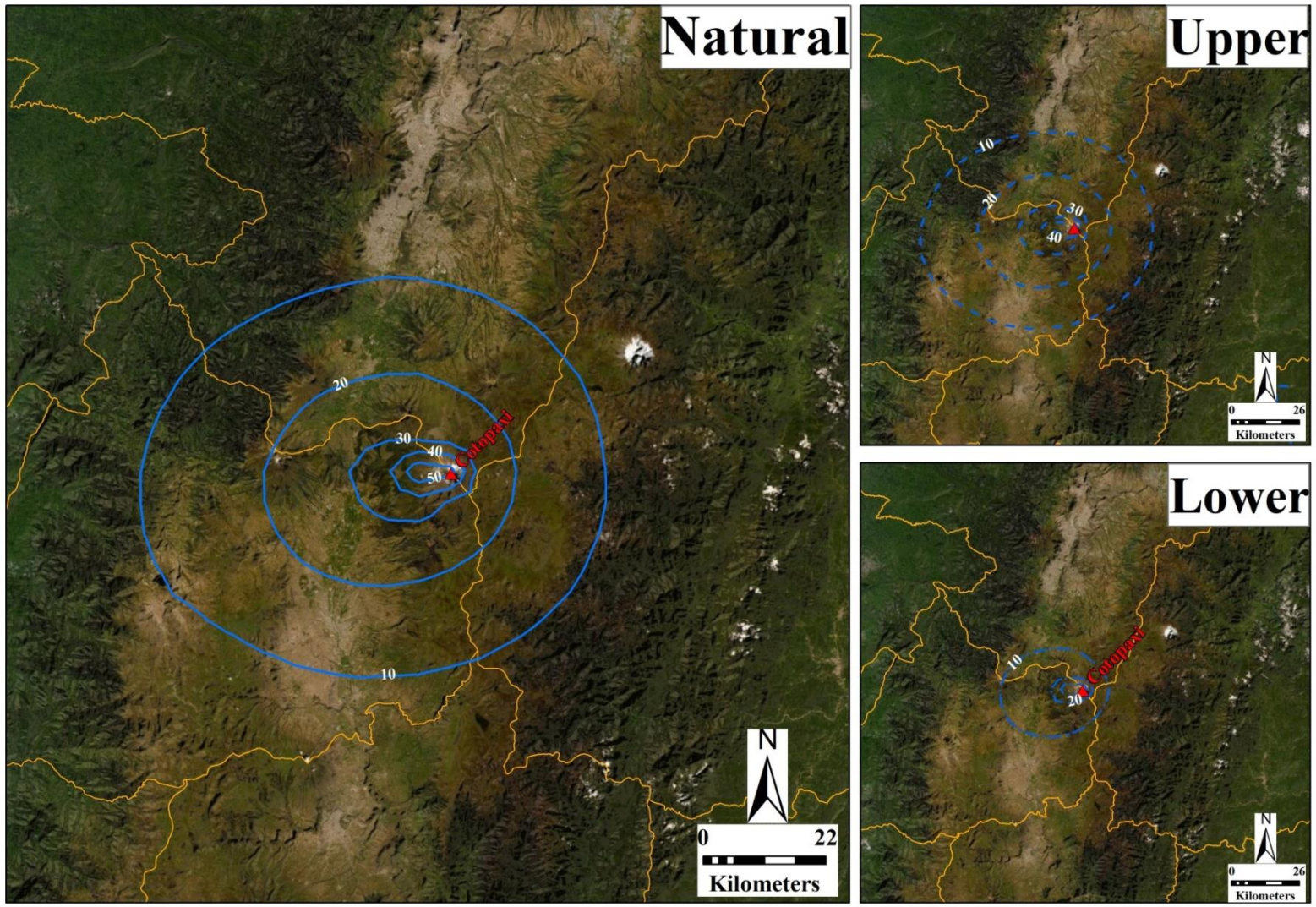

Figure S35. Cotopaxi volcano, Plinian andesitic eruption – Probabilistic map (100 mm)

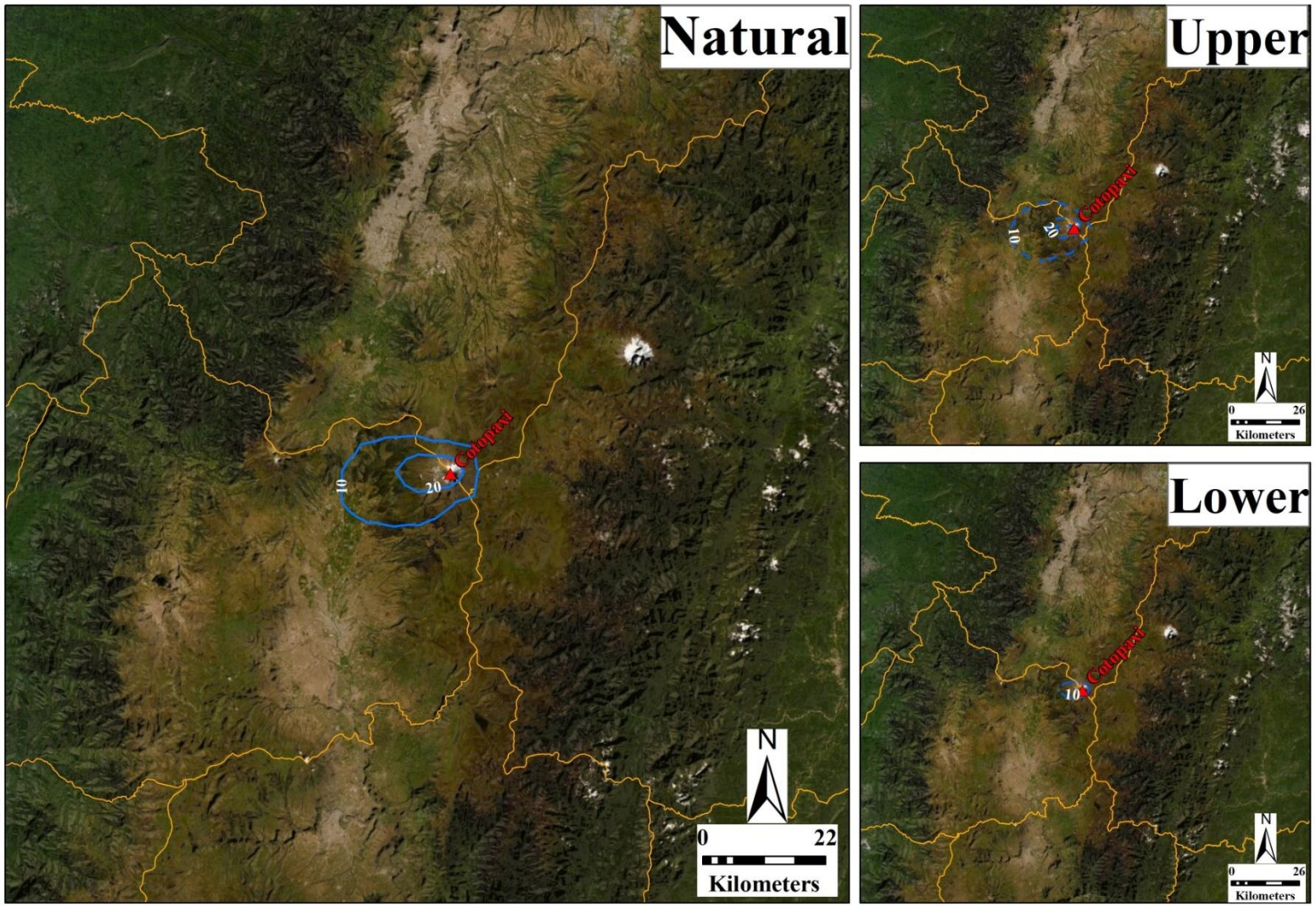

Figure S36. Cotopaxi volcano, Plinian andesitic eruption – Probabilistic map (300 mm)

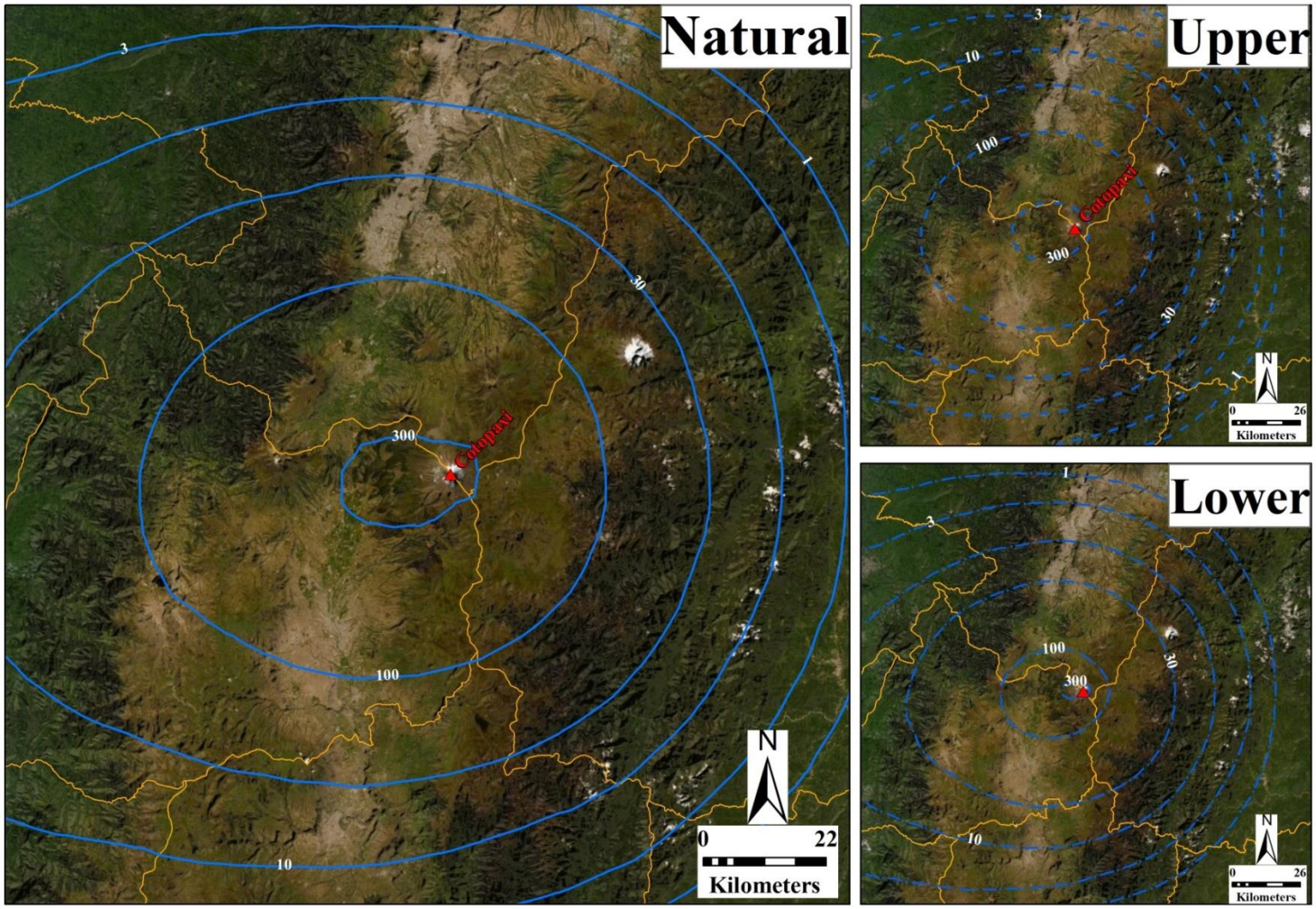

Figure S37. Cotopaxi volcano, Plinian andesitic eruption – Isopach map (10 %)

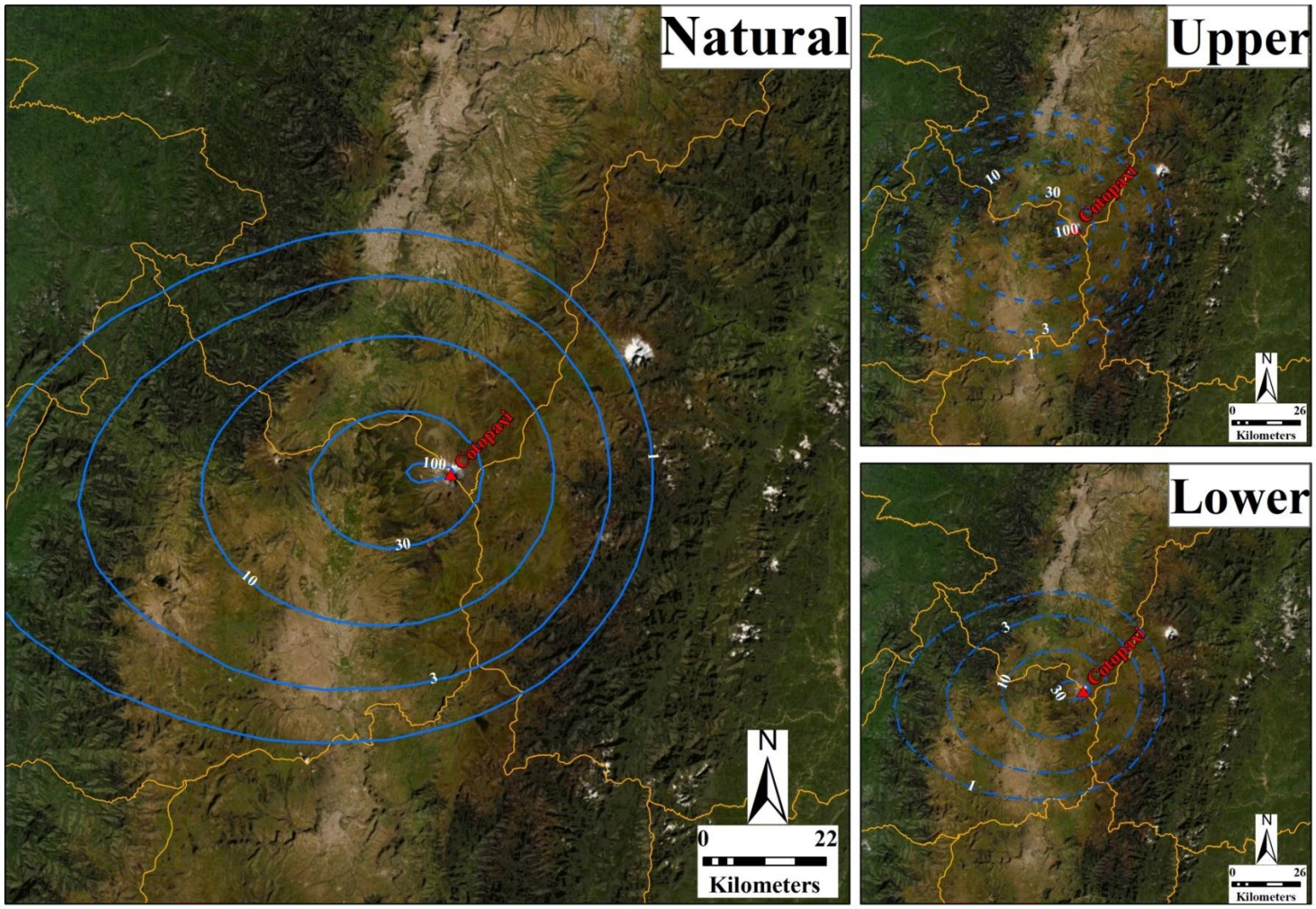

Figure S38. Cotopaxi volcano, Plinian andesitic eruption – Probabilistic map (50 %)

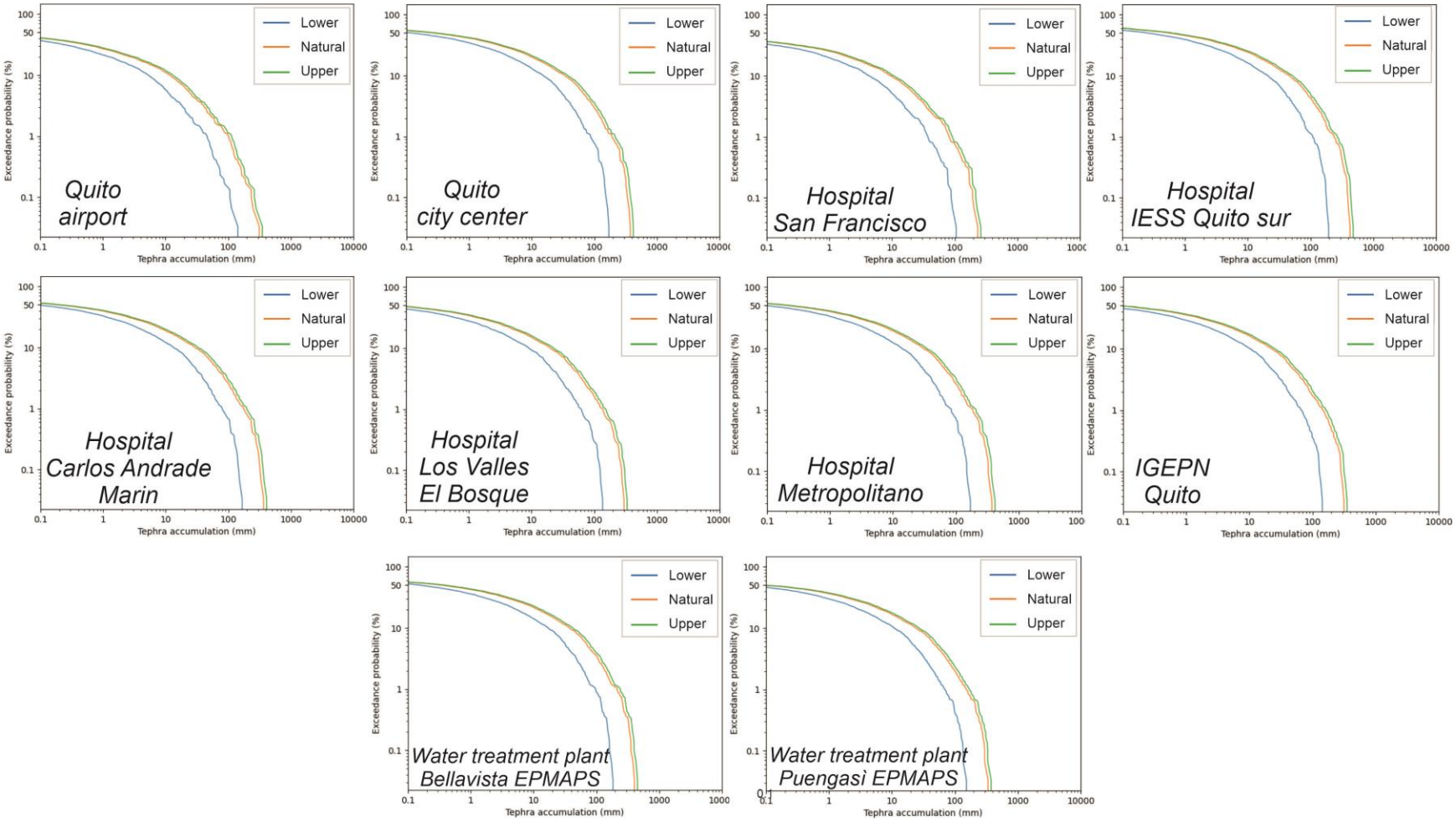

Figure S39. Cotopaxi volcano, Plinian andesitic eruption – Hazard curves

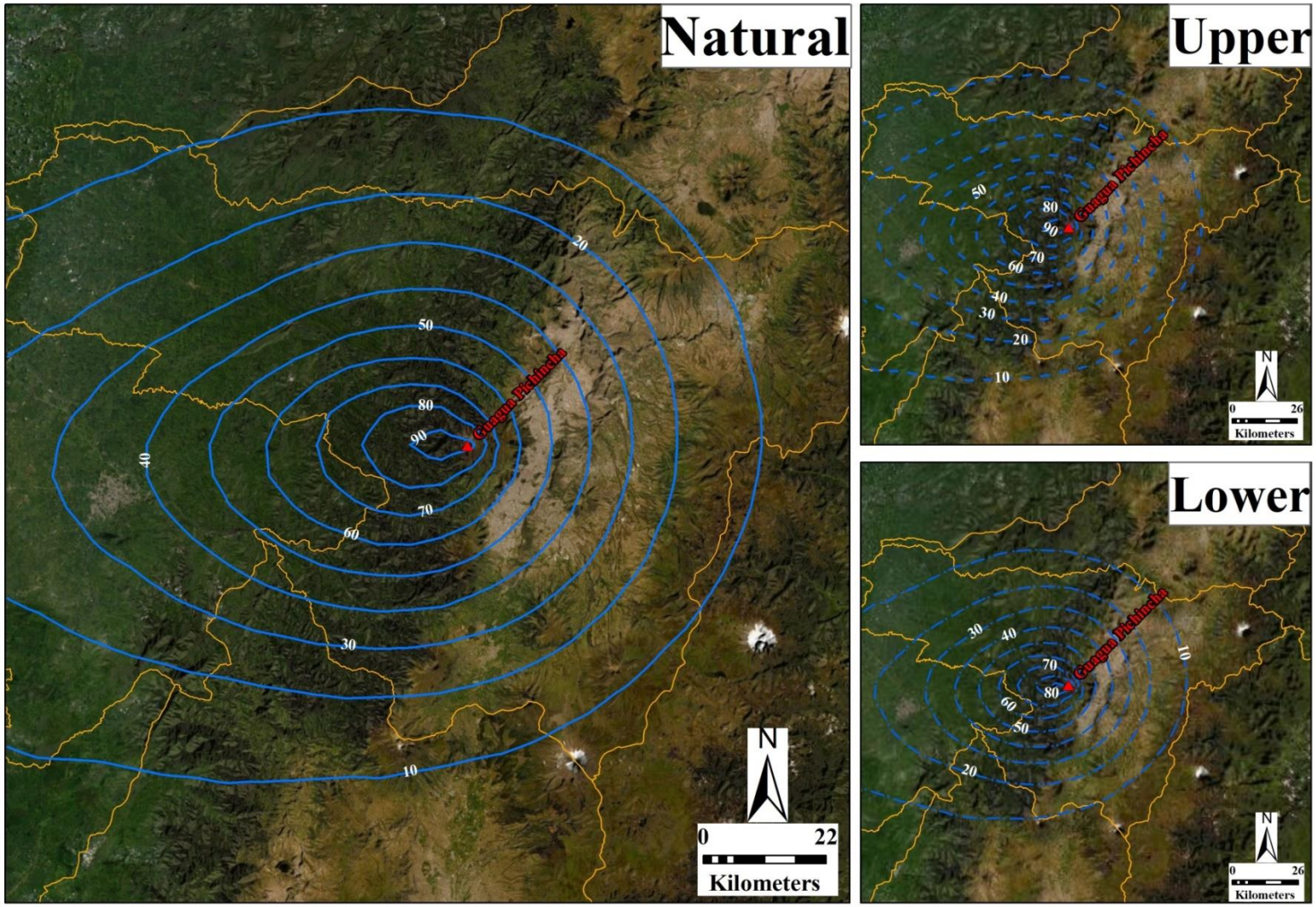

Figure S40. Guagua Pichincha volcano, sub-Plinian eruption – Probabilistic map (1 mm)

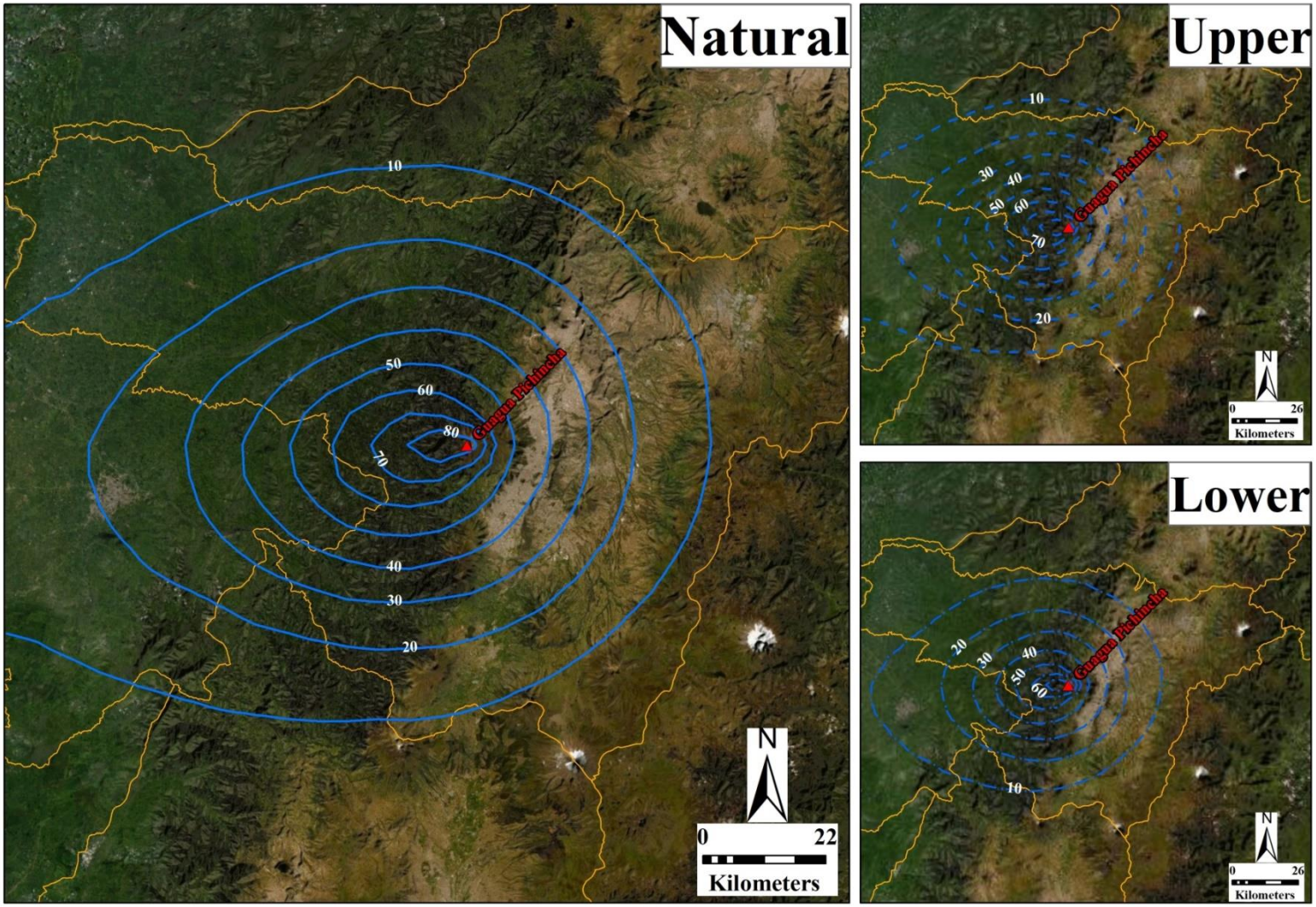

Figure S41. Guagua Pichincha volcano, sub-Plinian eruption – Probabilistic map (3 mm)

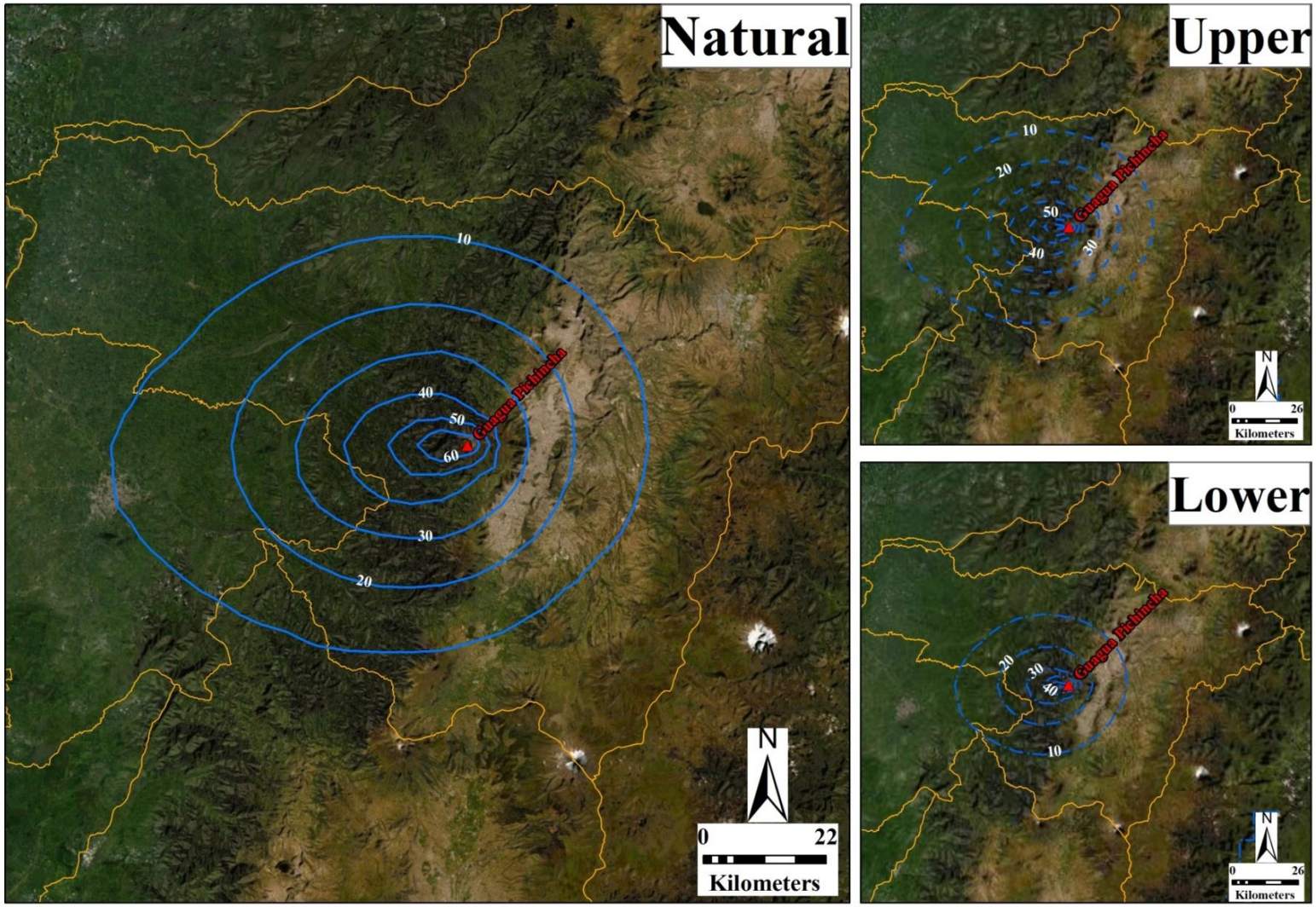

Figure S42. Guagua Pichincha volcano, sub-Plinian eruption – Probabilistic map (10 mm)

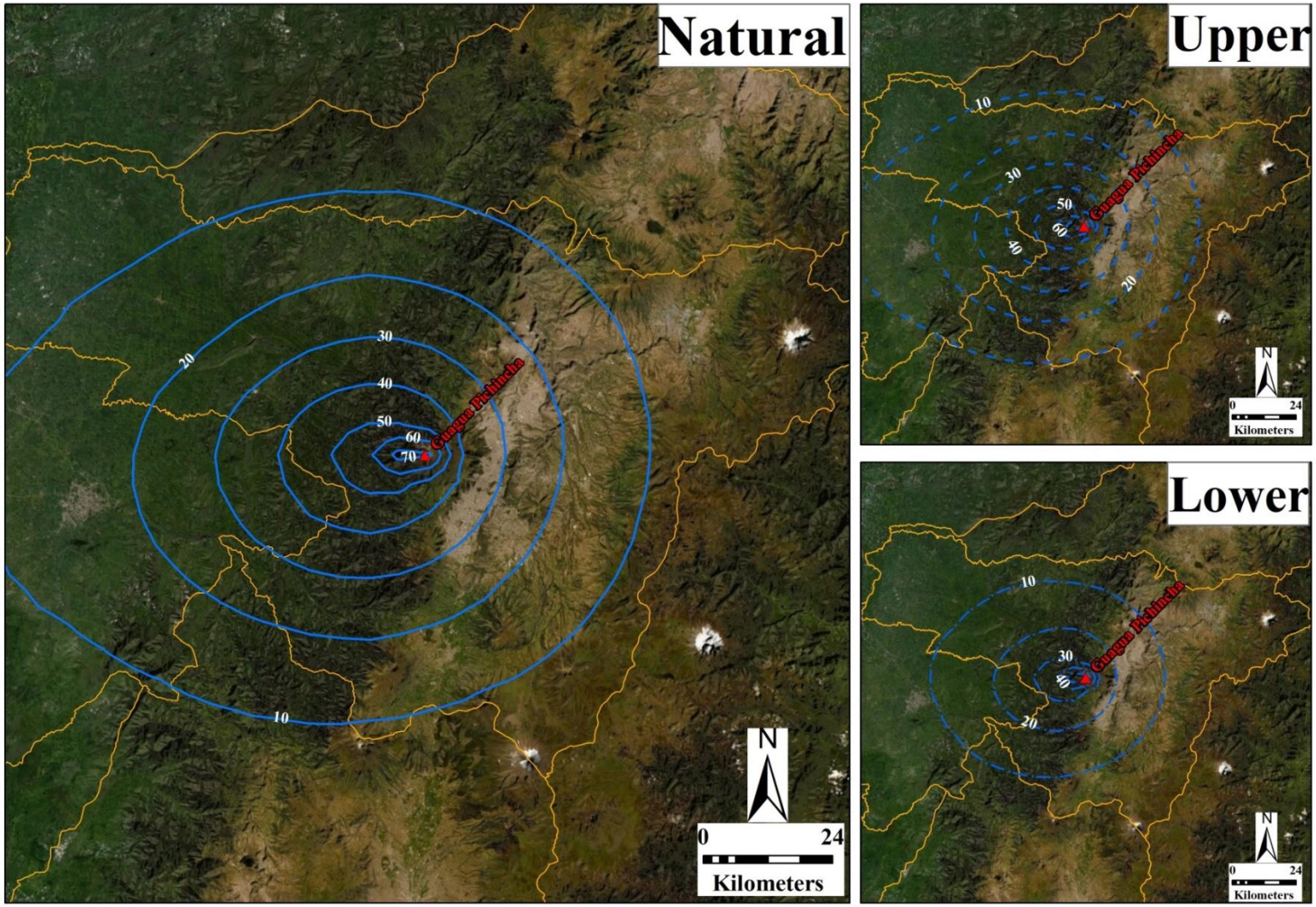

Figure S43. Guagua Pichincha volcano, sub-Plinian eruption – Probabilistic map (30 mm)

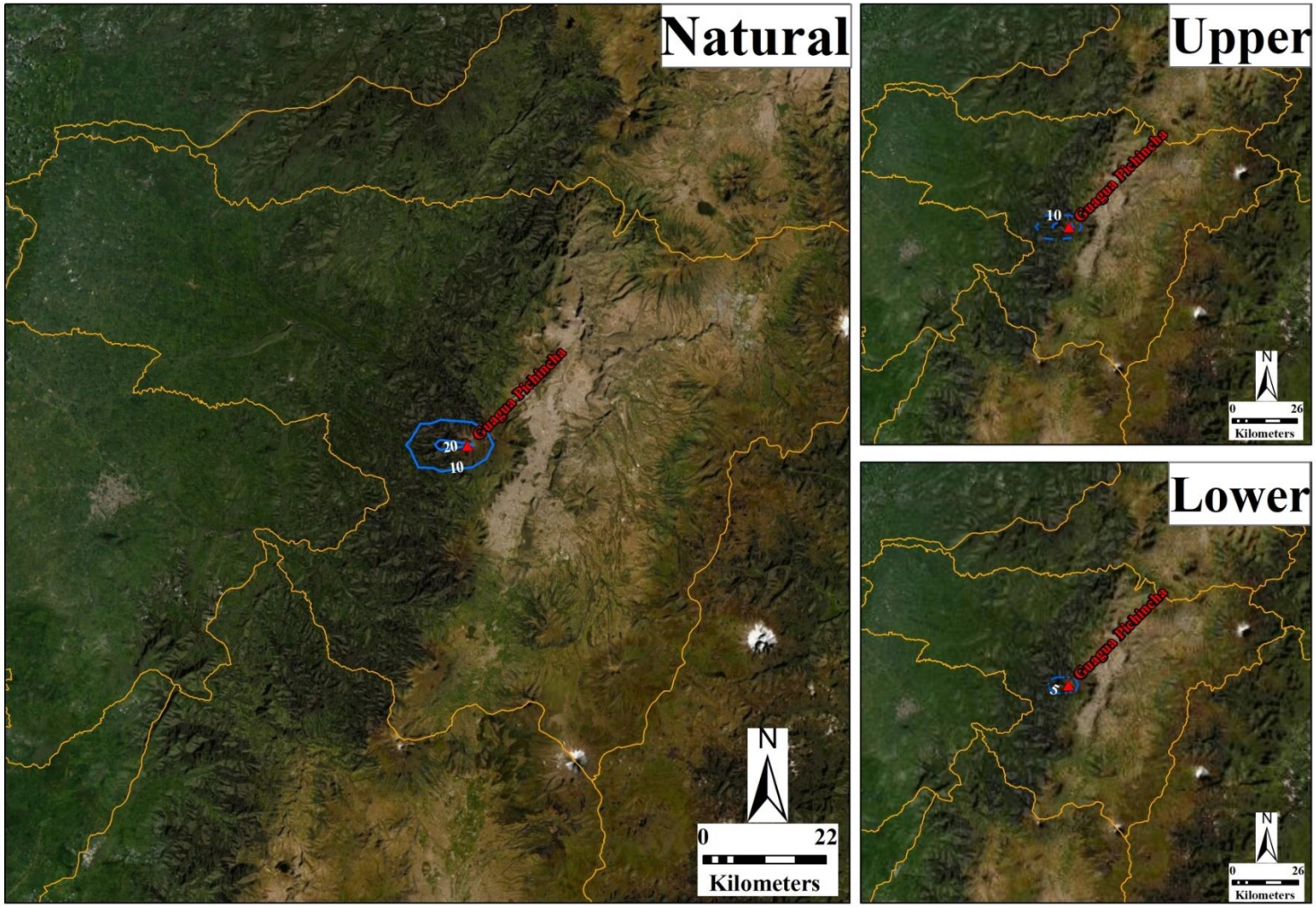

Figure S44. Guagua Pichincha volcano, sub-Plinian eruption – Probabilistic map (100 mm)

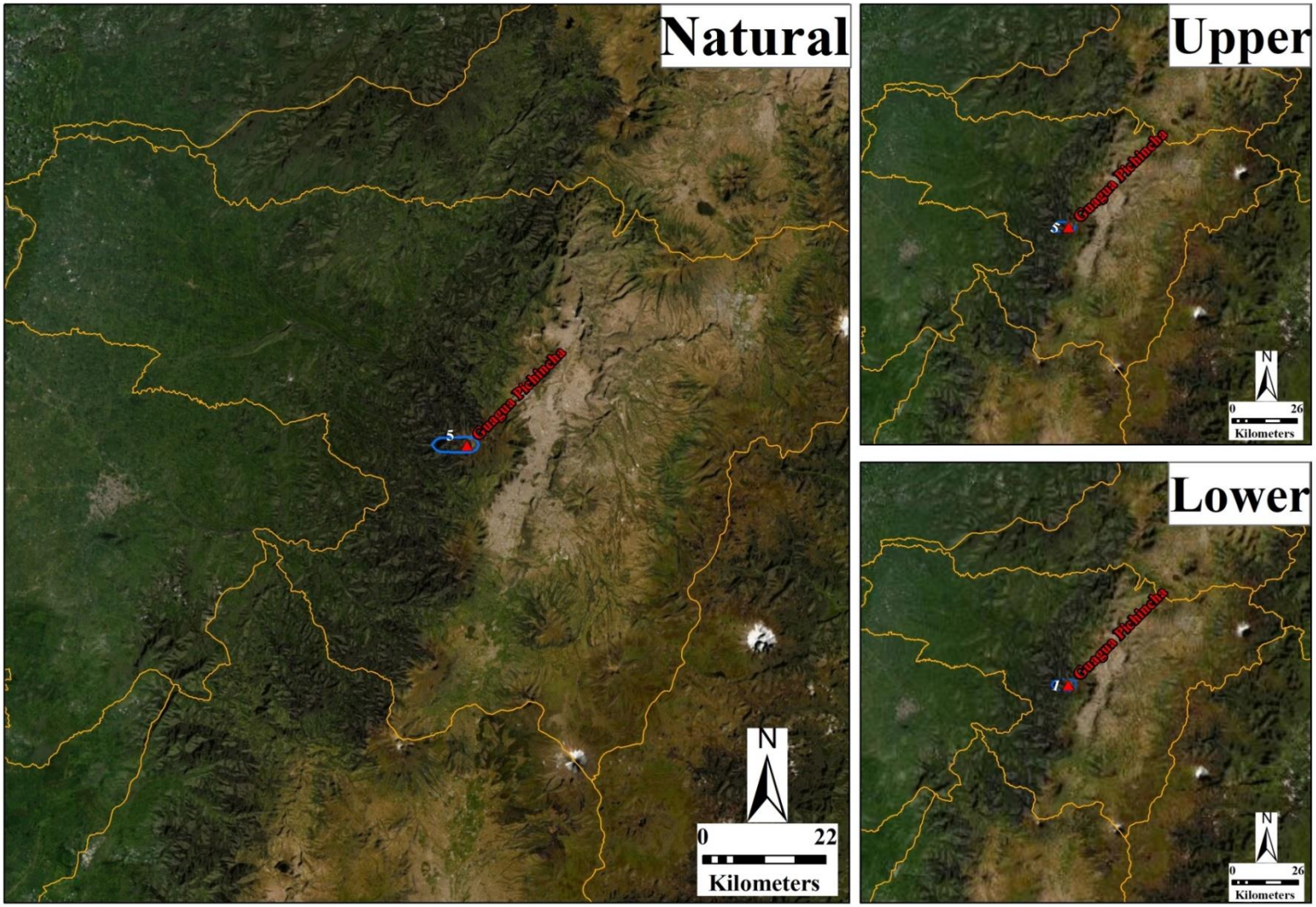

Figure S45. Guagua Pichincha volcano, sub-Plinian eruption – Probabilistic map (300 mm)

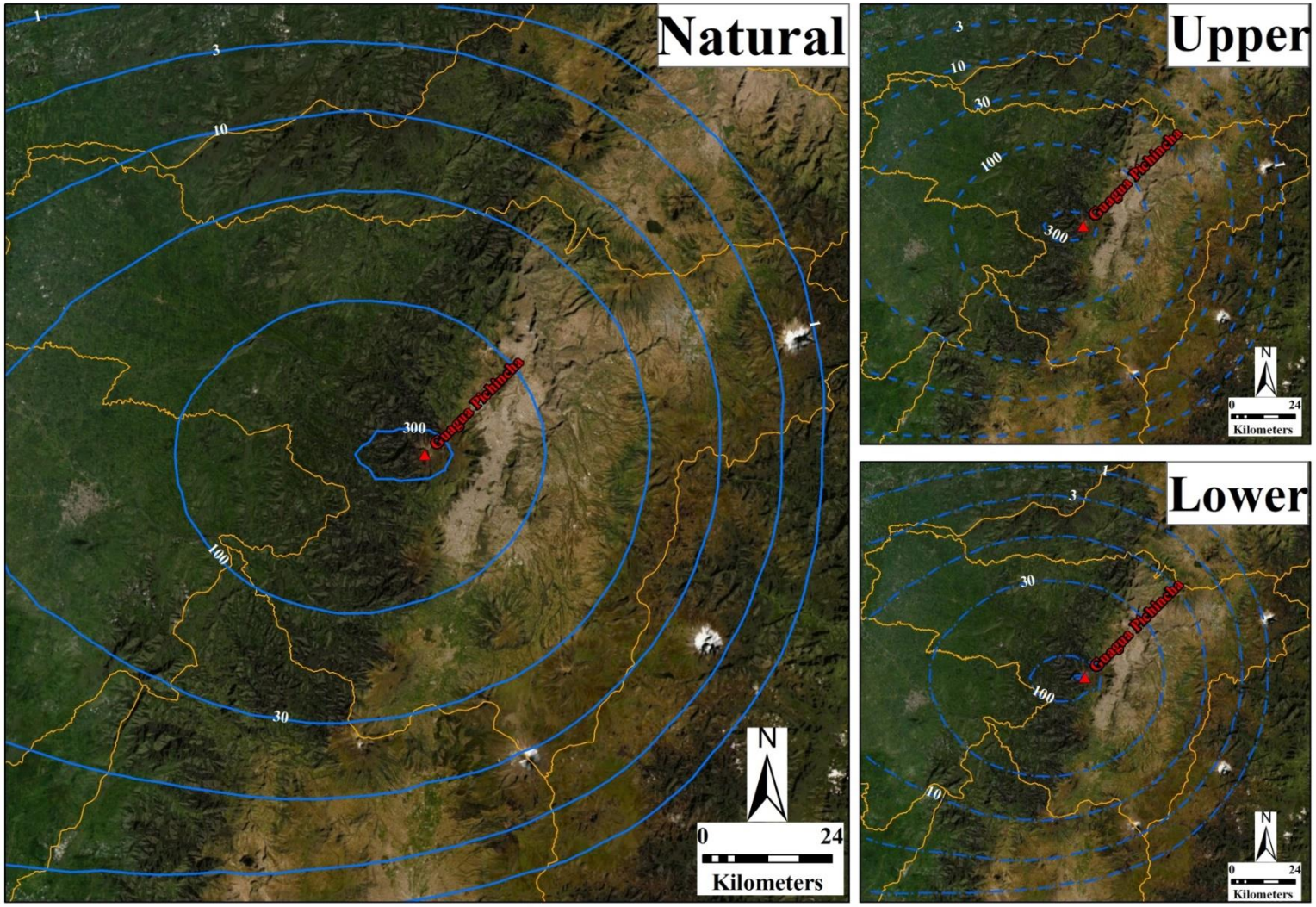

Figure S46. Guagua Pichincha volcano, sub-Plinian eruption – Isopach map (10 %)

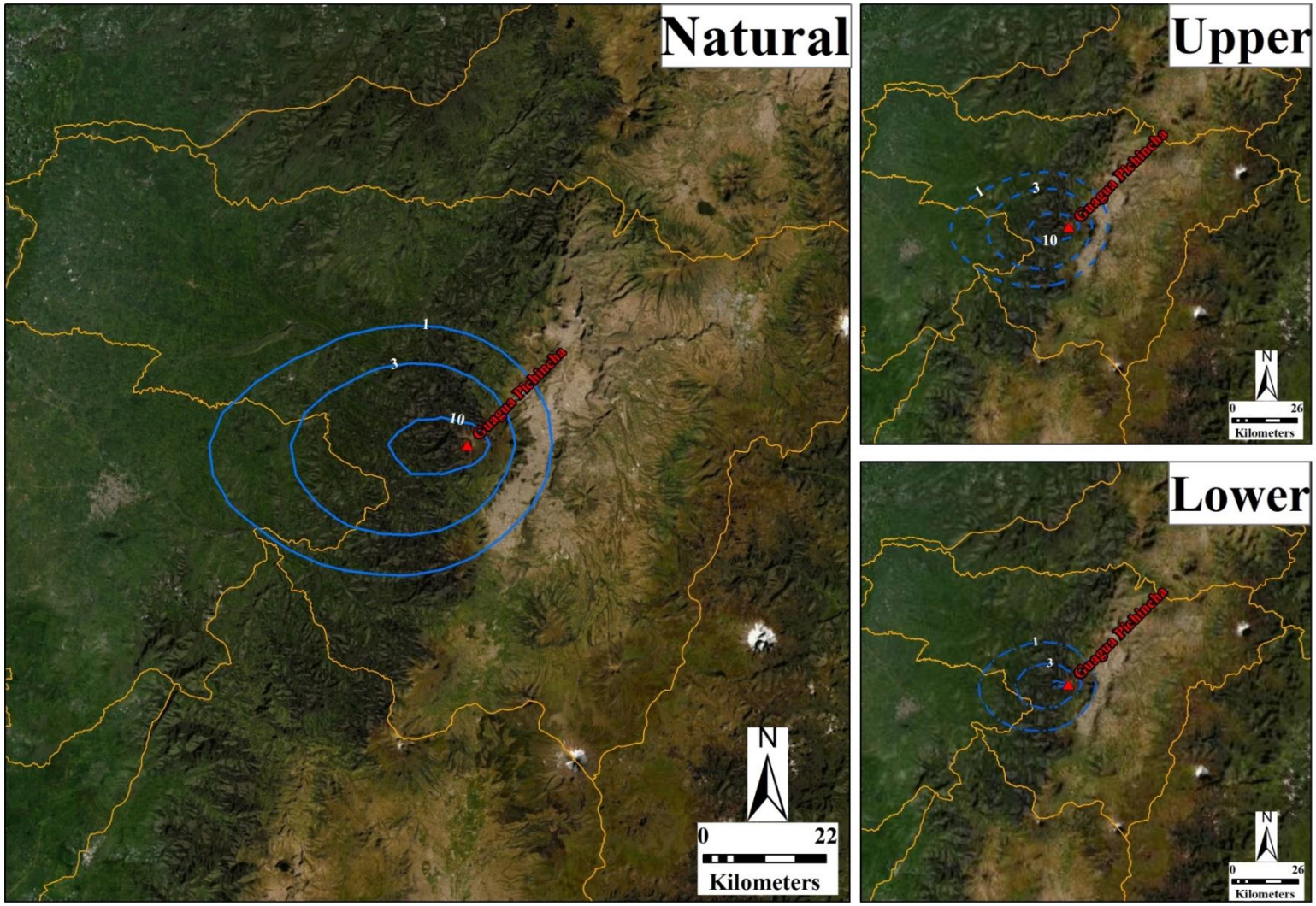

Figure S47. Guagua Pichincha volcano, sub-Plinian eruption – Isopach map (50 %)

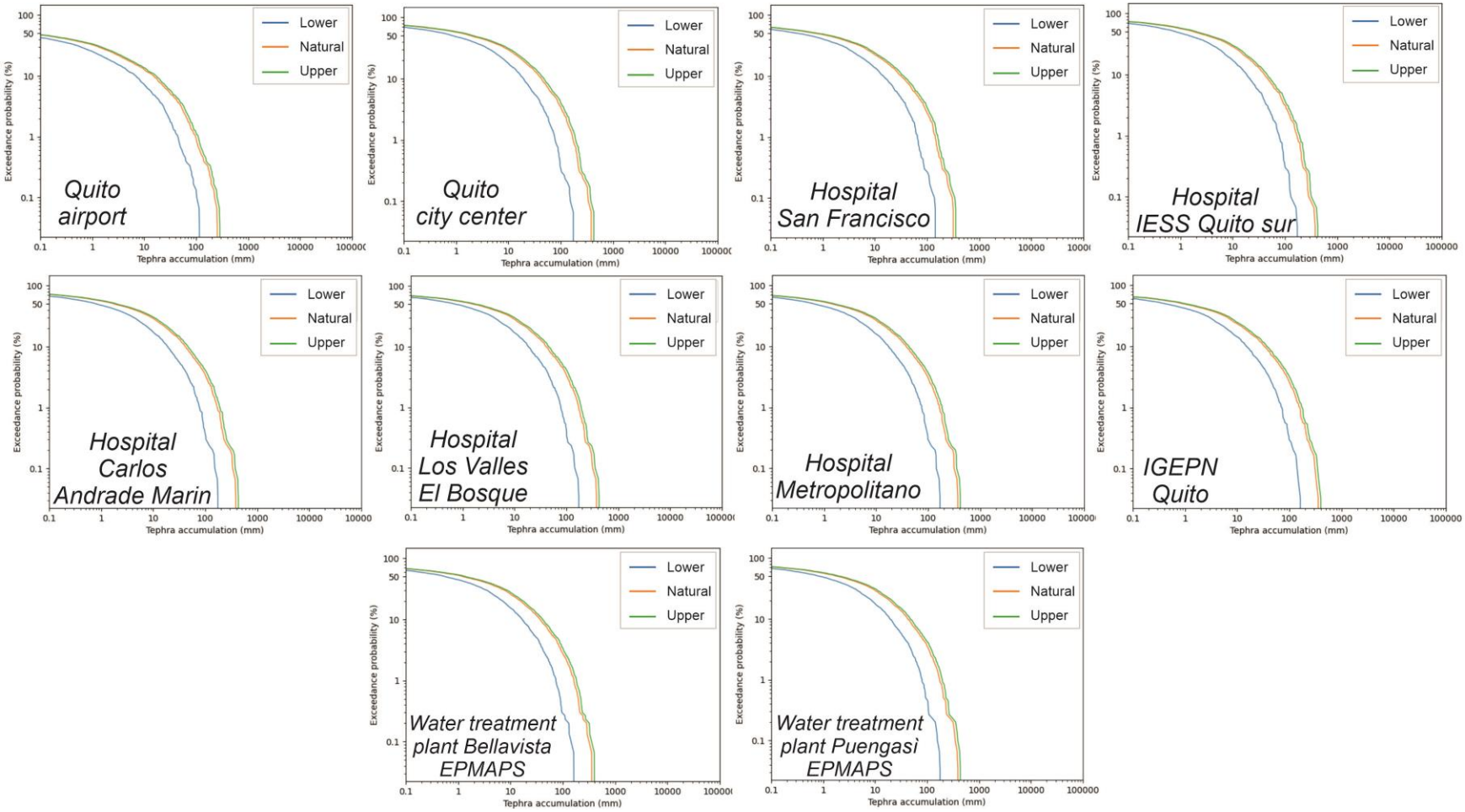

Figure S48. Guagua Pichincha volcano, sub-Plinian eruption – Hazard curves

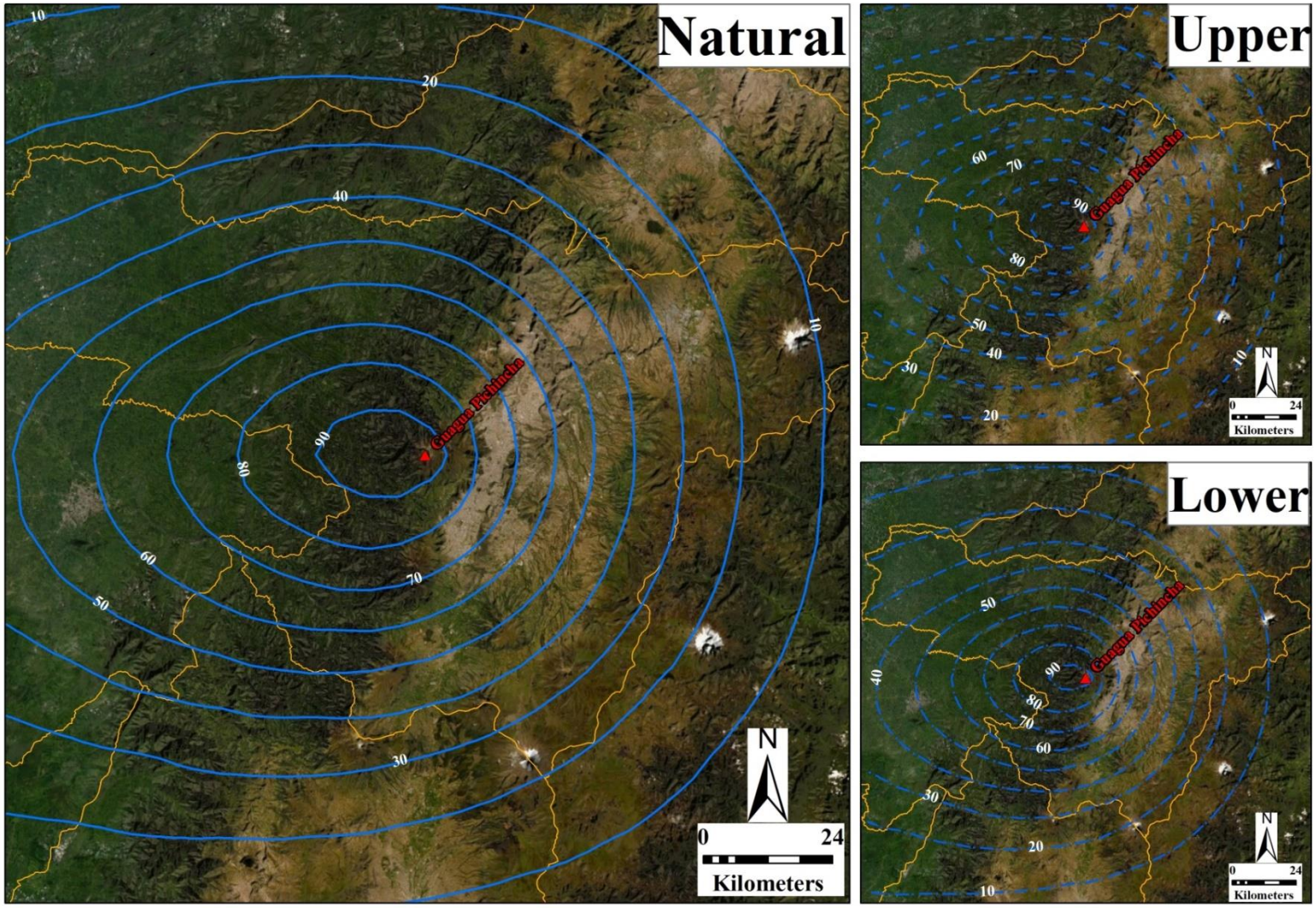

Figure S49. Guagua Pichincha volcano, Plinian eruption – Probabilistic map (1 mm)

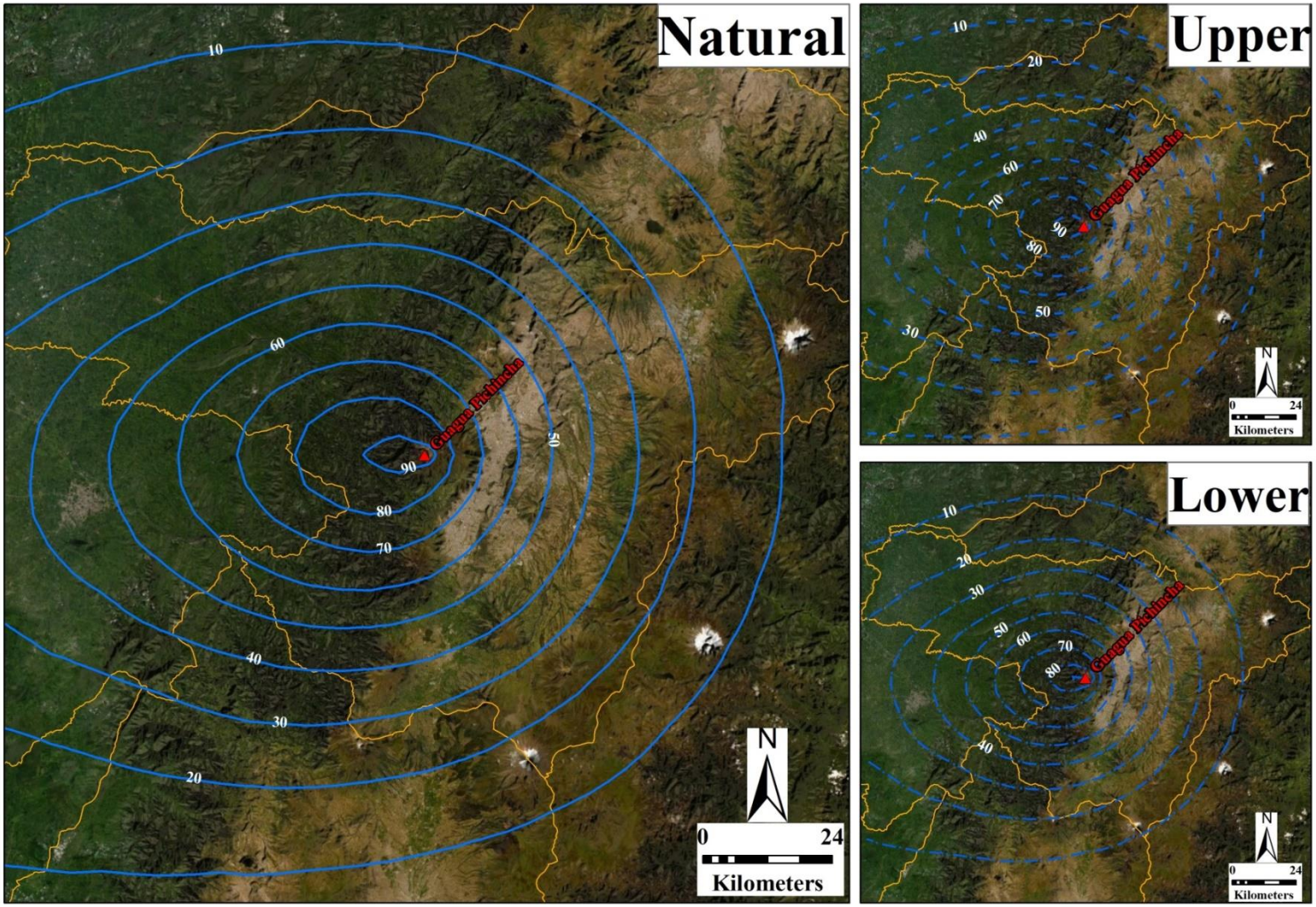

Figure S50. Guagua Pichincha volcano, Plinian eruption – Probabilistic map (3 mm)

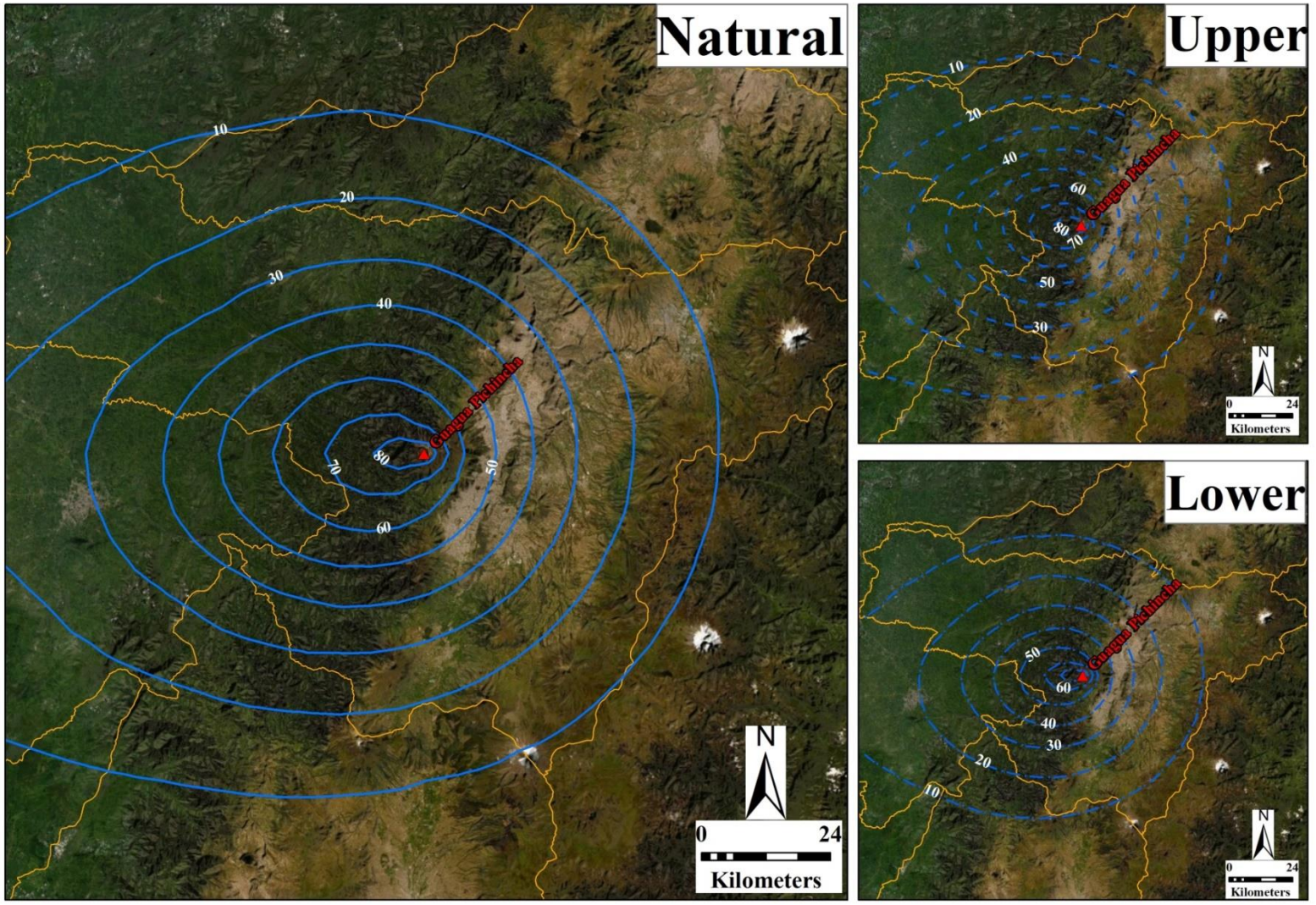

Figure S51. Guagua Pichincha volcano, Plinian eruption – Probabilistic map (10 mm)

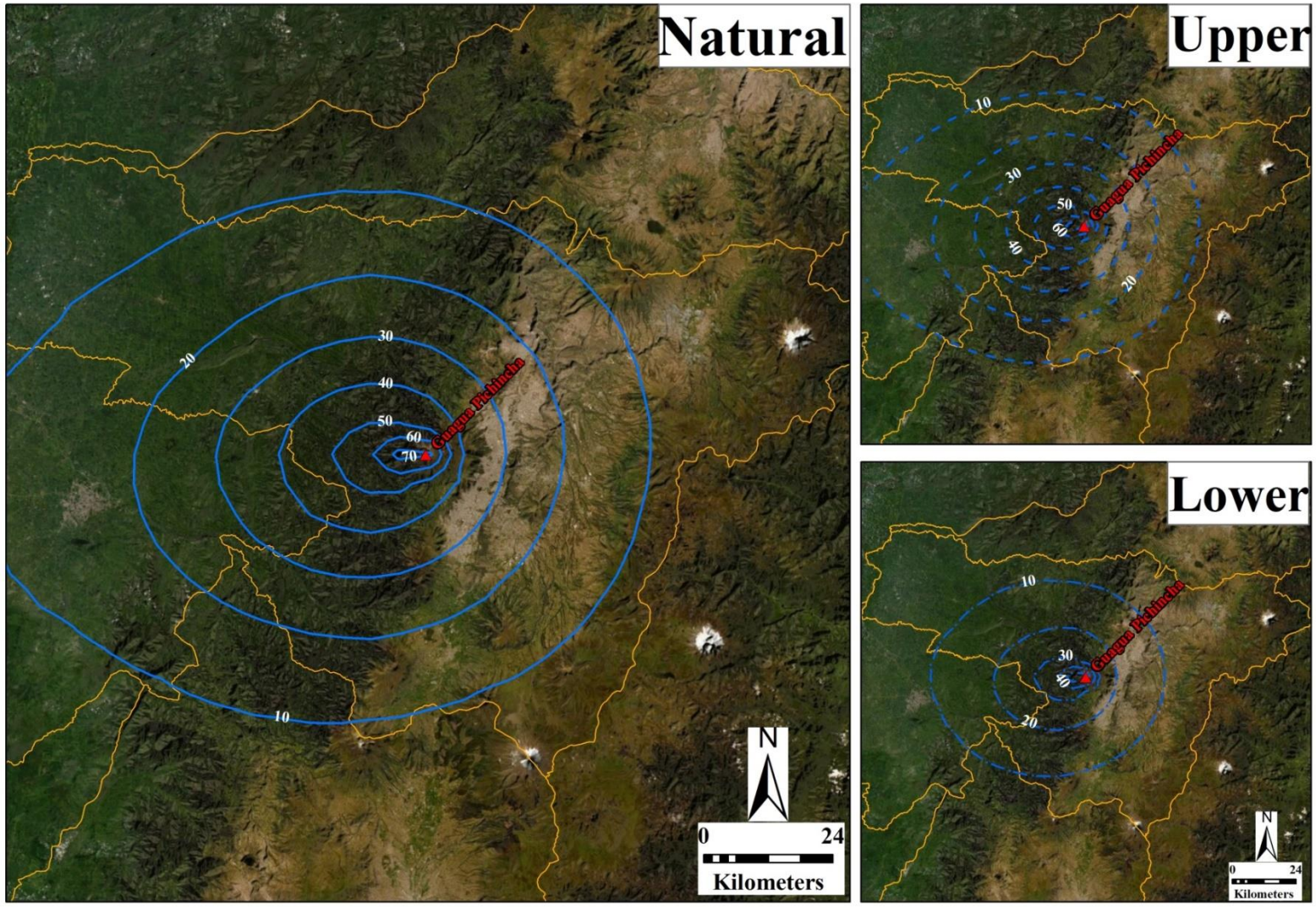

Figure S52. Guagua Pichincha volcano, Plinian eruption – Probabilistic map (30 mm)

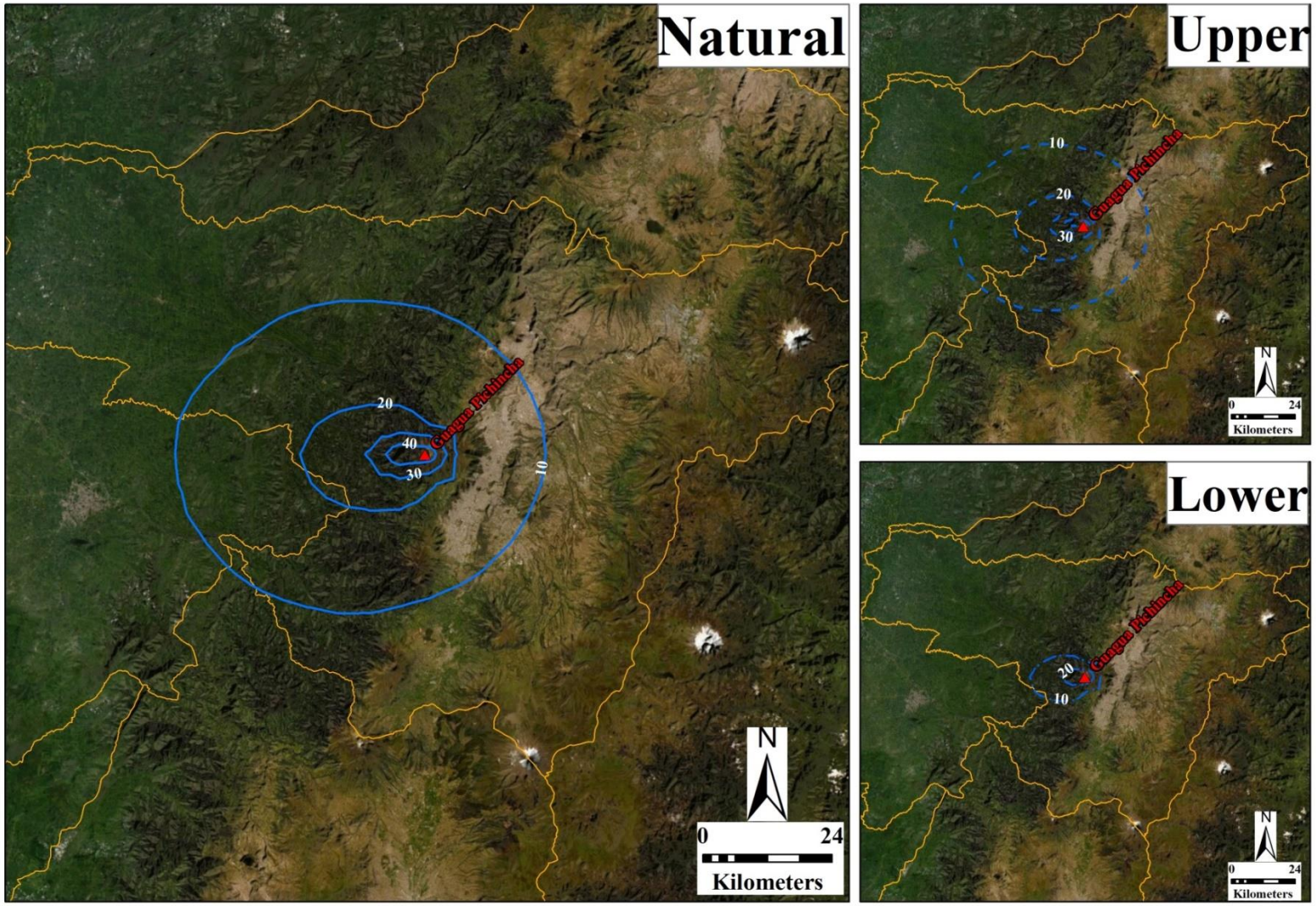

Figure S53. Guagua Pichincha volcano, Plinian eruption – Probabilistic map (100 mm)

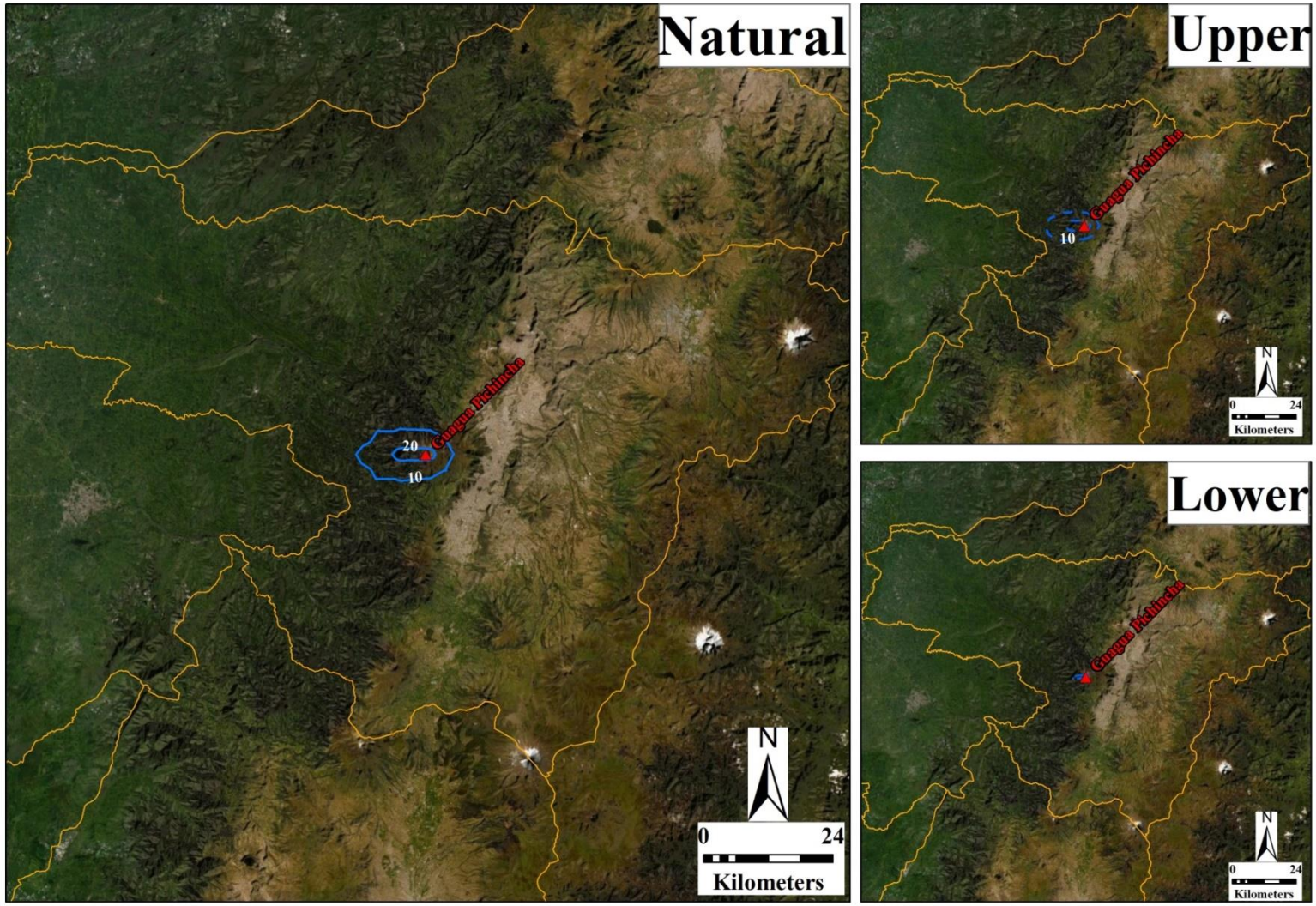

Figure S54. Guagua Pichincha volcano, Plinian eruption – Probabilistic map (300 mm)

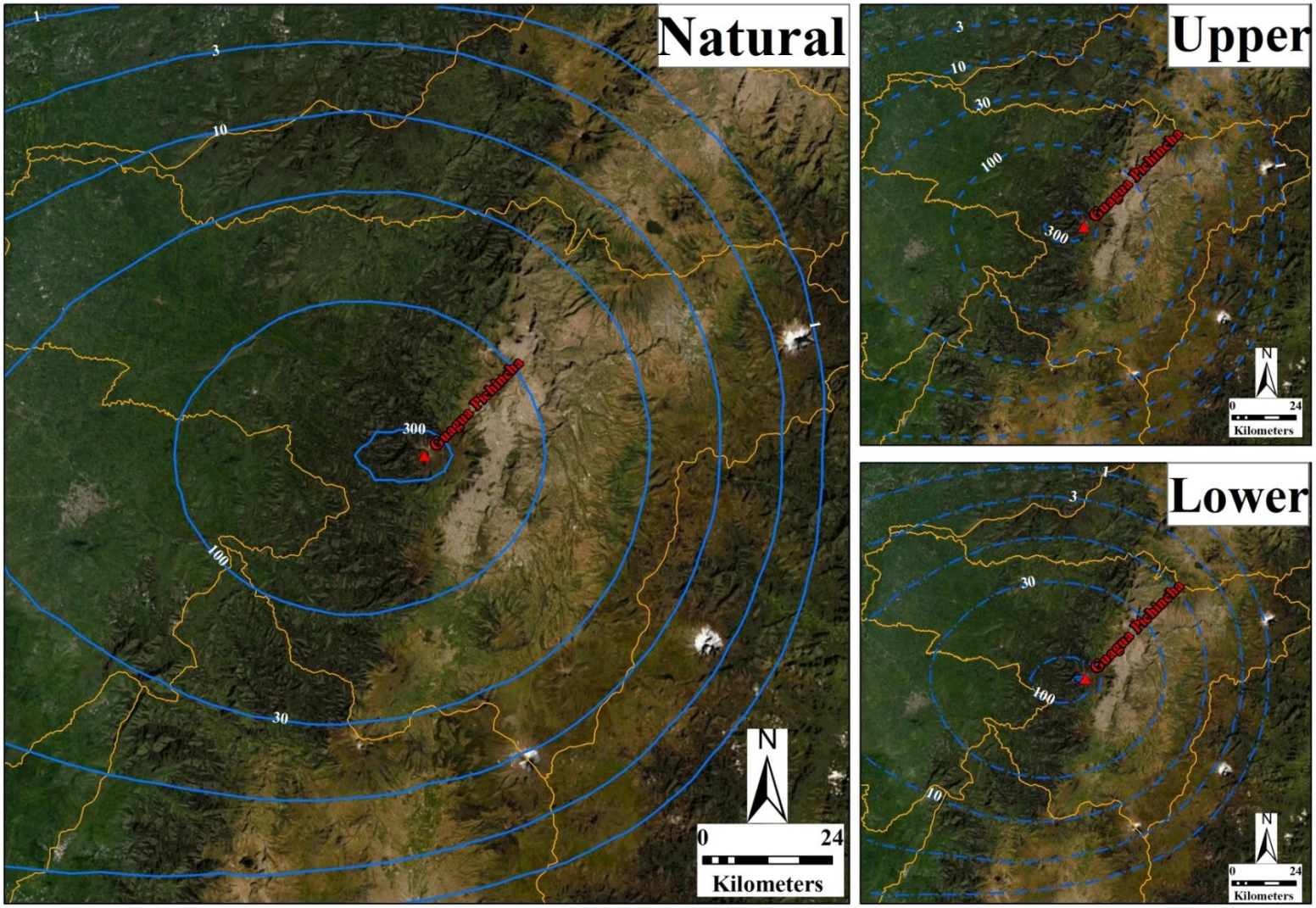

Figure S55. Guagua Pichincha volcano, Plinian eruption – Isopach map (10 %)

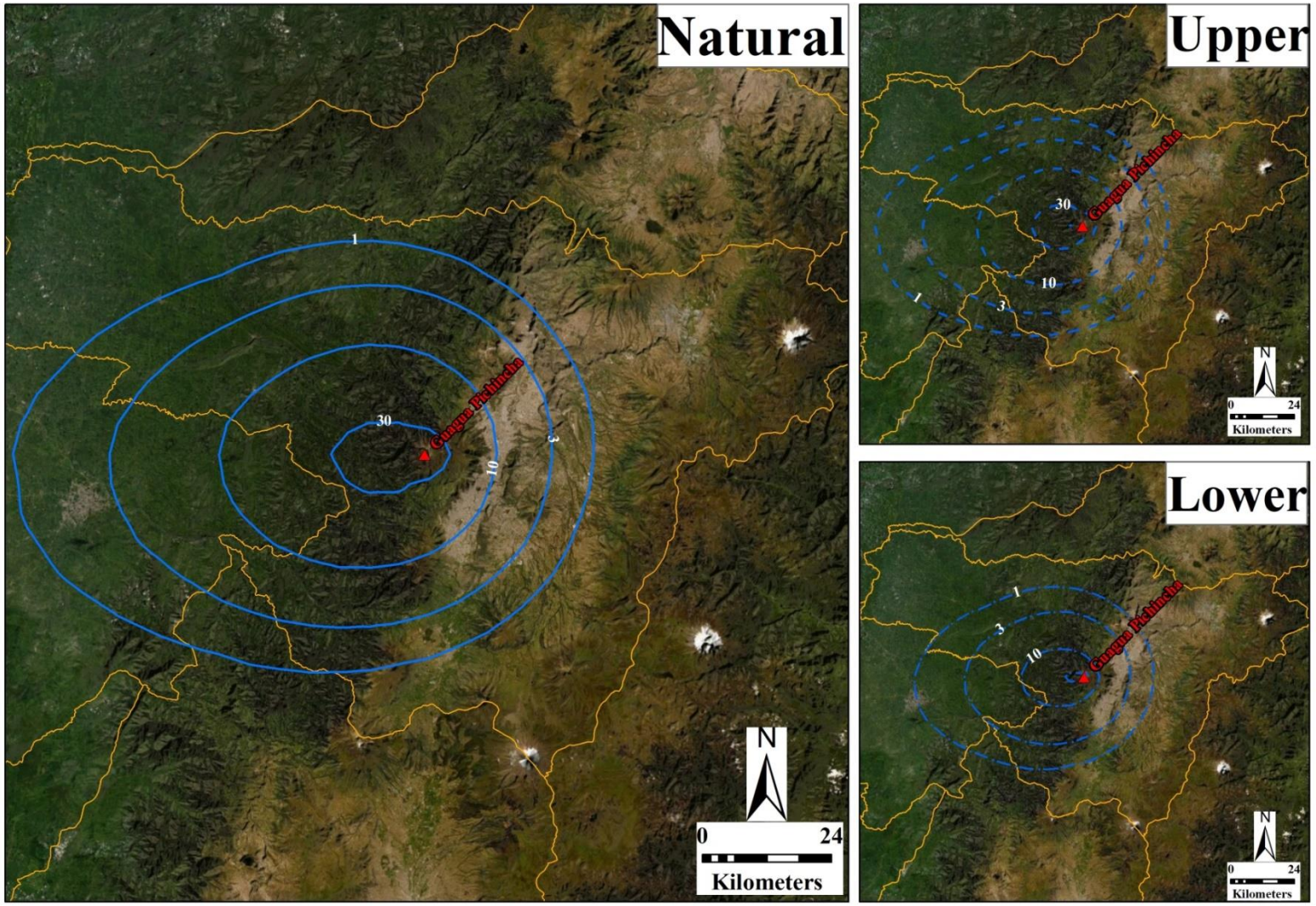

Figure S56. Guagua Pichincha volcano, Plinian eruption – Isopach map (50 %)

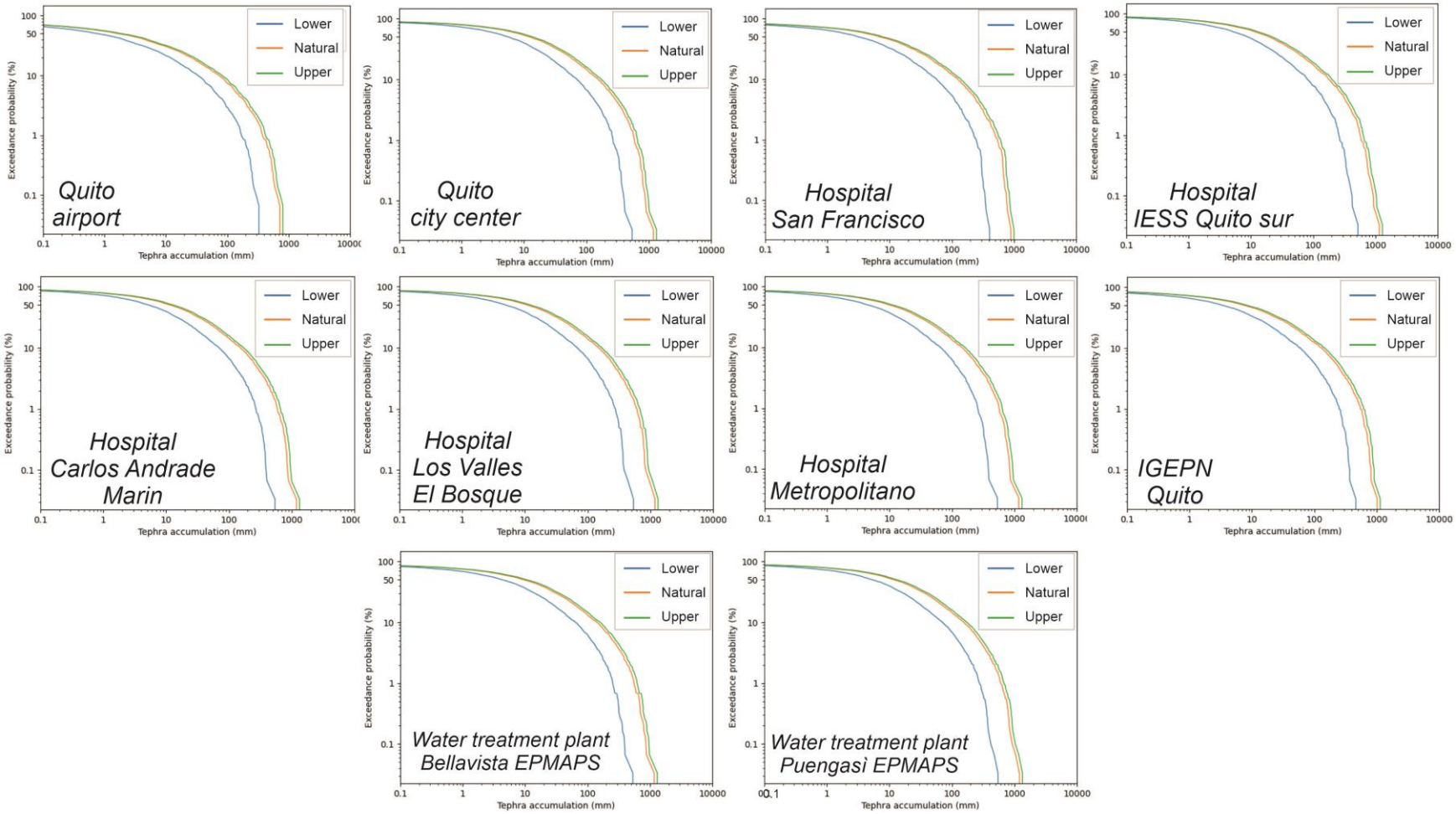

Figure S57. Guagua Pichincha volcano, Plinian eruption – Hazard curves